Università di Genova

Dibris

iit ISTITUTO ITALIANO DI TECNOLOGIA

Development of Functional Coatings for Different Applications: from Food Packaging to Fashion Industry

Marta Fadda

PhD program: Bioengineering and Robotics

Curriculum: Bionanotechnology

Cycle: XXXV

Tutors: Athanassia Athanassiou, Giovanni Perotto, Ilker S. Bayer

Abstract

Coatings are important in our society due to their contribution in terms of safety, health, comfort and well-being, for example, by offering protection from external agents to buildings, infrastructures, transports, food, and textiles. Since in our life most of the time we are in direct contact with them, for example in the shoes that we wear or in the food that we eat, it is essential that the materials used to develop the coatings are not toxic for our health. In addition, nowadays, the coating research-field and industry are looking for solutions to improve the sustainability of materials (e.g. biosourced, biodegradable, renewable materials) and processes (e.g. energy efficient manufacturing) in order to reduce their impact on the environment [1].

In this contest, the main objective of this work is to select sustainable materials in order to develop functional coatings for different applications, such as food packaging and leather industry. Concerning the food packaging, one of the main trend is to develop antimicrobial active coatings to reduce or avoid the bacterial growth on food, preserving its quality for a longer a time [2]. For this reason, a food grade sustainable copolymer and an antioxidant molecule, curcumin, have been combined to develop a sustainable and active coating for various substrates such as glass and polysaccharide films with the aim of proposing a coating for food packaging [3]. Due to the application, the coating presents appealing properties, such as reduction of gas exchange between the inside and the outside of the packaging, as well as transparency to allow the visibility of the food, and UV-filtering ability to protect the food from the UV light. Last but not least, the coating is characterized by low bacterial adhesion, making it a possible candidate for active food packaging.

Since the challenge of finding sustainable and green solutions for low environmental impact coatings has been evolving from avoiding petroleum-derivatives into the opportunity to get materials derived from renewable resources and waste [4], in this work, as next step, by-products of the food industry have been taken in consideration to develop a hydrophobic and water resistant coating for fish leather. Since salmon fish skin is one of the main waste of the aquaculture, the Horizon 2020 project, FISHSKIN [5], has considered it a sustainable raw material for fashion transforming it into leather. In this contest, the coating for fish leather has been developed by using the epoxidized soybean oil, which derives from the soybean oil produced in excess in many geographical areas respect to the consumption in cooking [6], and a sustainable trimer acid. As a result, it improved the waterproof ability of the leather in terms of water and humidity without affecting its breathability and softness.

Both the developed coatings could be easily scalable in an industrial process and considered as possible solutions in their fields of application, firstly because they respect the sustainability goal as main aim of the industries. In addition, the curcumin-based coating could be easily applied on different substrates, such as paper, PET and other food packaging materials, as well as the ESO-based coating could make water resistant cotton, as demonstrated, or other functional materials, such as paper, used also in other fields of application.

Key-words: coatings, sustainability, by-products, functionalization

Chapter 1. Introduction

1.1. Functional coatings

Coatings are thin layers applied on the surface a substrate, in order to protect and/or decorate it. For this reason, it is very common that in our life we are in contact with them, even if we are not conscious about it. Indeed, coatings are important in our society because they contribute to our safety, health and well-being, for instance, by offering protection from external agents to buildings, infrastructure, transports, food, and textiles [1]. Nowadays, it is more common talking about functional coatings, which have the aim of enhancing the properties of the substrate and/or giving to it new functionalities, creating, most of the times, multifunctional systems for a wide range of applications. Applying functional coatings aims to respond to specific needs. Generally, reducing the bad environmental impact of our life-style, in terms of pollution, energy consumption or production of waste, is one of the main issue.

For this reason, functional coatings have been proposed as possible solutions to face various problems. For instance, climate changes are causing the increasing of energy consumption: therefore, the demand of solutions to improve the energy efficiency of buildings is increasing. In this contest, transparent heat insulation coatings have been developed to improve the energy efficiency of glass windows, which satisfy esthetic purposes (e.g. greater brightness inside the buildings) causing, on the other hand, the increasing of heating during the winter and of cooling during the summer [7]. Or, coating mortar has been proposed in order to have optimized thermal and acoustic efficiency with the same weight of the material, reducing the demand for energy in buildings [8]. Our bad impact on the environment is caused also by the larger and larger amount of waste that we produce day by day: food, clothes, electronics etc. For this reason, various solutions have been proposed and developed to improve the durability of textiles. For instance, Dastjerdi et al. overcame the fact that already proposed TiO_2/Ag nanoparticles-based treatments lead a tournament in colour to brown of the fabrics, limiting their durability and, therefore, their application, by proposing a further coating with cross-linkable polysiloxane and obtaining more durable textiles in terms of antibacterial properties, UV-protection and washing [9]; or, Mazzon et al. shielded cotton fabrics' oxidative degradation with a bi-layer functional coating, where the first layer was made by incorporating butylated hydroxytoluene, as food grade antioxidant, into a polycaprolactone matrix, while the second one with polydimethylsiloxane to improve the stability in water of the treatment [10]. In addition, functional coatings made with zein have been proposed to protect stone surfaces in cultural heritage from water and humidity [11], or to make drug-eluting stents for treating

cardiovascular diseases [12]. Anyway, whatever the application, today the main goal in developing functional coatings is to moderate our impact on the environment, for example by facing climate changes decreasing the demand for energy, reducing the amount of waste that we produce improving the durability of materials, and proposing more and more socially, economic and environmentally sustainable solutions.

In this work, two functional coatings have been developed with the aim of reduce the bad environmental impact of some industries, in terms of processes and materials. First of all, an antioxidant and antibacterial coating was proposed in order to extend the shelf life of the packaged food and, therefore, reducing the amount of wasted food. As second project, a hydrophobic and water resistant coating was made in order to protect fish leather artefacts and products, such as bags and clothes, from rain. The reduction in the amount of waste was respected as aim of this project not only by improving the durability of the final products, but also by selecting by-products of the food industry to make the coating. Of course, due to the different application and substrate for the two projects diverse materials have been considered.

1.2. Polymer coatings

More specifically, when a thin layer of polymer is applied on the substrate, we talk about polymer coatings, with thickness in the order of 1-100 μm [13]. The type of substrate and the method of application of polymer coatings depend on the liquid or solid nature of the coating itself. Liquid coatings from solutions/suspensions of polymers and/or functional molecules can be applied with different techniques and the most common are spray drying, airbrush spraying, dipping, and casting. The choice of the method depends on several factors, such as the physico-chemical properties of the solution (e.g. concentration, viscosity) and the surface features of the substrate (e.g. morphology, porosity, roughness), influencing the homogeneity and the drying speed of the coating [14]. In this work, two liquid polymeric coatings were developed by dissolving the polymers in the respective solvents and then dipping manually the substrates in order to ensure good uniformity and coverage of large areas. Due to the type of solvent, different speed of drying were considered. In addition, in order to have multifunctional systems, polymer composite coatings have been developed with two parts: the matrix, usually represented by the polymer(s), and the filler, which usually are molecules/materials, for instance, in form of fibers or nanoparticles, with the aim of giving new functionalities or enhance some polymer's properties. The type of polymer and filler has been selected basing on the field of application and the type of substrate. In the first part of this work,

a polymer functional coating was developed for food packaging application. Therefore, in the next section coatings' properties and features for this application are investigated.

1.3. Functional coatings as sustainable solutions in food packaging

Nowadays, the food packaging industries are looking for alternative and innovative solutions in order to improve some fundamentals of packaging, such as [15]:
- Protection of the packaged goods from contaminations;
- Communication about both the state of the packaged food, for example whether it has gone bad or not, and information regarding its nutritional values and preparation;
- Convenience, since day by day people have been changing their way of live and, therefore, eating, consuming and demanding for more convenient food;
- Containment in order to make the transport of the food easier.

Additionally, safety, quality and freshness of the packaged food have to be preserved, and, simultaneously the packaging has to respect all the regulatory requirements without increasing the production costs [15]. Furthermore, the industries have to be taken into account all the sustainability issues in terms of reduction of produced waste also including recycle and reuse processes, efficient use of resources, and optimization of the processes [15]. Therefore, all these aspects have to be considered by the food packaging industries in order to reduce the environmental impact in terms of food loss and packaging waste. For this reason today the industries and several research fields are investing in active and intelligent sustainable food packaging, proposing not only new composite films but also functional coatings made of sustainable materials such as biopolymers and by products. Indeed, active functional coatings can reduce the food loss by extending the shelf life of the packaged food, but also improve the packaging recyclability by substituting traditional materials that are not recyclable (e.g. EVOH) in multi-layer packaging, with sustainable and easy-to-manage in terms of waste materials.

Concerning the materials used in packaging, in the last decades plastics and petroleum-based polymers have substituted conventional materials such as paper or metal because they are lighter, easier and cheaper to process. In addition, they protect the packaged food mechanically and chemically. The most used polymers in food packaging are: polyethylene (PE), polypropylene (PP), polyethylene terephthalate (PET). The main drawback of these materials is the permeability to gases and vapors [16]. However, due to the recent plastic-free feeling shared by industries, researcher and common people, now the market is considering again the paper due to its recyclability, biodegradability and compostability [17]. In spite of this, it presents some disadvantages for food packaging applications such as hydrophilicity,

poor barrier properties, and high sensitivity to microbial attack [18]. In order to overcome some of the drawbacks, different strategies have been proposed by the researchers and, then, adopted by the industries. First of all, by using natural polymers such as polysaccharides or proteins to make films. For instance, chitosan, which is one of the most abundant polysaccharide present in nature and a renewable resource, a part from being non-toxic, biocompatible, biodegradable and biocompatible, it presents antimicrobial activity and it is soluble in water [19]. To exemplify, Tanpichai et al. coated paper with chitosan obtaining an improvement in wettability, making the paper hydrophobic, and in mechanical properties, making the paper more robust, but still observing cellulose fibrils released from the coated paper in contact with food simulants [20]. Or, collagen and, consequently, gelatin (collagen's hydrolyzed form) that are the most abundant proteins in nature can be used as main part of bioplastic due to their good mechanical properties. About this, Battisti et al. improved the mechanical properties of paper by applying a coating made with gelatin crosslinked with transglutaminase enzyme, and encapsulating an antioxidant and antimicrobial agent to extend the shelf life of the packaged beef [21].

On the other hand, another strategy consists in applying coatings to overcome the main disadvantages of the already commercialized packaging materials that are poor in terms of gas barrier properties. Indeed, whey-protein-based coatings were applied on PET films in order to improve its barrier properties, obtaining results comparable to the ethylene vinyl alcohol copolymer (EVOH) used in food packaging composites, with side important effects such as good adhesion to the substrate, no fractures due to mechanical loads, and no affection of the transparency of PET, making easier the recyclability and biodegradability of the multi-layer system [22]. Or, an improvement of the barrier properties of polylactic acid (PLA) films was obtained by coating them with a PLA/SiO_2 hybrid material, maintaining relatively high optical transmittance [23]. Or, corn zein nanocomposite coatings were developed to reduce the water vapor and oxygen permeability of PP films [24]. Or, a functional coating is applied on the previous substrates to give to them new functionalities, for instance to avoid the spoilage of the food extending its shelf life without affecting its quality. Indeed, Al-Naamani et al. demonstrated the inactivation and the prevention of growth of food pathogens on PE films coated with chitosan-zinc oxide nanocomposite [25], or Munteanu et al. encapsulated essential oils into a chitosan matrix to obtain an antimicrobial and antioxidant coating for PLA films [26]. These are examples of active coatings for food packaging.

Therefore, in the last years active coatings have become an important sustainable solution in food packaging by putting the surface of the packaged food in contact with the

active agent (e.g. antioxidant, antimicrobial, enzyme). In particular, different techniques are reported in the state of the art to make active coatings for food packaging [27]:

- Coating with incorporated agent for controlled release, where the active agent is encapsulated in the polymeric matrix from where it migrates exercising its functionality onto the packaged food;

- Coating with agent's surface immobilization, where the surface of the substrate is initially functionalized by chemical or physical methods in order to immobilize the active agent. In this case, the agent will not migrate onto the packaged food;

- Coating with layer-by-layer assembly made by an attraction of alternating polyelectrolytes with opposite charges, where the active agent can be incorporated between layers or within the single layer. The active agent is not supposed to migrate onto the food;

- Coating with polymer chains grafted from the surface by UV light due to photoinitiators, where the active agent can be incorporated during or after the photografting.

Whatever the technique to incorporate the active agent into/onto the coating, the most used agents in active packaging are antimicrobials, antioxidant, and enzymes [27]. In particular, antimicrobial agents are used to control or prevent the growth of microorganisms on food, avoiding its spoilage. Indeed, Bastarrachea et al. reviewed some antimicrobial agents (e.g. essential oils, natamycicn, nisin) incorporated in coatings applied on PP, low density polyethylene (LDPE) or PLA films, in order to modulate their release and have inhibition effect against standard microorganisms such as *Escherichia coli*, *Salmonella Typhimurium*, or *Staphilococcus aureus* [27]. In addition, protecting packaged food from oxidative degradation is another important aim in order to maintain its quality during transport and storage. For this reason, different strategies are used to overcome this problem such as adding preservatives with antioxidant properties directly on food, incorporating the antioxidant agent into the packaging material, or developing antioxidant active coatings [27]. Bastarrachea et al. reported some examples of antioxidant active coatings, such as a citrus oil-based coating sprayed on the surface of PET trays with antioxidant activity on cooked turkey meat, or rosemary extract-based coating applied on LDPE plastic wrap to delay the lipid oxidation of chicken [27].

In Chapter 2 of this work it will be described how the first coating technology, the controlled release of the active agent, was used to develop an antioxidant and antimicrobial coating for food packaging. In particular, a both antimicrobial and antioxidant active agent,

curcumin, was encapsulated into a polymeric matrix made of polyvinyl acetate-vinyl laurate copolymer.

1.4. Functional coatings for textiles

Textile fabrics derive from an interlacement or intermingle of fibers that can be natural or synthetic. Natural fibers can be plant-derived (e.g. cotton, jute, flax) or protein-based (e.g. wool, silk). Plant-derived fibers are essentially made of cellulose with hydroxyl (-OH) functional groups, whereas the protein-based fibers have amine ($-NH_2$), hydroxyl (-OH), carboxyl (-COOH) and tiol (-SH) groups.

Textile fabrics from natural fibers present some advantages, for instance they are soft and breathable. On the other hand, they are hygroscopic, so they absorb water in form of both drop and moisture, and they are less durable. For this reason, it is a long time that the demand for hydrophobic and water-repellent treatments and coatings for textiles is increasing. In the last years, commercial textile fabrics have been treated with polymeric coatings in order to have high water repellency. For instance, famous commercial brands used C8 fluorinated products to make waterproof jackets, shoes and accessorize, in particular by adding expanded-poly (tetrafluoro-ethylene) (e-PTFE) membrane. However, in 2006 the U.S. Environmental Protection Agency (EPA) committed to reduce the use of this kind of materials by eliminating completely C8 chemistry till 2015 because they release perfluorooctanoic acid (PFOA) and perfluorooctane sulfonate (PFOS) after degradation, which are toxic for the environment as well as dangerous for human health [28]. Therefore, in the following years hydrophobic and water-repellent coatings made of polymers with six fluorinated carbon atoms (C6 chemistry) were proposed [29-32].

Nowadays, in spite of this regulamentation, the trend is to find out fluorine-free solutions for hydrophobic/superhydrophobic surfaces and textiles, since $-CF_3$ are harmful for the environment and for the human being, even if the carbon chain is shorter. For this reason, fluorine-free silicon-based polymers such as silan or siloxane have been proposed to develop hydrophobic coatings. For instance, polydimethylsiloxane (PDMS) was widely used as alternative to fluorinated polymers due to its low surface tension, easy workability, high durability and cheapness, also for textile fabrics [33]. In particular, this kind of polymers were often coupled with nanoparticles as filler to lead superhydrophobicity, as silica [33], TiO_2 [34], or ZnO [35] nanoparticles.

On the other hand, in the last years the environmental impact of materials and processes have been becoming more and more important in the production of hydrophobic or

superhydrophobic coatings. Therefore, the researchers and the industries are looking for materials that are not only more eco-friendly and bio-based, but also easy to recycle or to manage once discarded. Indeed, since inorganic nanoparticles are not degradable, they can represent a problem for the environment, as well as they make the recycle and waste management processes more complex [36]. Therefore, now the market is demanding not only for fluorine-free but also for nanoparticles-free solutions by giving a look at renewable resources and by-products of the industries. For instance, Cheng et al. used cellulose nanocrystals, that are renewable and biodegradable nanoparticles extracted from cellulose, as possible substitutes of inorganic nanoparticles for increasing the roughness of cotton fabrics and obtain superhydrophobicity and water/oil separation property [37]. On the other hand, nanoparticles-free superhydrophobic coatings for cotton fabrics were developed: Dong et al. firstly coated the fabric with polydopamine and then induced the roughness and surface energy with stearic acid obtaining a multi-functional fabric with not only high superhydrophobicity but also protection from UV, self-healing property due to solar light, and efficient oil-water separation [38]; Cheng et al. created the desired roughness on cotton by enzyme etching, then coated the surface with epoxidized soybean oil and lowered the surface energy with stearic acid, making superhydrophobicity and excellent oil/water separation properties [39]; or Cheng et al. obtained similar results as above but they induced the roughness with acid-etching [40].

Indeed, also in the field of hydrophobic coatings for textiles the researchers are looking for fully sustainable solutions basing on materials that are by-products of the industry or/and obtaining coated systems completely recyclable. For instance, paper, another cellulose-based material, is widely used by the industries for single-use items instead of plastic in packaging because it is biodegradable, light, cheap and recyclable [41]. Due to its hydrophilic nature and low moisture resistance, plastic-based and/or bio-based composites gather with by-products of the industries were developed to coat paper in order to improve its wettability properties were used. Concerning the use of biopolymers, for instance, Li et al. developed a coating from aqueous solution by grafting polydimethylsiloxane (PDMS) onto chitosan in order to make the paper hydrophobic and improve its moisture resistance demonstrating its recyclability [42]. Other research studies started to focus on plant oil-based coatings to improve the water resistance of paper in terms of both water and moisture by modifying chemically the oils to improve their performances. For instance, Parvathy et al. synthetized two bio-resins from transesterification and silanization of epoxidized castor oil and crosslinked them with paper by condensation: as a result, the coated paper presented hydrophobicity and high resistance to the moisture with the possibility to remove the coating in alkalinic solutions and recycle the paper

[43]. Or, Thakur et al. obtained similar results by crosslinking silane-modified epoxidized downstream corn oil with hydroxyl groups of the paper [44]. Or, Li et al. imparted water resistance to the paper with a coating made by synthetizing chitosan-*graft*-castor oil copolymer [45]. Therefore, now the research and the market are focusing their attention in proposing plant oils-based solutions for hydrophobic coatings for cellulose-based materials reducing the costs and improving the sustainability of the processes.

For these reasons, in Chapter 3 of this work epoxidized soybean oil, derived from soybean oil, was selected as main material to improve the water resistance of a protein-based textile fabrics, fish leather, and cotton fabrics.

Chapter 2. Antioxidant coatings from elastomeric vinyl acetate – vinyl laurate copolymer with reduced bacterial adhesion

This chapter is adapted from **Fadda M.** et al., Antioxidant coatings from elastomeric vinyl acetate – vinyl laurate copolymer with reduced bacterial adhesion, *Progress in organic coatings*, 2022.

2.1. Poly(vinyl acetate)-vinyl laurate copolymer

Since very few information about the copolymer poly(vinyl-acetate)-vinyl laurate (PVAc-VL) were found in the state of the art, first of all a literature review of the two components of the copolymer, polyvinyl acetate (PVAc) and its monomer vinyl acetate (VAc), and vinyl laurate (VL) was conducted, focusing much more on their sustainability in terms of non-toxicity and bio-degradation, and their application in composites.

VAc-based polymers are widely used as adhesives for paper and wood bonding [46]. A typical example is PVAc, which is non-toxic, cheap, biodegradable [47], and subjected to bio-deterioration by fungi [48]. The applications of PVAc are various, such as adhesives, coatings, emulsifiers, paints, and precursor in the synthesis of polyvinyl alcohol (PVA) [49]. It was demonstrated that PVAc presents low thermal stability, weak resistance against moisture, and partial hydrolysis: for this reason, to overcome these drawbacks VAc is often copolymerized with other monomers [50]. Indeed, VAc is usually copolymerized with vinyl chloride [51, 52], or acrylate [53] to produce latexes with a wide range of properties [54]. For instance, vinyl acetate-butyl acrylate emulsion copolymer is extensively used for architectural applications [54]. The ethylene-vinyl acetate copolymer (EVA) is well-known and used for a wide range of applications such as paints, encapsulation of photovoltaic modules [55], and for drug delivery systems due to its non-toxicity and biocompatibility [56]. More recently, composites of PVAc with natural polymers have also been developed [49]. For instance, cellulose nanofibrils were used to improve the mechanical properties of PVAc producing an adhesive nanocomposite [57]; graft copolymerization of VAc onto corn starch in an aqueous solution with a redox initiation system was performed [58]; the thermal stability of a starch-based wood adhesive was improved by using the co-monomers VAc and butyl-acrylate in order to promote the graft copolymerization [59]; a chitosan-graft-poly(vinyl acetate) copolymer was developed increasing the toughness and the water-resistance of chitosan for particular membrane

applications [60]; finally, the blending of PVAc with sugar cane bagasse lignin demonstrated that lignin protected PVAc from photochemical degradation [61].

The monomer VL is a vinyl ester that is mainly used in acylation processes [62, 63]. It was demonstrated to be biocompatible and non-toxic in different *in vitro* and *in vivo* models [64-66]. Moreover, it was implemented in various copolymerization processes, such as a carboxyl-terminated *N*-isopropylacrylamide/VL copolymer coupled with chitosan as a vector for gene transfection [67], a cotton-graft-VL with good water repellency even after repeated treatment with plasma [68], a microgel system based on *N*-isopropylacrylamide co-polymerized with VL [69], or nanoparticles with a poly(vinyl laurate-*co*-vinyl acetate) core and poly(ethylene glycol) shell to produce surfactant molecule in situ and to control oil-water interfaces [70].

Elastomeric resins based on VL are commercially available and particularly used as chewing gum base. Specifically, PVAc-VL (Figure 1) has been recently commercialized and is approved for food and drug packaging [57], while it is considered safe in cosmetic formulations [71] and certified with food-contact compliance according to the European Regulation 10/2011 [72].
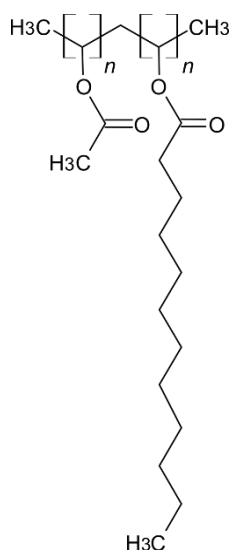

Figure 1. Molecule of PVAc-VL

Currently, PVAc-VL copolymer it is mainly used as a biodegradable chewing gum base to replace polyisoprene-based (synthetic rubber) (AU647719B2, US8409638B2, US20130071515A1). To the best of our knowledge, it has not been used to develop functional coatings. On the other hand, in this work it was taken in consideration as polymeric matrix in a functional coating thinking of its chemical structure: first of all, it was expected to have good adhesion properties due to the PVAc part, and then to be hydrophobic due to the VL segment.

12

2.2. Curcumin

Curcumin is a natural compound present in a pigment from Curcuma Longa L (turmeric). It is a symmetric molecule, also known as diferuloyl methane. It has three chemical entities in its structure: two aromatic rings connected by a seven carbon linker (Figure 2). It has been widely studied in several fields such as pharmacology [73, 74], biomedicine [75], dentistry [76], anti-cancer [77, 78], and sensors applications [79]. The use of this molecule was also investigated in food preservation and packaging due to its strong antioxidant and radical scavenging properties [80], and its antibacterial and bactericidal activity [81, 82]. Therefore, curcumin was widely used as additive in composite films for packaging applications. For instance, it was incorporated in low-density polyethylene films increasing their water vapor barrier properties [83], or in carbohydrate-based composite films to have strong antioxidant and some antimicrobial activity [84], or into gelatin composite films [85] or polylactic acid films [86] to improve mechanical, water vapor barrier and UV-barrier properties while maintaining the transparency of the films. Furthermore, aloe vera-starch composite films were reinforced with curcumin-loaded starch nanoparticles lowering their water vapor permeability [87]. Or, a combination of curcumin and anthocyanins were added in starch/polyvinyl alcohol blends to make pH-sensing composite films to monitor the real-time freshness of fish products [88].

Curcumin was also used as additive in coating for food packaging. For instance, cellulose-polycaprolactone composites with curcumin that can detect pH changes in food were developed [89], as well as edible coatings using curcumin doped iron-functionalized cellulose nanofibers and chitosan biocomposites to maintain the quality of kiwifruits during storage [90]; or, curcumin was loaded into gelatin-based and zein-based coatings, revealing promising release behaviour in contact with different food simulants [91]; finally, fabricated photoinduced antibacterial PVAc-curcumin coatings for active packaging applications were produced [92].
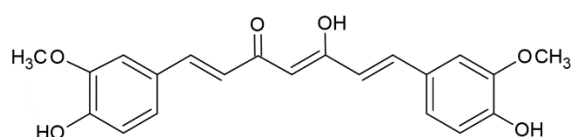
Figure 2. Molecule of curcumin

Therefore, in this work, a functional coating for food packaging was developed by using a food-grade copolymer, PVAc-VL, and curcumin for the first time. It was showed the biodegradable solvent 4-methyl-2-pentanone (MIBK, see: Environmental Health Criteria 117

by World Health Organization, 1990) (Figure 3) is a suitable solvent for both curcumin and the copolymer, and the coatings can be easily applied by dip coating technique. The elastomeric coating was applied not only on solid surfaces like glass, but also on natural polymer substrates, like gelatin and alginate films. Furthermore, these functional coatings demonstrate effective, antioxidant, UV-blocking and low bacterial adhesion properties while improving wettability and barrier properties of natural polymers films. Therefore, this functional coating can be a cost effective alternative in food packaging applications.
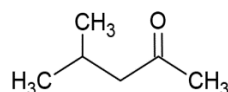

Figure 3. Molecule of 4-methyl-2-pentanone

2.3. Materials and methods

2.3.1. Materials

Poly(vinyl-acetate)-vinyl laurate copolymer (PVAc-VL; VINNAPAS® B 500/40 VL) was purchased from Wacker Chemie AG (Viscosity: 8.0-12.0 mPa.s; Molecular weight: 320000 g/mol; Glass transition temperature: 0 °C). Curcumin, 4-methyl-2-pentanone (Methyl isobutyl ketone, MIBK), ethanol, alginic acid sodium salt, gelatin from cold-water fish skin and glycerol were purchased from Sigma Aldrich. All chemicals are analytical grade and used as received. Deionized water was obtained from Milli-Q Advantage A10 purification system.

2.3.2. Preparation of the solution

Curcumin (1 g) was dissolved in 4-methyl-2-pentanone (100 mL) after stirring for 2 hours at room temperature to obtain 1 % (w/v) curcumin solution. Afterward, PVAc-VL (10g) was added to the curcumin solution until complete polymer dissolution after stirring for 2 hours at room temperature. This kind of solution produced a polymer coating containing 10 wt. % curcumin upon drying. In Table 1 are summarized all the concentration details relative to the other formulations including control solutions. For instance, the samples labeled as PC 10 (Polymer-Curcumin 90:10) indicated a dry coating with 10 wt.% of curcumin, or PC 2.5 indicated a dry coating with 2.5 wt.% of curcumin; and finally PC 10A or PC 10G indicate the PC 10 coating applied on alginate (A) or gelatin (G), respectively.

14

Sample label	Substrate	% PVAc-VL (dry coating)	% Curcumin (dry coating)
PC 0	Glass	100	0
PC 100	Glass	0	100
PC 10	Glass	90	10
PC 0A	Alginate	100	0
PC 10A	Alginate	90	10
PC 0G	Gelatin	100	0
PC 10G	Gelatin	90	10
PC 1.25	Quartz	98.75	1.25
PC 2.5	Quartz	97.5	2.5
PC 5	Quartz	95	5
PC 7.5	Quartz	92.5	7.5

Table 1. Coating labels and dry weight percentages. Coatings in the last four rows were made for detailed UV filtering measurements on quartz slides as substrates.

2.3.3. Preparation of the alginate and gelatin films

Glycerol (0.5 g) was mixed with deionized water (100 mL) at room temperature. Afterward, alginic acid sodium salt (3 g) was dissolved in the previous solution under shaking overnight at room temperature to obtain a 3 % (w/v) sodium alginate solution. Likewise, 3 % (w/v) gelatin solution was made. 70 mL of the solution were casted on squared Petri-dish (12 cm × 12 cm), previously covered with a layer of PDMS, and dried under an aspirated hood for 24 hours. The thicknesses of alginate and gelatin films were measured to be 145 ± 20 µm and 155 ± 35 µm, respectively.

2.3.4. Preparation of the coatings

Microscope glass slides were dip-coated in 20 mL of various solutions for 30 seconds and left to dry under an aspirated hood for 24 hours in standard conditions (21-23 °C, 40-50 % R.H.). The coatings were made with PC 10 (8 ± 2 µm, thick), PC 0 (8 ± 2 µm, thick) and PC 100, respectively. Similarly, alginate films and gelatin films were dip-coated in the same solutions to apply the coatings. Figure 4 summarizes the solution and coating preparation processes schematically.
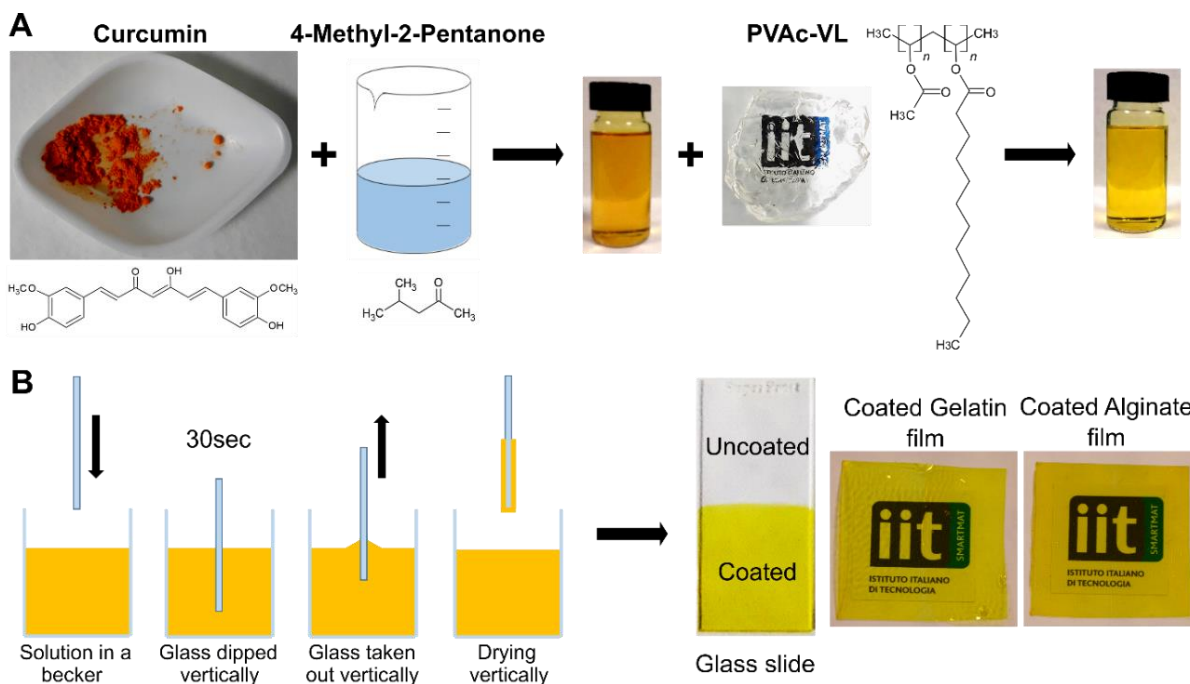
Figure 4. (A) Schematic illustration of solution fabrication steps. (B) Schematic illustration of the dip coating steps. The photos show coatings on glass (PC 10), gelatin (PC 10G) and alginate (PC 10A).

2.3.5. Morphological characterization: SEM and AFM

Scanning electron microscope JSM-6490LA (JEOL, Tokyo, Japan) was used to investigate the microstructure of the surface and cross-section of PC 100, PC 0, PC 10, pure alginate film, PC 10A, pure gelatin film and PC 10G with 5 kV acceleration voltage. The samples were previously mounted on a tilted stub, framed with silver paste, and sputter-coated by using a Cressington Sputter Coater – 208 HR (Cressington, Watford, UK) with a 10 nm thick layer of gold.

An AFM system XE-100 (Park Scientific, Suwon, South Korea) with a NCHR probe (f = 320 kHz, c = 42 N/m) was used to investigate the topography of PC 100, PC 0, PC 10. Areas of 5 x 5 µm (256 x 256 pixels) were scanned. The images were acquired in non-contact mode and then processed by Gwyddion software.

2.3.6. UV-Vis absorbance, light transmittance and opacity

A Varian CARY 6000i Scan UV-Vis spectrophotometer (Walnut Creek, CA, USA) was used to investigate the absorbance, transparency, and UV-blocking properties of the coatings. The spectral region scanned was from 200 to 800 nm. To study the transparency and the UV-blocking properties of the coatings, the light transmittance was measured. In particular, the transmittance at 660 nm (T_{660}) and 280 nm (T_{280}) of the coatings was evaluated, following the

protocol of Roy et al. [84]. Coatings were made on quartz slides. An uncoated quartz slide was used as a reference to take the measurements.

On the other hand, the opacity was calculated at 600 nm as indicated in previous works [93, 94] using the following equation:

$$Opacity = \frac{Abs_{600}}{X} * 100$$

where Abs_{600} is the value of absorbance at 600 nm and X is the thickness of the coating (mm).

2.3.7. Yellowness and whiteness index

The yellowness (YI) and whiteness (WI) indexes, of PC 10, pure alginate film, PC 10A, pure gelatin film, and PC 10G were evaluated. Photographs of the samples were processed by using a free app "RGB Color Detector" for Android to obtain R, G and B values from all samples. These values were converted from RGB to CIELAB values using a free online color converter (http://colormine.org/convert/rgb-to-lab) and YI and WI values were estimated by using the following equations reported in previous works [86, 95], respectively:

$$YI = \frac{142.86 \times b}{L}$$

$$WI = L - 3 \times b$$

where L is the lightness and b is the yellowness/blueness. A sheet of printing paper was used as white support for the samples to take the pictures. There different films from each film were photographed and there different zones on each sample were photographed to ensure reliable results.

2.3.8. Chemical characterization: ATR-FTIR and μRaman spectroscopy

Chemical characterization of curcumin, PVAc-VL (polymer resin), PC 0, PC 10, pure alginate film, PC 10A, pure gelatin film and PC 10G, was performed by using a single-reflection ATR accessory with a diamond crystal (MIRacle ATR, Pike Technologies) coupled to FTIR spectrophotometer (VERTEX 70v FTIR, Bruker). The spectral region scanned was 4000-600 cm^{-1} with a resolution of 4 cm^{-1}. The spectra were normalized to their maximum.

A Horiba Jobin-Yvon μRaman LabRAM HR800 (Horiba Scientific, Kioto, Japan) operating with a He-Ne laser source (632.8 nm) was used to study further the molecular vibration modes of curcumin, PC 0, and PC 10. The objective used was a 50× with a slit aperture of about 150 μm. The spectral region scanned was 3500-1000 cm^{-1} with a resolution of 1 cm^{-1}. The spectra were normalized with maximum absorption peaks.

2.3.9. Thermogravimetric analysis

Thermogravimetric analysis (TGA) of curcumin, PVAc-VL, and PC 10 samples were carried out by using a TGA Q500 (TA Instruments, USA) instrument. Measurements were performed placing the samples (4-7 mg) in platinum pans under inert N_2 flow (50 mL/min) in a temperature range from 30 to 800 °C with a heating rate of 10 °C/min.

2.3.10. Mechanical characterization: AFM-nanoindentation and tension test

The Young's modulus of PC 0 and PC10 coatings applied on glass slides was measured with an AFM Nanowizard III-JPK (Bruker, Billerica, MA, USA), operated in nano-indentation mode called QI. The system was placed on an active anti-vibration platform inside an anti-acoustic box. A probe CP-NHC-BSG-C-5 (sQUBE, Germany) with a tapping silicon cantilever (thickness 4±1 µm, length 125±10 µm, width 30.0±7.5 µm, resonance frequency 204-497 kHz, spring constant 10-130 N/m) and a borosilicate glass bead of 20 µm diameter as the tip was used for the indentation. The cantilever was calibrated to obtain the actual sensitivity and spring constant. Regions with 5 µm × 5 µm area were scanned with a rate of 0.5 Hz. For each area, 64 force-distance curves (8×8 array) were acquired, and three different areas were scanned. The force versus indentation curves were analyzed using the Hertz model with the Poisson's ratio taken as 0.3.

Coatings applied on alginate and gelatin films were tested with uniaxial tension tests on a dual column universal testing machine Instron 3365 (Instron, Norwood, MA, USA) as composites (coating and substrate). Namely, pure alginate film, PC 10A, pure gelatin film and PC10G were cut in dog bone specimens (ten samples tested for statistical analysis) with a width of 4 mm and length of 25 mm. They were conditioned at 24 °C and 50 % R.H. in an Espec SH-262 Environmental Chamber (ESPEC, Hudsonville, MI, USA). Displacement was applied at a rate of 3 mm/min. The Young's modulus, stress at maximum load, and elongation at break were calculated from the stress–strain curves.

2.3.11. Water contact angle

Static water contact angles of PC 0, PC 10, pure alginate film, PC 0A, PC 10A, pure gelatin film, PC 0G, and PC 10G were measured by using a contact angle goniometer OCA-20 (DataPhysics Instruments GmbH, Filderstadt, Germany) at room temperature. Deionized water droplets of 3 µL were deposited on the surface and the contact angle was calculated from the side view with the help of the built in software. Six measurements for each coating were taken to ensure repeatability.

2.3.12. Water vapor permeability measurement

The water vapour permeability (WVP) of pure alginate film, PC 0A, PC 10A, pure gelatin film, PC 0G and PC 10G was evaluated under 100 % relative humidity gradient ΔRH (%) by following the ASTM E96 standard method. In detail, 400 µL of deionized water were placed in the permeation chambers (Inner diameter = 7 mm; height = 10 mm) to generate 100 % R.H.. Samples were mounted on the top of the permeation chamber, sealed and placed at 0 % R.H. by using anhydrous silica gel. The chambers were weighted every hour for 7 consecutive hours by using a sensitive electronic balance (0.0001 g of accuracy) to monitor the transfer of water from the chamber to the desiccant, through the sample, evaluating the water mass loss, which was plotted as a function of time. The slope of each line was calculated by linear regression. Afterwards, the water vapor transmission rate (WVTR) was determined by using the following equation:

$$WVTR(g(m^2d)^{-1}) = \frac{slope}{A}$$

where A is the area of the sample.

The water vapor permeability (WVP) of the samples was calculated by using the following equation:

$$WVP\ (g(mdPa)^{-1}) = \frac{WVTR \times L \times 100}{p_s \times \Delta RH}$$

where L is the thickness of the sample (m), p_s is the saturation water vapor pressure at 25 °C (Pa). Each measurement was replicated four times to ensure reliability of the results.

2.3.13. DPPH and ABTS radical scavenging assays

DPPH (2,2-diphenyl-1-picrylhydrazyl) radical scavenging assay (RSA) was performed with PC 10 samples (2 cm x 2 cm) that were placed in a 6-well plate in a standing position. 12 mL/well of 0.2 mM solution of DPPH˙ radical molecule in ethanol were added. Samples were covered with aluminum and kept in darkness. 3 mL of extract was taken at specific time points (0, 0.25, 0.5, 1, 2, 3, 4, 6, 24 hours), placed in a polystyrene cuvette and its light absorbance was measured at 517 nm by using a Cary 6000i Scan UV-Visible spectrophotometer (Walnut Creek, CA, USA), in dark condition and at room temperature. Separately, PC 0 (2 cm x 2 cm) sample was immersed in 12 mL of DPPH˙ radical ethanol solution to control if pure PVAc-VL had any antioxidant activity.

ABTS (2,2'-azino-bis(e-ethylbenzothiazoline-6-sulphonic acid) radical scavenging assay (RSA) was performed in the same conditions previously described.

The percentage RSA was calculated by using the following formula:

$$RSA\ (\%) = \left[\frac{A_{control} - A_{sample}}{A_{control}}\right] * 100$$

where $A_{control}$ is the absorption of the control PC 0 sample and A_{sample} is the absorption of the PC 10 sample at the specific time point.

2.3.14. Release tests in food simulants, water and acidic environment

The release of curcumin from PC 10 samples in 3% (v/v) acetic acid, 10%, 50% and 95% ethanol-water solutions was measured to simulate aqueous foods (10 vol.% ethanol), oil-in-water emulsions (50 vol.% ethanol) and fatty foods (95 vol.% ethanol), respectively [96, 97]. Measurements were made by using a Cary 6000i Scan UV-Visible spectrophotometer (Walnut Creek, CA, USA). Curcumin had a characteristic UV absorbance peak at 428 nm in 3% acetic acid, 10%, 50% and 95% ethanol solutions, whereas presented a peak at 416 nm in water. Calibration curves of curcumin were constructed, to extrapolate the molar extinction coefficient (ε), which resulted in $\varepsilon = 2,653\ cm^{-1}M^{-1}$ for 3% acetic acid, $\varepsilon = 2,546\ cm^{-1}M^{-1}$ for water, $\varepsilon = 18,951\ cm^{-1}M^{-1}$ for 10% ethanol solution, $\varepsilon = 59,933\ cm^{-1}M^{-1}$ for 50% ethanol solution and $\varepsilon = 69,702\ cm^{-1}M^{-1}$ for 95% ethanol solution. PC 10 samples (2 cm $\times$ 2 cm) were placed in a 6-wells plate and immersed in 4 mL of mediums at room temperature. 3 mL of extract was taken at specific time points (0, 0.25, 0.5, 1, 2, 3, 4, 6, 24, and 48 hours), and the measurements were carried out. At each time point, 3 mL of respective solution was added to the sample. Six samples for each liquid were analyzed.

2.3.15. Bacterial adhesion study

The bacterial anti-adhesion property of PC 0, PC 10, and uncoated glass (control) was evaluated by using *Escherichia coli* (*E. coli*) (ATCC 25922) and *Staphylococcus aureus* (*S. aureus*) (8325-4). A single colony of *E. coli* or *S. aureus* was inoculated in Luria-Bertani (LB) broth medium (25 ml) and incubated at 37 °C overnight (o.n.) with shaking at 200 rpm. 1 mL of *E. coli* or *S. aureus* o.n. culture, approximately 10^9 CFU/mL, was centrifuged and suspended in 100 µL of LB. 10 µL of *E. coli or S. aureus* suspension was gently placed, under sterile conditions, onto the PC 0, PC 10, and uncoated glass, previously sterilized by UV irradiation for 30 minutes. To allow the bacterial adhesion on the material surface, the samples were left to dry for 90 minutes at room temperature. Afterwards, the bacteria were stained with 0.3 % crystal violet (CV) (Merk, Germany) for 15 minutes to understand if the bacteria adhered to the surface of the samples, following the method previously described with slight modifications

[98, 99]. To remove unattached or weakly adherent bacteria, the stained samples were carefully rinsed in sterile distilled water (SDW). Then, the uncoated glass, PC 0 and PC 10 were immersed in 25 mL of LB broth and incubated at 37 °C with shaking at 200 rpm. 1 mL of each sample was removed after 1, 2, 3, 4, 5 hours, and the absorbance of the solutions was estimated using a UV−Vis spectrometer at 590 nm (OD_{590}).

To determine the percentage of the adhered bacteria to the samples, the same amount of *E. coli* and *S. aureus* were spotted on PC 0, PC 10, and uncoated glass. The samples were left to dry for 90 minutes at room temperature. After rinsing with SDW, the adhered bacteria were harvested by detaching with 1 mL of SDW. 10 µl of the *E. coli* or *S. aureus* original suspension was added to 1 mL of SDW and used as control. The absorbance of the bacteria solution was measured at 590 nm (OD_{590}). The percentage of adhered bacteria was calculated respect to the control. The results are presented as mean ± the standard error of the mean (SEM). The significance of the differences in the mean values of groups was evaluated using the analysis of variance (one-way ANOVA). Results with a p-value <0.05 were considered statistically significant.

2.3.16. Biocompatibility study

2.3.16.1. Cell culture

Chinese Hamster Ovarian (CHO) cells (ATCCs, UK) were cultured in Dulbecco's modified Eagle medium (DMEM, Euroclone) 10% fetal bovine serum inactivated, and 1% penicillin streptomycin in a humidified incubator at 37°C and 5% CO_2. All reagents were products of ThermoFisher. CHO cells were seeded in DMEM at a density of 2×10^4 cells ml^{-1} and let to grow until they were confluent. Cells were then treated with trypsin-EDTA, detached, and centrifuged (1000 rpm, 5 min); the cell pellet was re-suspended in DMEM, and the cell density was precisely determined with an automated cell counter. Further, the cell density was precisely adjusted to 400 cell μl^{-1} to conduct the indirect biocompatibility test.

2.3.16.2. Cell proliferation assay

Prior to conduct the test, PC 0 and PC 10 were sterilized under UV for 30 minutes, then rinsed with sterile water, and submerged in DMEM culture medium for 48 hours. The proliferation assay was performed with an xCELLigence device (ACEA Biosciences) equipped with E-plate 16. The xCELLigence device allows the real-time monitoring of cell viability based on electrical impedance read out. For each condition (i.e., DMEM conditioned with PC 0, DMEM conditioned with PC 10, and normal DMEM) 4 different wells were used. Each of the 4 wells was filled with 150 µL of DMEM (either conditioned or not). After a background

measurement, 50 µL of CHO cell suspension in DMEM was added to each well in order to plate $2x10^3$ cells/wells. The proliferation assay was run for 50 hours in the incubator. Sampling of the cell proliferation was done every 15 minutes by reading out the impedance of the electrodes and converting it to a dimensionless parameter, named Cell Index (C.I.), proportional to the electrode area covered by the cells [100]. The C.I. matrix was then processed by IgorPro (Wavemetrics). At the end of the experiment, the cells were inspected by fluorescence microscopy. For fluorescence imaging, CHO cells plated on glass coverslips in the identical conditions were fixed using 4% (w/v) Paraformaldehyde (PFA, SCBiotechnology,USA) in 1X Phosphate Buffer Saline (PBS). The cells were washed once with pre-warmed PBS, pH 7.4, and fixed using 4% PFA for 10 min at room temperature. The fixed cells were first permeabilized with 0.1% Triton X-100 in PBS for 3 to 5 minutes and then incubated for 10 min in 1% w/v bovine serum albumin (BSA) in PBS to reduce nonspecific background. For selective F-actin staining, the cells were stained with Alexa Fluor-647 phalloidin (life Technologies, USA) diluted in PBS 1X and placed at room temperature for 20 min. The nuclei were stained with Hoechst 33342 (ThermoFisher Scientific). The confocal analysis was finally carried out using a Nikon Inverted Microscope TiE equipped with a Nikon Confocal Laser System (Nikon Optical Co., Ltd., Japan) at an excitation wavelength $\lambda_{ex} = 405$ nm, and $\lambda_{ex} = 647$ nm.

2.4. Results and discussion

2.4.1. *Morphology of the coatings*

The microstructure of the coatings PC 100, PC 0 and PC 10 was investigated by SEM. Images of the surface and of the cross section are reported in Figure 5. In Figure 5A PC 100 surface showed a relatively compact coating as a further demonstration of the complete dissolution of curcumin in the selected solvent. However, its cross-section (Figure 5D) revealed a somewhat porous internal structure that could be attributed or to the sub-microscopic particles of curcumin or to some cutting effects (e.g. glass fibers after the breaking of the sample). On the other hand, PC 0 presented both a uniform surface without visible separation between VAc and VL segments (Figure 5B) and a uniform cross section (Figure 5E). Similarly, the coating PC 10 showed a uniform and smooth surface (Figure 5C) and cross section (Figure 5D), revealing a good encapsulation of curcumin in the polymeric matrix. In addition, the cross section images of PC 0 and PC 10 gave information about the coatings' thickness of about 8-10 µm.
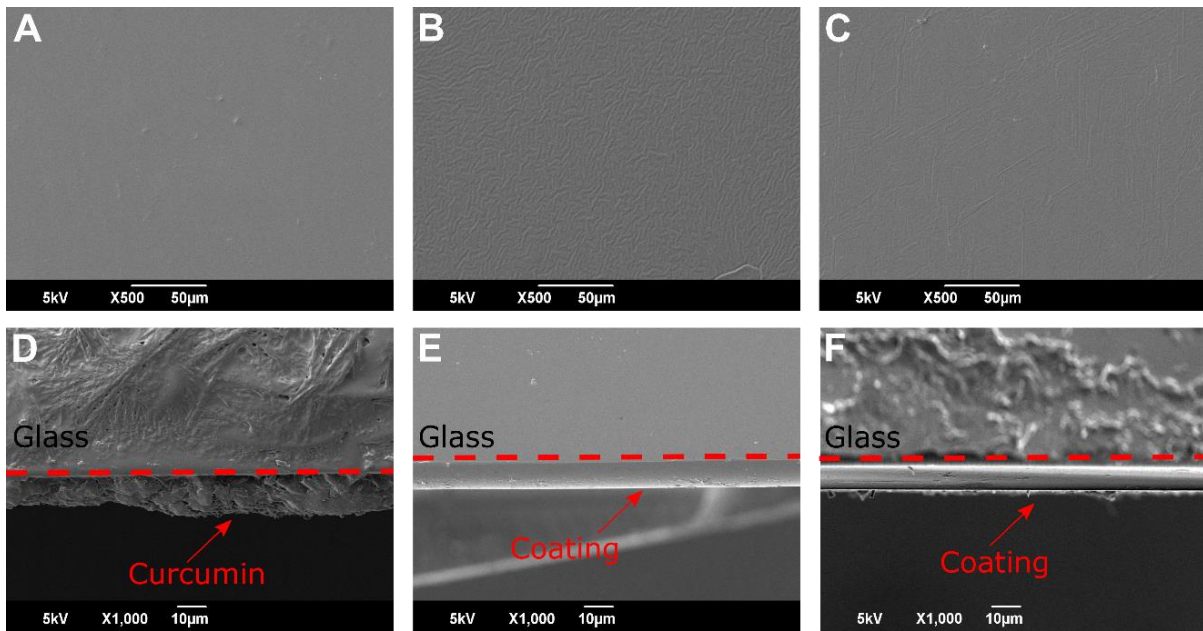
Figure 5. (A-C) SEM images of the surface of PC 100, PC 0 and PC 10 coatings. (D-F) SEM images of the cross section of PC 100, P C 0 and PC 10.

Further surface analysis of PC 100, PC 0 and PC 10 were conducted by AFM (Figure 6). The scanned area of PC 100 (Figure 6A and Figure 6D) confirmed the results obtained by SEM, showing the sub-microscopic particulate nature of the curcumin coating. Furthermore, the analysis of the topography conducted by Gwiddion gave information about the surface roughness (Ra) of nearly 0.6 nm and root mean square (RMS) of nearly 1 nm, indicating a high variability in the peak-valley distribution. On the other hand, PC 0 (Figure 6B and Figure 6E) showed a smoother topography without microscale surface rugosity formation after the coating and drying process as confirmed by the lower Ra (~ 0.1 nm) and RMS (~ 0.1 nm). Similar results were obtained on the PC 10 coating, with roughness parameters comparable to PC 0's ones, confirming again a good encapsulation of the filler curcumin into the polymeric matrix.
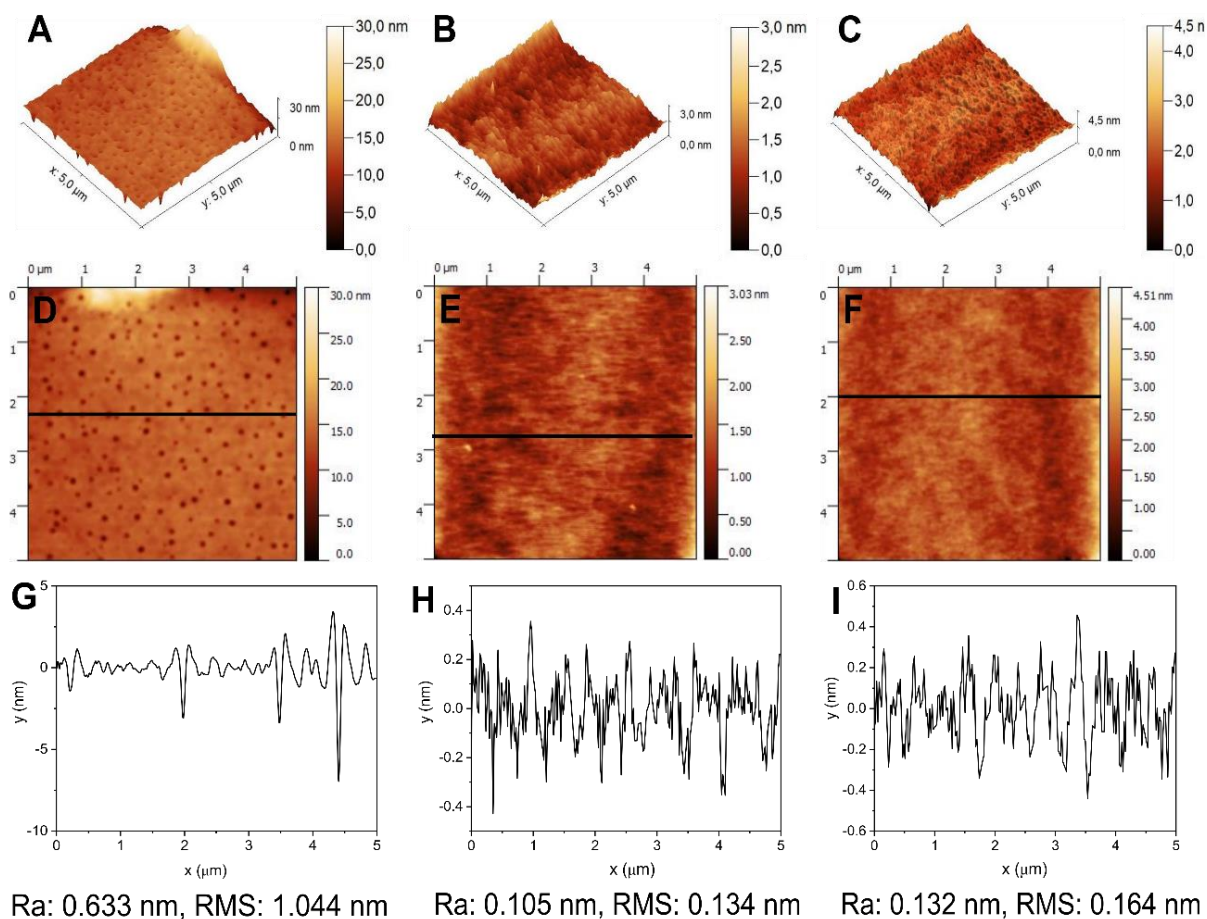
Figure 6. (A-C) AFM topography (3D view) of PC 100, PC 0 and PC 10. (D-F) AFM topography (2D view) with a random cross section (black line) of PC 100, PC 0 and PC 10. (G-I) Roughness graph, Roughness average (R_a) and Root Mean Square (RMS) parameters of PC 100, PC 0 and PC 10.

Additionally, the microscale morphology of alginate and gelatin films without and with PC 10 coating on them was inspected by SEM. Figure 7 shows the pictures and SEM images, both of the surface and cross section, of the uncoated (Figure 7A-C) and coated (Figure 7D-F) alginate film. From the photographs it can be immediately noticed that the application of the coating, a part from a change in color, did not affect the transparency of the film. From the comparison between the Figure 7B and Figure 7E, it can be noticed that the uncoated alginate film microstructure featured a rough surface that changed in a smoother, more homogeneous and pores-free one due to the application of the coating, revealing a pattern similar to the PC 10 one observed previously (Figure 5C). In addition, the estimated thickness of the PC 10 was also confirmed by the SEM image of the cross section of the PC 10A (Figure 7F), resulting to be around 5-8 μm. Furthermore, it can be observed that the coating adhered well to the natural film, without showing defects ad cracks.
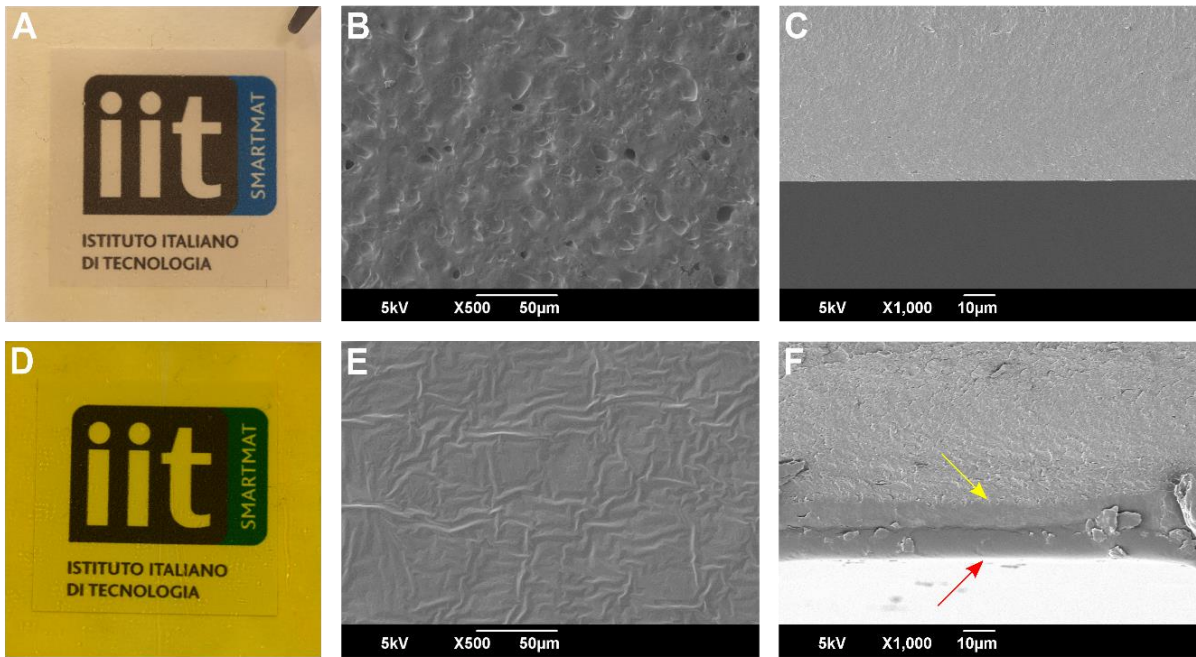
24

Figure 7. (A) Photograph and SEM images of the (B) surface and (C) cross section of the uncoated alginate film. (D) Photograph and SEM images of the (E) surface and (F) cross section of the PC 10A sample.

Similar results were obtained by the photographs and SEM images, both of the surface and cross section, of the uncoated (Figure 8A-C) and coated (Figure 8D-F) gelatin film. From the photographs a good degree of optical transparency was demonstrated. In addition, the surface of the gelatin film (Figure 8B) appeared smoother respect to the alginate's one, but the PC 10G's surface (Figure 8E) revealed the same pattern as for PC 10A and PC 10, previously observed. The cross section image of PC 10G (Figure 8F) confirmed the coating thickness of about 5-8 μm and a good adhesion to the substrate.
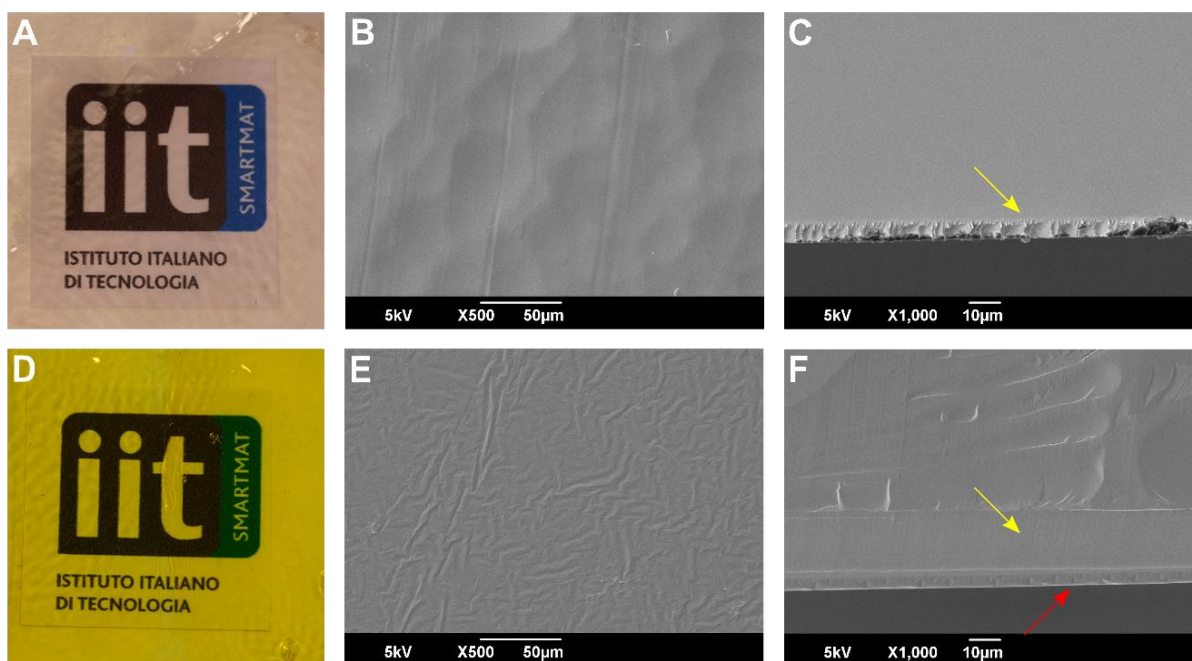
Figure 8. (A) Photograph and SEM images of the (B) surface and (C) cross section of the uncoated gelatin film. (D) Photograph and SEM images of the (E) surface and (F) cross section of the PC 10G sample.

Therefore, the coating was demonstrated to be homogeneous with an excellent encapsulation of the filler curcumin into the PVAc-VL polymeric matrix, demonstrated both by the picture of the samples where it was visible that the yellow color due to the curcumin was homogeneously distributed, as it will be discussed in the study of yellowness of the samples (Section 2.4.3), and then by the SEM and AFM images. In addition, it can be concluded that the coating adhered well not only on glass but also on natural substrates, as demonstrated by the cross section images, where any delamination or breaking of the coating was observed, with an average thickness of 8 μm.

2.4.2. *Optical features*

In this section, the optical features of the various coatings were investigated in terms of absorption, transparency and UV-filtering ability.

The UV-Vis absorption spectra of the coatings PC 100 and PC 10 on quartz slides with their photographs are reported in Figure 9A and Figure 9B, respectively. For the PC 100 coating, the intense absorption band of curcumin at 431 nm was ascribed to a combination of $\pi \rightarrow \pi^*$ and n $\rightarrow$ n* transitions, and a weaker band at 267 nm was due to $\pi \rightarrow \pi^*$ transitions [101]. On the other hand, in PC 10 the two curcumin-related absorption peaks shifted to 421 nm and 264 nm due to the presence of the copolymer in the formulation.
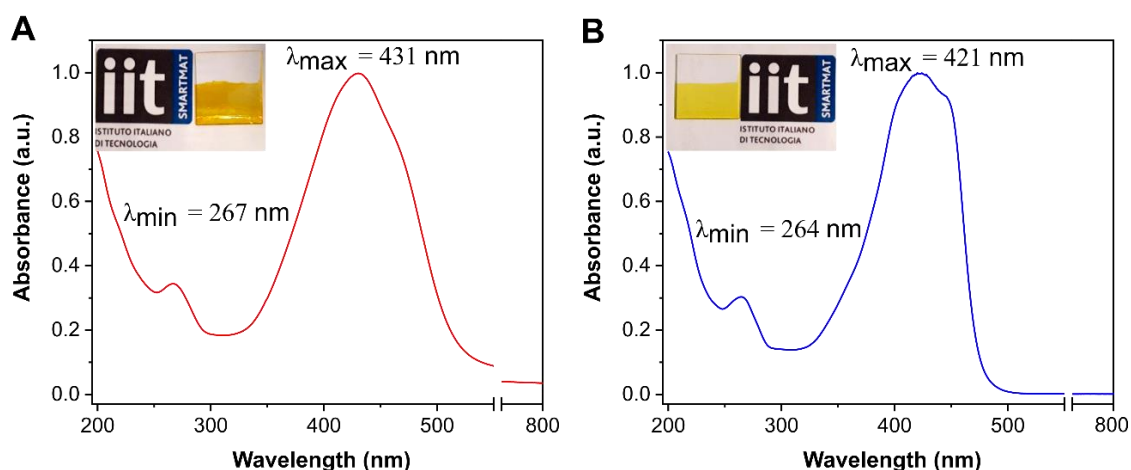
Figure 9. UV-Vis absorption spectra and photographs of (A) PC 100 and (B) PC 10.

Afterwards, the transparency of the coating was evaluated because it was considered an important feature in order to allow the consumer to look through the packaging, evaluating the freshness and the quality of the packaged food. Results were showed in Figure 10. In particular, the photographs of PC 0 and PC 10 coatings on quartz attached on Figure 10A demonstrate their transparency to the naked eye. In addition, a further investigation of this property was done on PC 0, PC 1.25, PC 2.5, PC 5, PC 7.5, and PC 10 coatings by evaluating the percent transmittance (%T) from 400 to 800 nm as visible range (Figure 10A). The spectra indicated that the coatings, whatever the amount of curcumin, were transparent in all the visible range, obtaining same results as for PC 0. In particular, the percent transmittance at 660 nm (%T_{660}) was took in consideration to evaluate the transparency. Values were practically 100 % for all the samples. The transparency of the coatings was also evaluated in terms of percent opacity in the visible (600 nm) (Figure 10B). As can be noticed, the PC 0 sample had the lowest opacity but also all the curcumin coatings' opacity did not exceed 5%.
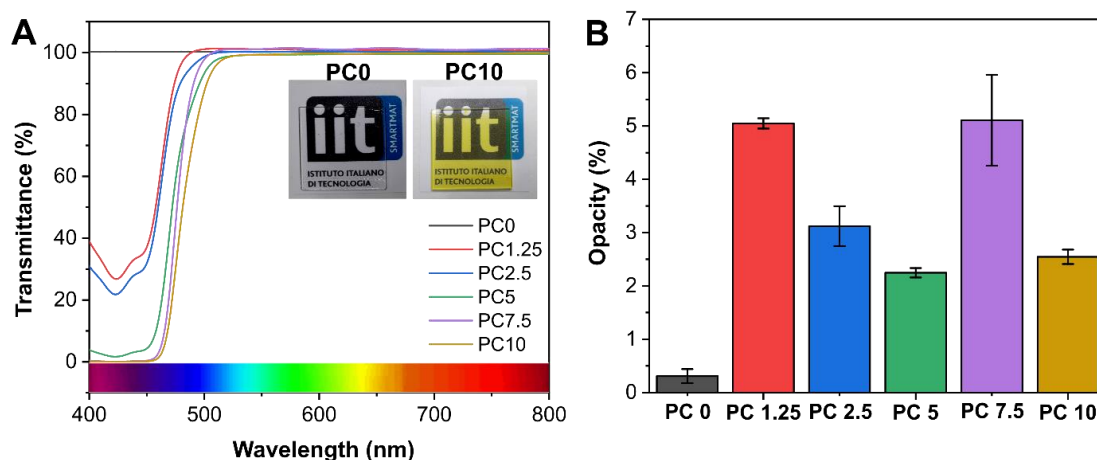

Figure 10. (A) Light transmittance (%T) of PC 0, PC 1.25, PC 2.5, PC 5, PC 7.5, and PC 10 coatings in the range 400-800 nm (visible range), with attached photographs of PC 0 and PC 10. (B) Percent opacity (%) of PC 0, PC 1.25, PC 2.5, PC 5, PC 7.5, and PC 10 coatings.

The protection from UV light conferred by the coating was evaluated, first of all because it was expected that the curcumin gave this property as previously reported for curcumin-based composites [86], and then because it was considered important that the coating protected the packaged food from the deterioration of the UV light during transportation and storage. For this reason, the UV-filtering ability of PC 0, PC 1.25, PC 2.5, PC 5, PC 7.5, and PC 10 was evaluated (Figure 11). The %T of all the coatings in the range between 200 nm and 450 nm are showed in Figure 11A. Between UVC and UVB bands, the %T increased for all the coatings as the wavelength increased. In particular, at the start of the UVC range, the coatings PC 1.25 and PC 2.5 showed lower %T values respect to PC 0 of about 20% and 30%, respectively, indicating a slight UV barrier effect. On the other hand, they presented much higher %T values compared to the others indicating insufficient curcumin concentration levels for proper filtering. PC 10 had a minimal increase with a maximum of about 30%. Generally, between UVB and UVA (UVA1) region, the %T decreased for all the coatings except for PC 0. More specifically, in the UVB region no significant changes in %T were observed for all the samples. The UVA range is classified as UVA2 (320-340 nm) and UVA1 (340-400 nm). In the UVA2 region, the %T of PC 10 ranged from 30 to 16%, whereas in the UVA1 region it further declined from 16% and finally to 0% due to high levels of curcumin dispersed in the polymeric matrix [102, 103]. The promising effect observed in the UVA region has been as good as other polymer nanocomposites that contain ZnO or TiO_2 nanoparticles [104]. Furthermore, the UV filtering ability was evaluated in terms of percent transmittance at 280 nm (%T280). Values were plotted in Figure 11B as a function of curcumin concentration. As expected, the higher the concentration of curcumin the lower the $\%T_{280}$. As previously demonstrated by Roy et al. [86], the T_{280} decreased exponentially with increasing the amount of curcumin in the coating in the way:

$$T_{280} = 98.98e^{-0.15x} \ (R^2 = 0.999)$$

where x is the concentration of curcumin (%), even if different results in terms of UV filtering ability depend on the amount of curcumin in the final system.

Therefore, PC 10 demonstrated superior filtering performance compared to all the other coatings.
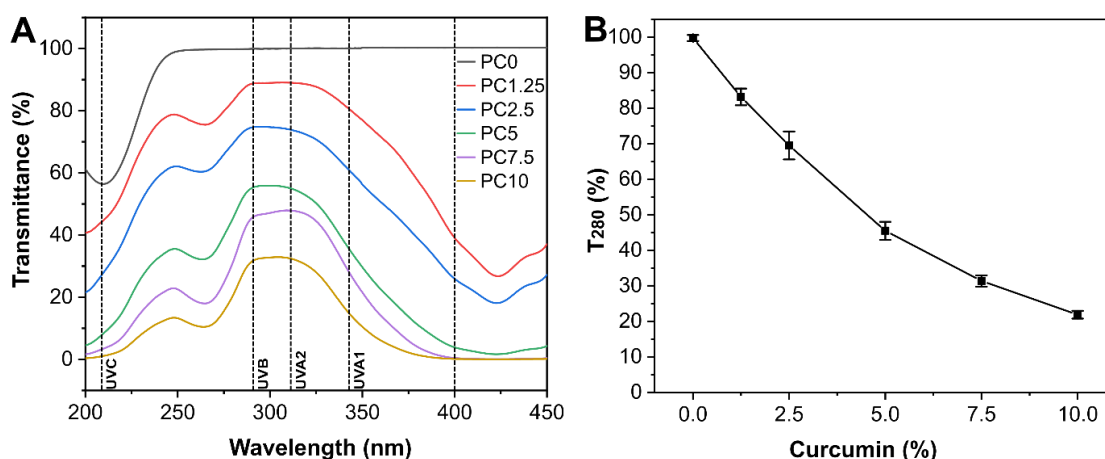
Figure 11. (A) Light transmittance (%T) of PC 0, PC 1.25, PC 2.5, PC 5, PC 7.5, and PC 10 coatings in the range 200-450 nm (UV range). (B) Percent transmittance values at 280 nm (%T_{280}) vs curcumin concentration.

In conclusion, PC 10 coating was demonstrated both to be transparent and to have UV filtering ability. Therefore, the curcumin did not affect the transparency but on the other hand maintained its functionality even if it was encapsulated into the polymeric matrix.

2.4.3. Yellowness and whiteness index

CIELAB color space presents three coordinates: *L* is the lightness of the color in a range 0-100, where 0 is black and 100 is white, *a* represents the redness/greenness, where negative values indicate green while positive red, *b* represents the yellowness/blueness, where negative values indicate blue while positive yellow.

For this study, these values were considered and reported in Table 2 for PC 10, alginate film, PC 10A, gelatin film, and PC 10G. As expected, both PC 10, PC 10A and PC 10G presented similar negative *a* values, therefore in green region that is closer to yellow, and positive *b*, therefore in yellow region. However, *b* values were not similar due to the different substrate that influenced the yellowness of the final coated sample. Furthermore, both alginate and gelatin films presented positive *b* value, which was uniformed by the presence of the curcumin coating.

As confirmation of these observations, both the increasing of YI and the decreasing of WI were observed in PC 10A and PC 10G respect to their uncoated controls. Again, the YI of PC 10A and PC 10G was observed to be higher than the control PC 10, since the natural films had a certain degree of inherent yellowness, as previously stated and as can be noticed in Figure 7A and Figure 8A for alginate and gelatin, respectively. In particular, alginate appeared brownish while gelatin more transparent with YI comparable to values observed for other transparent films, also in presence of curcumin [86].

In conclusion, a part from some differences in the values that could be attributed also to the quality of the camera and/or to the different exposures to the lights, this analysis confirmed that the coating PC 10 did not change its color features once applied on various substrate. In addition, the statistical analysis revealed that, whatever the substrate, the yellow color and, therefore, the curcumin, was homogeneously distributed into the polymeric matrix, confirming the versatility of the developed coating for food packaging, since it could be expected that the release of the antioxidant active agent was beneficial for all the packaged food.

Sample	L	a	b	YI	WI
PC 10	61.60 ± 0.57	-5.28 ± 0.68	46.34 ± 1.67	107.48 ± 4.12	-77.42 ± 5.09
Alginate	56.46 ± 1.62	4.20 ± 0.20	9.02 ± 0.84	22.89 ± 2.76	29.40 ± 4.08
PC 10A	62.86 ± 3.51	-6.12 ± 0.45	61.20 ± 2.62	139.20 ± 2.09	-120.74 ± 4.43
Gelatin	64.32 ± 0.84	5.68 ± 0.23	4.80 ± 0.42	10.66 ± 0.93	49.92 ± 1.47
PC 10G	61.80 ± 1.78	-6.00 ± 0.76	54.86 ± 1.69	126.82 ± 1.82	-102.78 ± 3.58

Table 2. Surface color values of PC 10, alginate film, PC 10A, gelatin film, and PC 10G. The values presented as mean ± standard deviation.

2.4.4. Chemical characterization

First of all, the IR spectrum of PVAc-VL copolymer (red) was compared with the IR spectrum of PVAc (black) (Figure 12A). The pure PVAc spectrum showed the typical band of the molecule: C=O stretching vibration at 1728 cm^{-1}, associated to the acetate groups of the polymer, CH$_3$ asymmetric and symmetric bending vibrations at 1433 and 1370 cm^{-1}, respectively, C-O asymmetric stretching vibration at 1233 cm^{-1}, C-C stretching vibration at 1016 and 942 cm^{-1}, and C-H rocking vibration at 795 and 631 cm^{-1} [105]. The PVAc-VL spectrum presented: C-H asymmetric and symmetric stretching vibrations at 2920 and 2853 cm^{-1}, C=O stretching vibration at 1732 cm^{-1}, CH$_2$ vibration at 1463 cm^{-1}, CH$_3$ asymmetric and symmetric bending vibration at 1433 and 1370 cm^{-1}, C-O asymmetric stretching vibration at 1228 cm^{-1}, C-O stretching vibration at 1171 and 1111 cm^{-1}, C-C stretching vibration at 1019 and 944 cm^{-1}, and C-H rocking vibration at 797, 720 and 630 cm^{-1}. Peaks at 2920 and 2853 cm^{-1} are the most evident contribution of vinyl-laurate to the copolymer (blue). In addition, the

appearance of a shoulder at 1463 and 1171 cm^{-1}, as well as, of a new peak at 720 were attributed to the vinyl-laurate [63].

Afterwards, the FTIR spectra of PVAc-VL and the coatings PC 0, PC 10, and curcumin powder were acquired (Figure 12B). PC 0 coating presented the same peaks as for the copolymer PVAc-VL as a confirmation of the fact that there is not delamination of the copolymer after the dissolution in the solvent, as previously observed by morphological investigation of the surface of this polymeric coating. Similarly, in the PC 10 spectrum is clearly visible the contribution of the polymeric part in all the peaks previously assigned for PVAc-VL. However, new peaks were individuated and assigned: C=C and C=O stretching vibration at 1628 cm^{-1}, C=C stretching vibration a 1600 cm^{-1}, C=O stretching vibration, C-C-C and C-C=O bending vibration at 1513 cm^{-1}. The spectrum of the curcumin powder allowed to understand if these peaks were due to the presence of curcumin as filler in the composite coating. The spectrum of curcumin showed the typical bands such as C=C and C=O stretching vibration of the inter-ring chain at 1625 cm^{-1}, C=C stretching vibration of aromatic rings at 1600 cm^{-1}, C=O stretching vibration, C-C-C and C-C=O bending vibration at 1506 cm^{-1}, C-C-C, C-C-H and C-O-H bending vibration of aromatic rings connected with "enolic" part at 1425 cm^{-1}, C-C-C, C-C-H bending vibration of aromatic "keto" part and C-O-H bending vibration of "keto" part at 1278 cm^{-1}, C-O-H bending vibration connected to aromatic rings and of "enolic" form at 1230 cm^{-1}, C-C-H bending vibration at 1203 cm^{-1}, C-O-C bending vibration at 1180 cm^{-1}, C-C-H bending vibration of aromatic rings and C-C-H bending vibration of inter-ring chain at 1149 cm^{-1}, O-CH$_3$ stretching vibration and C-C-H bending vibration of aromatic ring connected to "enolic" part at 1111 cm^{-1}, C-O-C stretching vibration and C-C-H bending vibration of aromatic ring connected with "enolic" part at 1022 cm^{-1}, C^{12}O stretching vibration and C^{12}OH bending vibration at 959 cm^{-1}, C-C-H out of plane bending vibration of aromatic ring connected with "enolic" part of the molecule at 881 cm^{-1}, C-C-H out of plane bending vibration of aromatic rings and inter-chain ring at 853 cm^{-1}, C-C-H out of plane bending vibration aromatic ring connected with "keto" part of the molecule at 808 cm^{-1} [106]. Therefore, from this analysis, it was possible to understand that the peaks at 1628, 1600 and 1513 cm^{-1} were the most evident contribution of the curcumin in PC 10.

To understand if there was in interaction between curcumin and PVAc-VL in PC 10 formulation, both the spectrum of PC 0 was subtracted from the spectrum of PC 10, and Raman spectroscopy was used. The results are reported in Figure 13. In particular, in Figure 13A the comparison between PC 10-PC 0 and curcumin is reported. As can be noticed, in the subtracted spectrum a peak at 1713 cm^{-1} was visible differently from the curcumin spectrum. This peak

was assigned to C=O stretching vibration, characteristic of the "diketo" form of the curcumin molecule. On the other hand, the peaks at 1230 cm^{-1} and 882 cm^{-1} were visible in the curcumin spectrum but not in the PC 10-PC 0 spectrum. They were assigned to C-O-H bending vibration and to C-C-H out of-plane bending vibration of the "enolic" part of the molecule, respectively [107]. Therefore, the curcumin molecule changed, partially, from the "enolic" to the "diketo" form (Figure 13C), due to its interactions with PVAc-VL that are mostly hydrophobic-hydrophobic interactions.
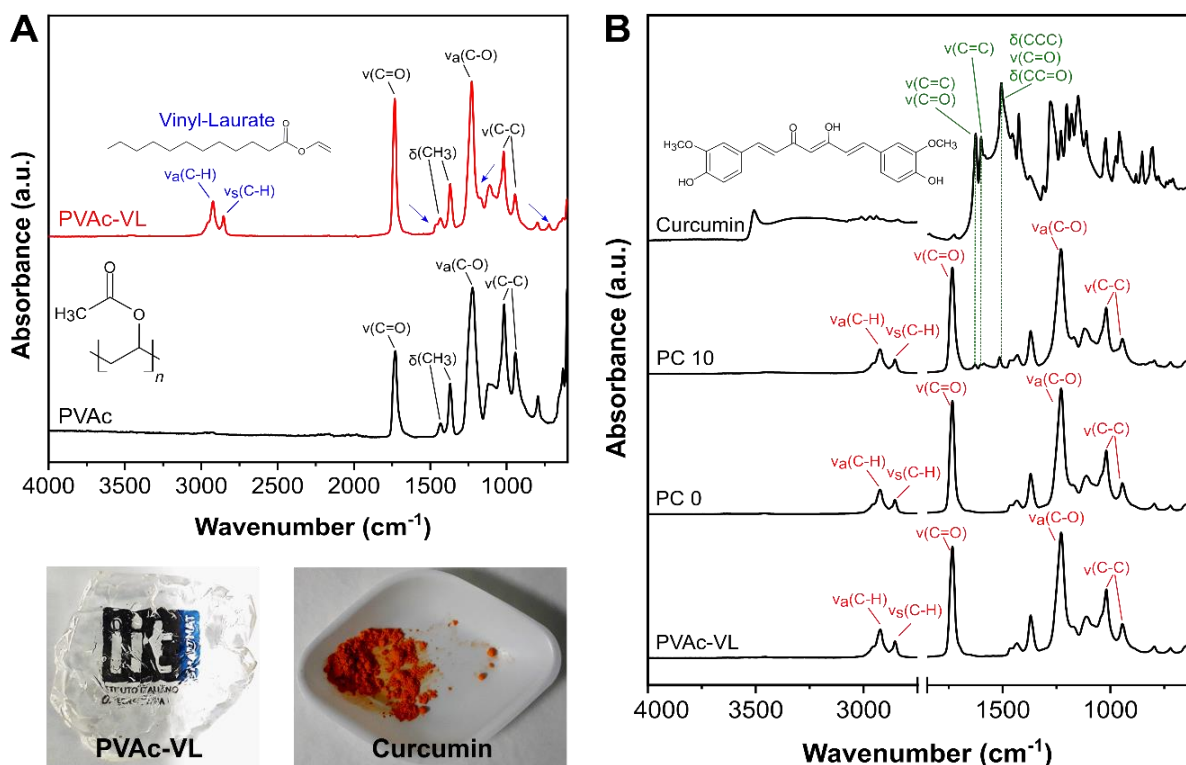

Figure 12. (A) ATR-FTIR spectra of (from the bottom) PVAc and PVAc-VL copolymer. The assignments relative to VL are reported in blue. (B) ATR-FTIR spectra of (from the bottom) PVAc-VL copolymer, PC 0, PC 10, and curcumin powder. The assignments relative to PVAc-VL are reported in red, whereas the assignments of the peaks in PC 10 due to curcumin are reported in green.

To provide additional information about the molecular interactions between curcumin and PVAc-VL, Raman spectroscopy was used. Figure 13B shows the Raman spectra of curcumin, PC 10 and PC 0. The spectrum of PC 0 showed: C=O stretching vibration at 1739 cm^{-1}, CH$_2$ bending vibration at 1444 cm^{-1}, CH$_3$ bending vibration at 1365 cm^{-1}, C-C stretching vibration at 1305 cm^{-1} and C-O-C stretching vibration at 1126 cm^{-1}. On the other hand, the spectrum of curcumin shows: C=C and C=O stretching vibration of the aromatic ring and ketone group, respectively, at 1627 cm^{-1}, C=C stretching vibration of the aromatic ring at 1600 cm^{-1}, and C-C-H bending vibration of aromatic rings and C-C-H bending vibration of inter-ring chain at 1150 cm^{-1}. As can be noticed, in the PC 10 spectra three changes were observed

respect to the controls: the peak at 1627 cm^{-1} in curcumin shifted to 1636 cm^{-1}, and its intensity increased. In addition, the intensity of the peak at 1600 cm^{-1} decreased, and the peak at 1150 cm^{-1} shifted to 1160 cm^{-1}. These changes indicated that there was an interaction between the inter-ring chain and the aromatic rings of the curcumin and PVAc-VL, due to the hydrophobic interactions [106, 107].
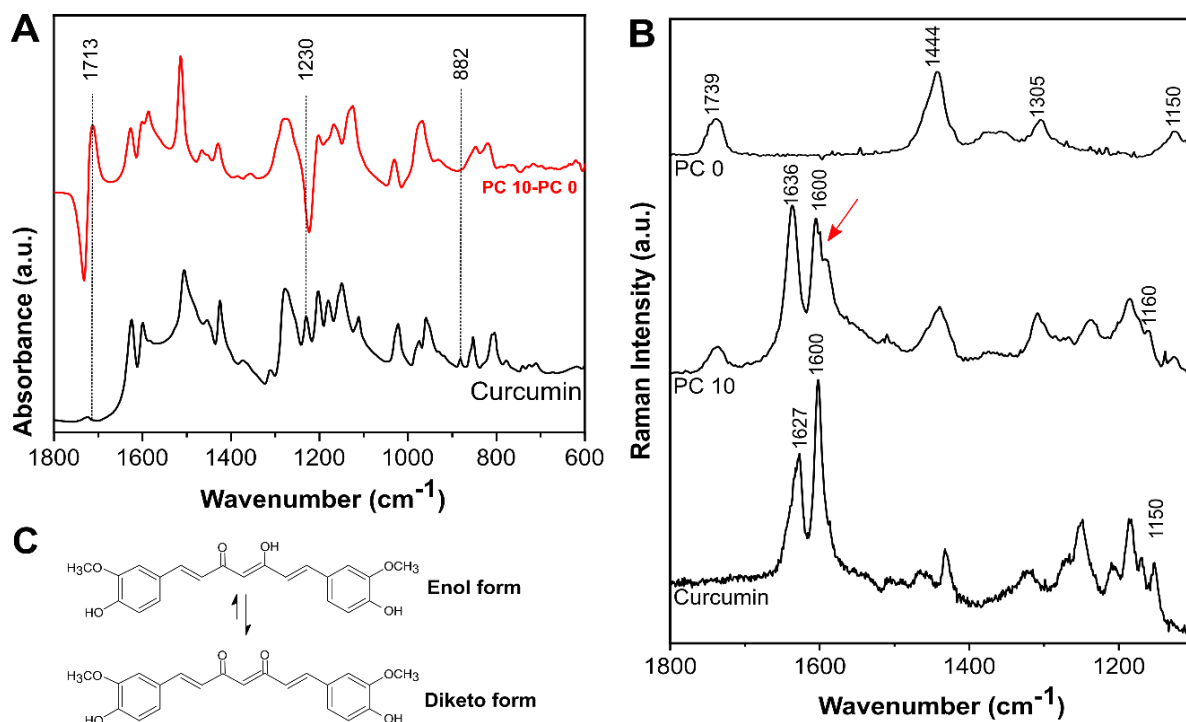

Figure 13. (A) ATR-FTIR spectra of curcumin and PC 10-PC 0 in the range 1800-600 cm^{-1}. (B) Raman spectra of (from the bottom) curcumin, PC 10 and PC 0. In PC 10, the red arrow highlights the decrease in the intensity of the peak at 1600 cm^{-1} due to curcumin-polymer interactions. (C) Schematic representation of the curcumin tautomerisms without PVAc-VL ("enol" form) and with PVAc-VL ("diketo" form).

Finally, Figure 14 shows FTIR spectra of pure alginate, PC 10A, pure gelatin and PC 10G. The spectrum of pure alginate presented the typical bands of the sodium alginate [108, 109], as well as pure gelatin [110]. The FTIR spectra of coated natural films, PC 10A and PC 10G, did not show any peaks of alginate and gelatin, respectively, but they presented PVAc-VL and curcumin' characteristic peaks, which have been previously described and discussed. These results suggested that the coatings were homogenous and they did not mix or dissolved in the natural polymers but rather remained as protective layers over the films or the substrates.
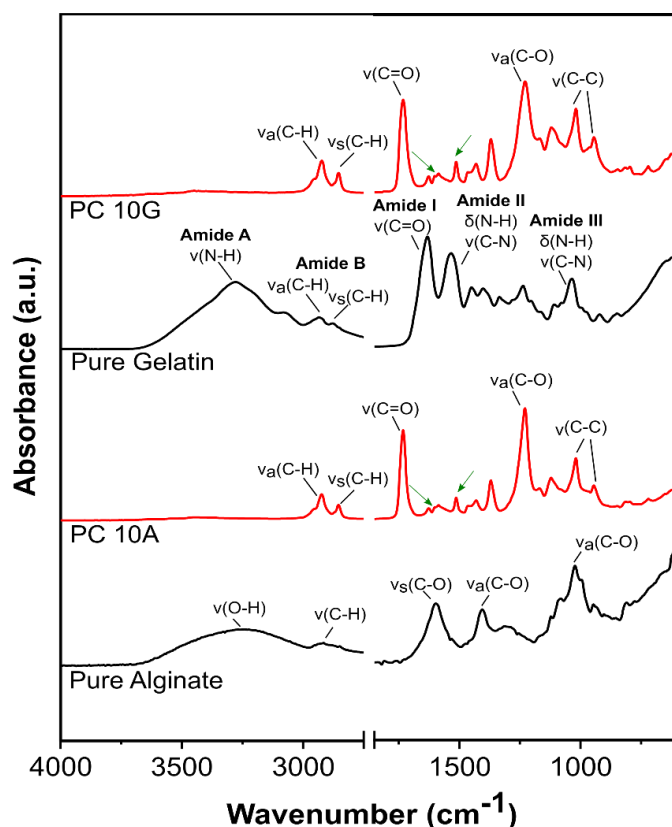
Figure 14. ATR-FTIR spectra of (from the bottom) pure alginate film, PC 10 A, pure gelatin film, and PC 10G. The green arrows highlight the peaks due to the curcumin's contribution.

2.4.5. *Mechanical characterization*

All the results relative to the mechanical properties of the coating are reported in Figure 15 and Figure 16. As a coating the strategies to evaluate them were: AFM nano-indentation technique to have a local value of the Young's Modulus and to understand if curcumin gave any mechanical contribution once encapsulated in the polymeric matrix, and the tension test on coated natural films to understand if the coating changed their mechanical features.

Young's Moduli of PC 0 and PC 10 coatings were measured locally by using AFM nano-indentation technique. All the details considered for the measurement, the Young's Modulus and the calculated error are reported in Table 3. In particular, the Poisson's ratio was 0.3 for both the samples and the sensitivities were comparable. In order to have statistically appreciable results, as many indentation measurements as possible had to be taken by scanning three different and randomly chosen areas of the two coatings. Each area was scanned as an 8×8 array, therefore for each of the 64 points the Young's Modulus was measured. The distribution of the measured Young's Modulus per each area is reported in Figure 15 for PC 0 (Figure 15A) and PC 10 (Figure 15B). Each area is coloured differently (black, red and blue), and each measurement is represented by one point. Per each area the average Young's Modulus

was calculated and reported in the graph. In Table 3 is reported the average of these averages. The Young's Modulus of PC 0 was ~ 3.1 MPa while the PC 10's one was ~ 4.2 MPa, therefore they were comparable indicating that the curcumin did not introduce extra hardness or stiffness to the polymer coating, confirming again both a good encapsulation of the filler into the polymeric matrix, and a defect-free surface as previously demonstrated from the AFM study. In addition, even if the percent error for PC 10 resulted to be higher than the PC 0's one probably due to the dispersion of curcumin, both of them were considered acceptable for this kind of coatings [111].

Sample	Poisson's ratio [v]	Sensitivity (nm/V)	Young's Modulus (MPa)	Error (%)
PC 0	0.3	22.4	4.28 ± 0.93	7
PC 10	0.3	23.8	3.14 ± 0.31	25

Table 3. Assumed details and obtained results for the AFM nanoindentation measurement for PC 0 and PC 10 coatings.
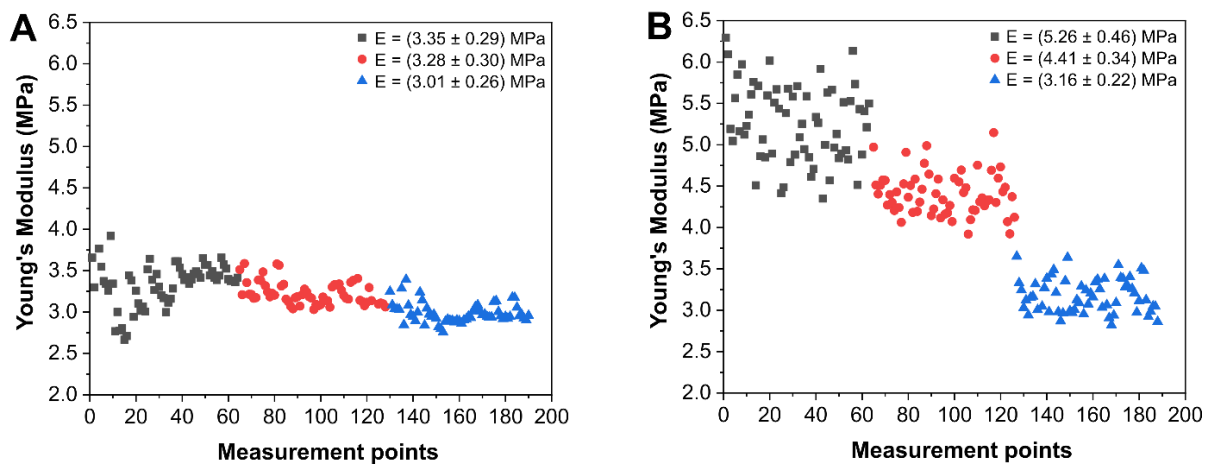

Figure 15. Young's Modulus distribution per each scanned area (black, red, and blue) of (A) PC 0 and (B) PC 10.

Applying a polymer coating could change the mechanical properties of the substrate in terms of flexibility and ductility, which in packaging are extremely important features, in order to protect the packaged food from possible breaking and/or spoilage during the transportation. For this reason, the mechanical properties, in terms of Young's Modulus (YM), Ultimate Tensile Strength (UTS) and Elongation at Break (EB), of the coating applied on alginate and gelatin films were investigated. Therefore, the analyzed samples were: alginate film, PC 10A, gelatin film, and PC 10G. Representative stress-strain curves, YM, UTS and EB of the samples are reported in Figure 16. First of all, UTS and EB of gelatin films resulted in the range reported

by Said et al. for gelatin from different types of fish species, 6.23 - 43.62 MPa, and 2.96 – 76.73 %, respectively, explaining higher values with higher contents of amino-acids [112]. For alginate, similar UTS and EB were obtained by Rhim with 33 MPa and 15 %, respectively [113]. Both results on control films demonstrated their accordance with already proposed natural films for food packaging applications. In addition, it was demonstrated that the coating did not change significantly (ANOVA, $p < 0.05$) the mechanical properties of the alginate film, while some changes were observed on gelatin films. In particular, PC 10G presented a decreasing of about 50% in the YM respect to uncoated gelatin, as well as an increasing of about 60% in the EB, while the coating did not affect significantly the UTS. In other words, the coating decreased the stiffness of gelatin films while it increased their ductility, making it more flexible and more resistant to plastic deformations before the breaking. This final result was considered valuable due to the application because the coating could help the packaging to resist more to the breaking in case of bad transportation.
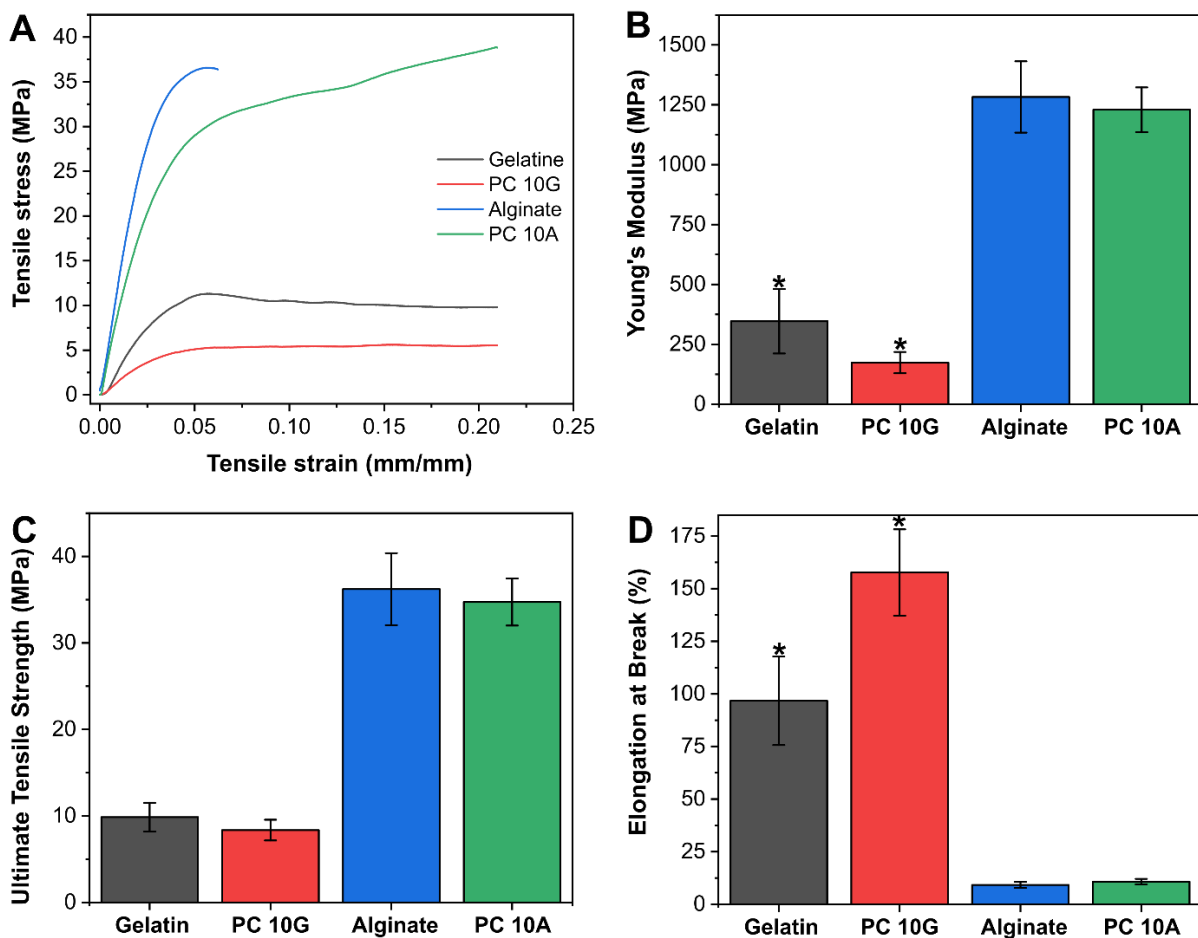

Figure 16. (A) Representative (in terms of Young's Modulus) stress-strain curves of gelatin film, PC 10G, alginate film, and PC 10A. (B) Young's Modulus (MPa) of gelatin film, PC 10G, alginate film, and PC 10A. (C) Ultimate Tensile Strength (MPa) of gelatin film, PC 10G, alginate film, and PC 10A. (D) Elongation at Break (%) gelatin film, PC 10G, alginate film, and PC 10A. *ANOVA test, $p < 0.05$.

2.4.6. Thermal stability

The thermal stability of the curcumin powder, PVAc-VL and PC 10 was evaluated by TGA, and the thermograms including the derivative of weight loss curve are reported in Figure 17. As can be noticed, curcumin (blue line) started its thermal degradation at 190 °C and showed two thermal degradation peaks at about 300 °C and 400 °C, showing a residual weight of 30 % at 800 °C. On the other hand, PVAc-VL (red line) started its degradation at 250 °C and presented two thermal degradation peaks at 330 °C, losing 70% of its weight, and at 440 °C, showing a 3% residual weight at the end of the test. PC 10's thermal degradation (black line) was similar to PVAc-VL: it started its degradation at 240 °C and presented two thermal events at 333 °C, losing 65% of its weight, and at 432 °C, showing a 4% residual weight at the end of the test. These results suggested that the polymer protected the filler from the thermal degradation, shifting the curcumin's degradation starting point of 50 °C. In addition, it can be summarized that the curcumin was well encapsulated without changing the thermal stability of the copolymer, as previously observed [86].
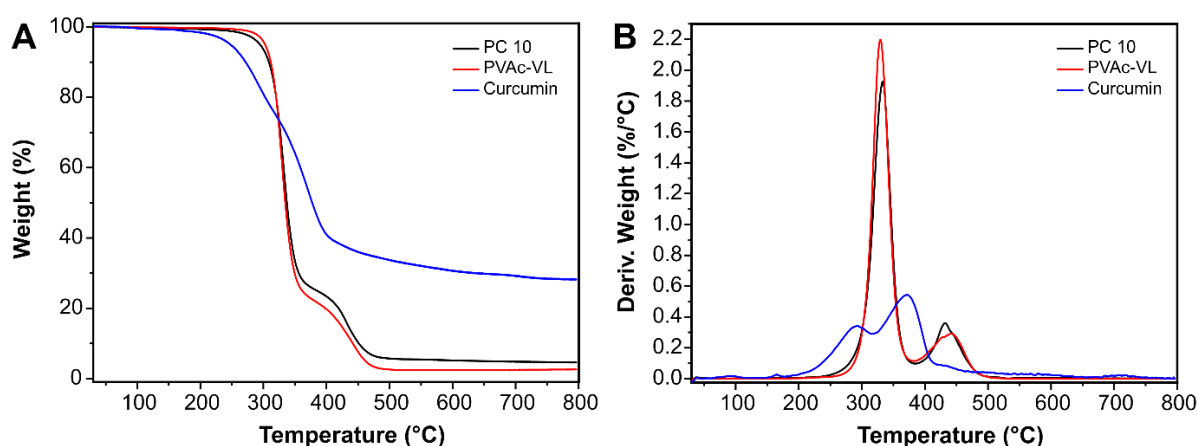

Figure 17. (C) Mass loss and (D) derivatives of the thermograms of curcumin (blue), PVAc-VL (red) and PC 10 (black).

2.4.7. Water contact angle

The wettability properties of the packaging were evaluated in order to understand if the coating protected the packaging, which could be applied on, from external agents such as rain avoiding the destruction of the packaging itself and the deterioration of packaged food. Therefore, water contact angles of PC 0, PC 10, alginate film, PC 0A, PC 10A, gelatin film, PC 0G and PC 10G were measured and reported in Figure 18. The WCA of PC 0 and PC 10 was quite hydrophobic with no significant changes due to the curcumin. As expected, alginate presented a hydrophilic behaviour, in accordance with the state of the art [114]. Gelatin was hydrophilic, as well, with a WCA close to 80°, probably due to the orientation of hydrophobic

amino acids [115]. As can be noticed, the coating significantly improved the wettability properties of natural films with WCA up to 100°. Furthermore, the presence of curcumin did not influence the wettability properties of the coatings, as previously observed for PC 10.

Therefore, since the coating improved the wettability properties of the natural substrates protecting them from water, could be considered a good candidate for food packaging applications.
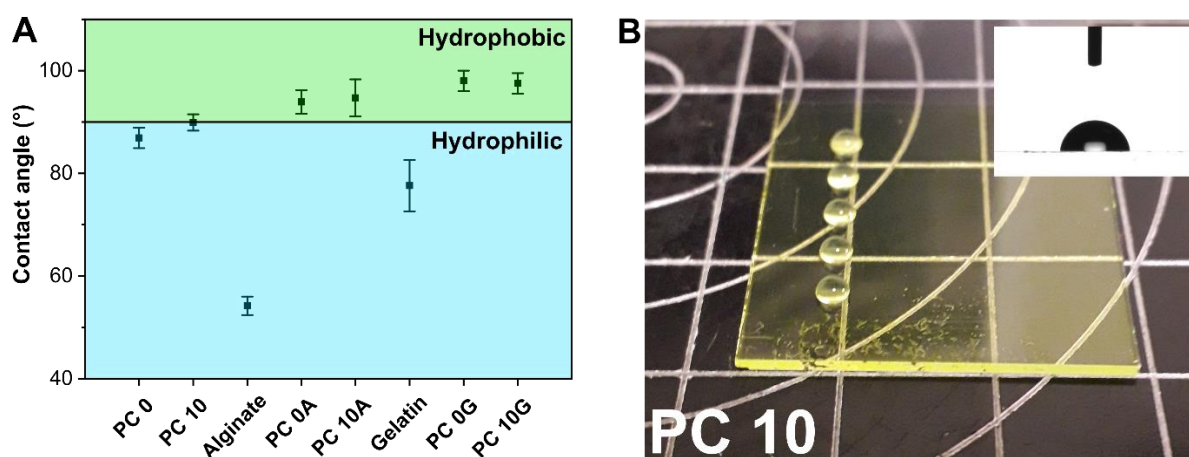

Figure 18. (A) Water contact angles (°) of PC 0, PC 10, alginate film, PC 0A, PC 10A, gelatin film, PC 0G, and PC 10G. (B) Photo of PC 10 with 3 μL water drops on it and respective picture acquired with the camera of contact angle goniometer.

2.4.8. Barrier properties: water vapor permeability

As previously reported, a good packaging material has to avoid gas exchange between the outside and the inside of the packaging, making as slow as possible the spoilage of the food. For this reason, the water vapour transmission rate (WVTR) and the water vapour permeability (WVP) of alginate, PC 0A, PC 10A, gelatin, PC 0G and PC 10G were evaluated. Results are reported in Table 4.

Sample	WVTR (g / m² · day)	WVP (g / m · day · Pa)
Alginate	$(5.92 \pm 0.57) \cdot 10^3$	$(2.44 \pm 0.12) \cdot 10^{-4}$ [a]
PC 0A	$(2.55 \pm 0.48) \cdot 10^3$	$(1.86 \pm 0.22) \cdot 10^{-4}$
PC 10A	$(2.10 \pm 0.38) \cdot 10^3$	$(1.54 \pm 0.36) \cdot 10^{-4}$ [a]
Gelatin	$(5.03 \pm 1.30) \cdot 10^3$	$(3.10 \pm 0.37) \cdot 10^{-4}$ [b,c]
PC 0G	$(2.17 \pm 0.48) \cdot 10^3$	$(1.50 \pm 0.31) \cdot 10^{-4}$ [b]
PC 10G	$(1.91 \pm 0.19) \cdot 10^3$	$(1.33 \pm 0.18) \cdot 10^{-4}$ [c]

Table 4. WVTR (g / m2 · day) and WVP (g / m · day · Pa) of alginate film, PC 0A, PC 10A, gelatin film, PC 0G, and PC 10G. Values are reported as mean ± standard deviation. *a,b,c ANOVA test, p<0.05.*

As can be noticed, both the WVTR and the WVP decreased in presence of the coating. In particular, a significant improving of the barrier properties was observed for the natural films with the coating containing curcumin, PC 10A and PC 10G. Anyway, especially from the results obtained for alginate it can be deduced that curcumin did not influence the barrier properties of the composites as a confirmation of the good encapsulation without phase separation of the filler curcumin in the polymeric matrix.

2.4.9. *Antioxidant activity and release in food simulants*

The DPPH and ABTS scavenging activities of PC 10 and PC 0 are reported in Figure 19. In the DPPH assay PC 10 demonstrated an RSA of 71 ± 3 % and 91 ± 2 % after 15 minutes and 24 hours, respectively, whereas in the ABTS assay PC 10 demonstrated an RSA of 7 ± 1 % and 85 ± 3 % after 15 minutes and 24 hours, respectively. On the other hand, in both assays PC 0 did not show any radical scavenging activity. These results confirmed that curcumin did not lose its antioxidant activity once encapsulated in the polymeric matrix.
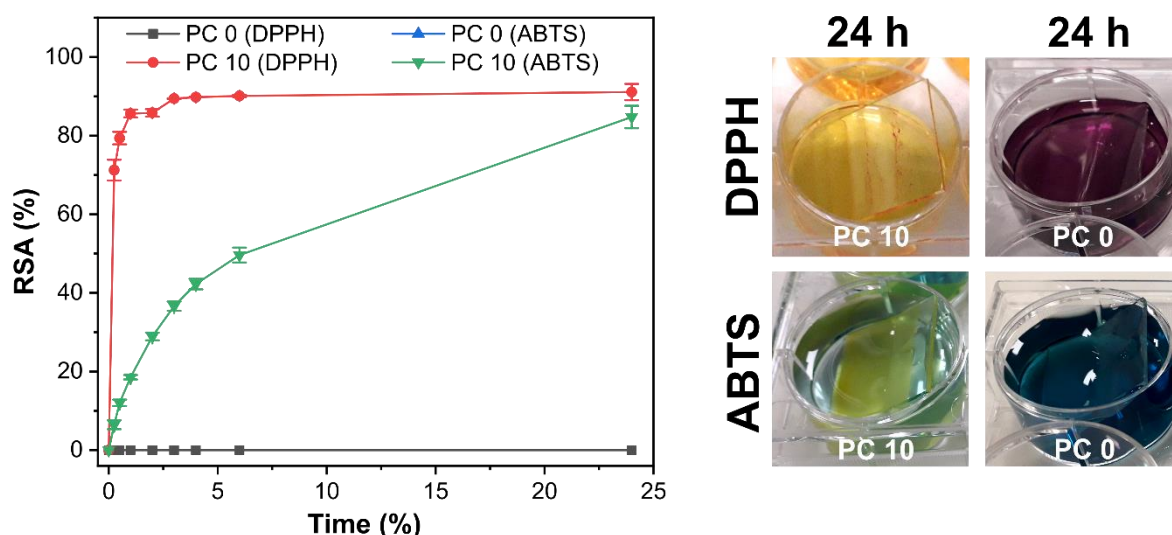

Figure 19. Radical scavenging activity RSA (%) with both DPPH assay of PC 0 (grey) and PC 10 (red), and ABTS assay of PC 0 (blue) and PC 10 (green). Photos of PC 10 (on the left) and PC 0 (on the right) immersed in DPPH (up) and ABTS (bottom) solutions after 24 hours.

Percentage cumulative curcumin release data from PC 10 are plotted in Figure 20. In particular, in Figure 20A the release in the first 6 hours is shown, whereas in Figure 20B the release was extended to 48 hours. As can be noticed, in EtOH 95:5 solution, as fatty food simulant, 70% of the encapsulated curcumin was released in the first 15 minutes, 90% in 30 minutes and practically 100% after 1 hour. However, in EtOH 50:50 solution, as emulsion food simulant, 20% of the encapsulated curcumin was released in the first 15 minutes, 50% in 1 hour and 100% after 48 hours. In EtOH 10:90 solution, as aqueous food simulant, only about 10%

of the curcumin was released within 48 hours. In acidic condition (3% acetic acid), as acidic food simulant, there was a slight release of curcumin after 30 minutes (1%) until 23% after 48 hours. The differences in the release rate was previously explained with the diffusion of the active compound throughout the polymer matrix and with its solubility in the release medium [86]. Indeed, the high release rate of curcumin in EtOH 95:5 solution was due to its high solubility in the alcoholic solvent. On the other hand, curcumin has got very low solubility in water based mediums. Therefore, with the increasing of the percentage of water in the alcoholic solution, a slower burst release was observed. All these results indicated that this system allows a controlled release in different conditions, from the fatty food to acidic environments.

Figure 20. Percentage cumulative release of curcumin from PC 10 (A) in the first six hours up to (B) 48 hours in different solutions: EtOH 95:5 (grey), EtOH 50:50 (red), EtOH 10:90 (blue) and 3% (v/v) acetic acid (purple).

2.4.10. Bacterial adhesion study

Staphilococcus aureus and *Escherichia coli* are standard microorganisms to study the antimicrobial properties of a material that could be proposed as candidate for food packaging applications [27, 86]. Figure 21A and Figure 21B show the growth curves of S. aureus and E. coli, respectively, on PC 0, PC 10, and glass, used as control. As expected, on glass the bacterial growth increased exponentially after 2.5 hours. On the other hand, after 2.5 hours *S. aureus* and *E. coli* growth was much lower for PC0 and PC 10 respect to the control, even if no significant differences was observed between PC 0 and PC 10 due to the filler curcumin. These results demonstrated anti-adhesion properties of the coatings, as confirmed by the photographs in Figure 21C, which show higher adhesion of bacteria on glass than on PC 0, and PC 10. Indeed, the purple spot due to the crystal violet staining was clearly visible on glass, differently from coatings, for both bacteria strains. The brownish colour of the spot on PC 10 was due to the change in colour of curcumin because of the basic environment created by the crystal violet.

Therefore, the spot did not represent adhered bacteria, but simply the curcumin's change in colour due to the pH of the staining medium.

Furthermore, the percentage of bacterial adhesion was evaluated and results are reported in Figure 21D. In particular, a stronger adhesion of S. aureus (45.7%) than E. coli (30%) to the glass surface was observed due to the different polysaccharides structural components of its cell wall [98]. On the other hand, a considerable reduction (between 40-20% less) in bacterial adhesion to PC 0 and PC 10 surface was observed for both the bacteria strains. Furthermore, the adhesion on PC 10 was lower than PC 0 due to the presence of curcumin, which was demonstrated to have antibacterial properties [116-118].
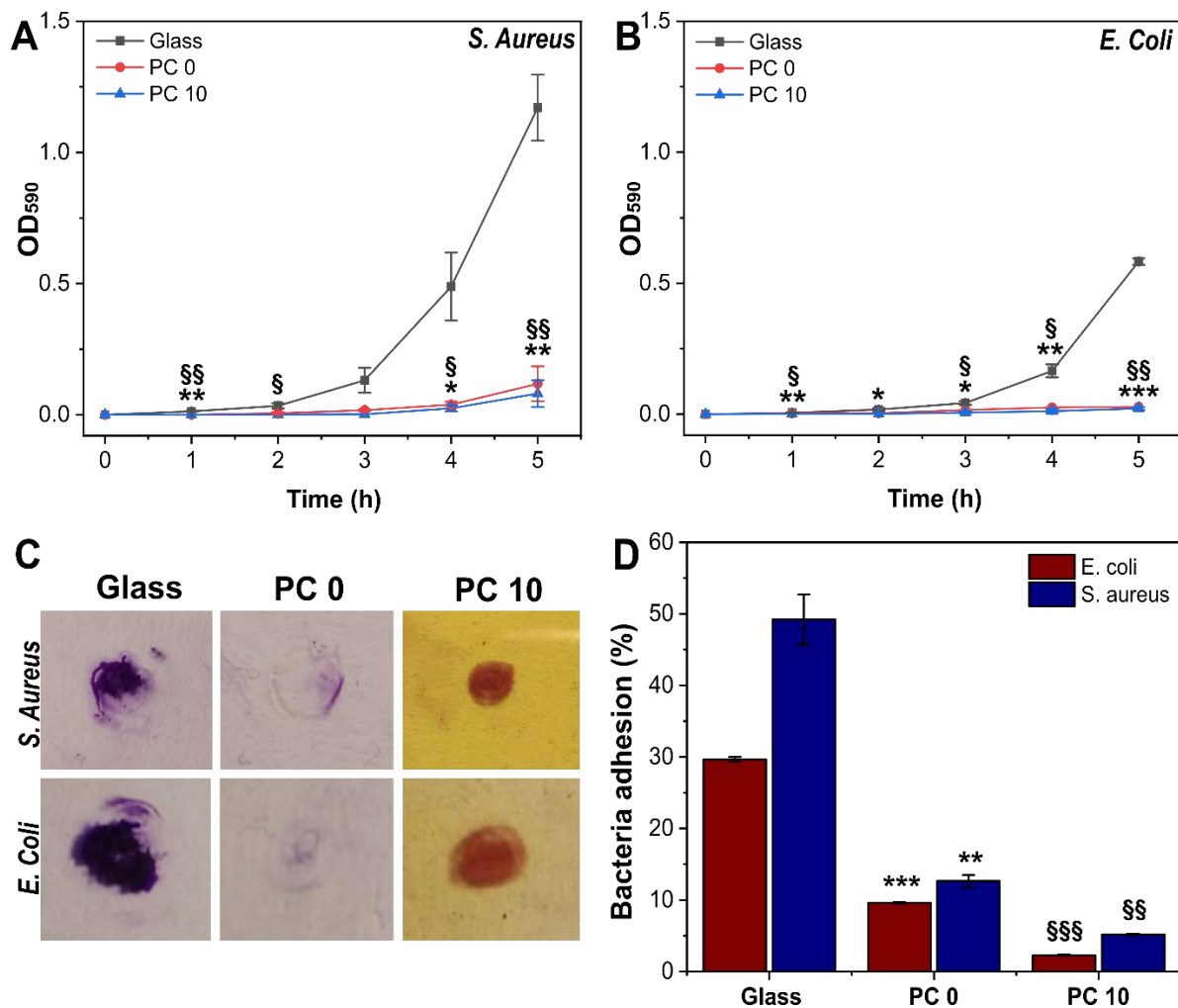

Figure 21. Bacterial growth of (A) S. Aureus and (B) E. Coli strains on glass (control), PC 0 and PC 10. (C) Photographs of glass, PC 0 and PC 10 after staining with crystal violet of the adhered bacteria and rinsing with de-ioinized water. (D) Percentage bacteria adhesion on glass, PC 0 and PC 10 for S. Aureus (blue) and E. Coli (red). The values are presented as mean $\pm$ standard error of at least 3 independent experiments. *$p<0.05$, **$p<0.01$, ***$p<0.001$: PC 0 vs glass. §$p<0.05$, §§$p<0.01$, §§§$p<0.001$: PC 10 vs glass.

2.4.11. Biocompatibility study

The indirect biocompatibility test was performed *via* a proliferation assay conducted in culture medium (DMEM) previously conditioned with PC 0 and PC 10 samples. Chinese Hamster Ovarian (CHO) cells are widely used in biological and medical research [119]. They are an epithelial adherent cell line, very well characterized and exploited for many purposes, due to their high stability and safety profile. One of the advantages of using CHO cells is that they produce proteins similar to those produced in humans. For these reasons, they are often employed also for toxicity screening [120]. For this reason, it was possible to determine if toxic chemical reagents were released by the materials, affecting cell viability. The results as cell index vs time are reported in Figure 22A. The graph shows that the proliferation phase started shortly after the adhesion of the cells to the electrodes and rapidly increased until the cells were confluent onto the electrodes after 50 hours. No differences were detected between CHO cells cultured in normal DMEM, as control, and CHO (Chinese Hamster Ovarian) cells cultured in conditioned DMEM. In particular, the curves obtained from media conditioned by PC 0 and PC 10 were perfectly superimposable. In addition, the fluorescence images acquired at the end of the proliferation tests (Figure 22 B-D) demonstrated that cell survival and proliferation were allowed in the culture medium conditioned in the materials. The fluorescence images showed no differences in the cell shape and morphology.
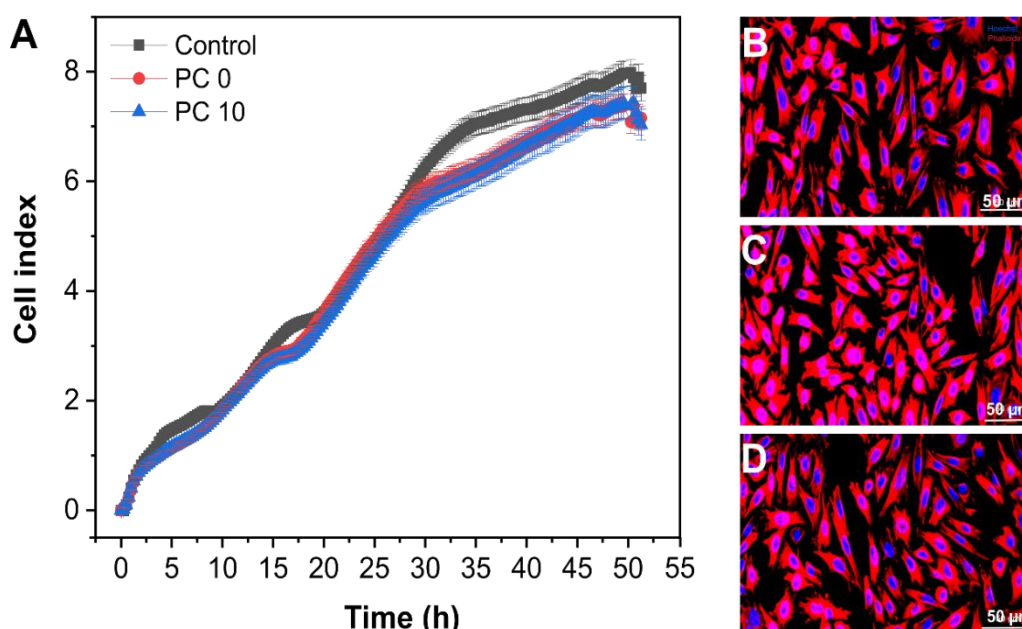

Figure 22. (A) The real-time proliferation curves measured for CHO growing in normal culture medium (DMEM) as control (grey), in DMEM conditioned with PC 0 (red) and in DMEM conditioned with PC 10 (blue). Confocal images of CHO cells growing in (B) normal DMEM, (C) DMEM conditioned with PC 0, and (D) DMEM conditioned with PC 10. Cells nuclei are labeled with Hoechst (blue), and the cytoskeleton with phalloidin (red).

2.5. Conclusions

In conclusion, coherently with the presented state of the art about coating for food packaging, in this part of the work an active antioxidant and antimicrobial filler, curcumin, was encapsulated into a PVAc-VL matrix. The functional coating was developed and was applied by dip-coating technique, resulting suitable not only for glass substrates but also for natural free standing films, such as alginate or gelatin-based. Curcumin was demonstrated to be homogeneously distributed and well encapsulated into the polymeric matrix, without affecting the transparency but conferring a good protection from UV light, preventing photo-degradation of the substrate and of the packaged food. As expected, curcumin made the coating strongly antioxidant with different release behaviors into various liquid food simulants, therefore, if it is applied on packaging substrates (e.g. PET, LDPE, PP, PLA), it will protect the packaged food from oxidative degradation, that is one of the main aims in developing packaging systems. In addition, the coating improved significantly the wettability and barrier properties of the substrates, allowing the protection of the food from water, for instance during the transportation, and from the gas exchange with the outside, preserving the environment inside the packaging. Last but not least, the coating was not toxic to cell proliferation, therefore, the developed system is expected to not be dangerous for the human health, and prevented the adhesion of bacterial colonies, obtaining antimicrobial properties, as well. All these results and, especially, the combination of antimicrobial and antioxidant properties, suggested that this coating can be used in food preservation and packaging applications.

Chapter 3. Epoxidized soybean-oil based coating for water resistant fish leather

This chapter is partially adapted from the patent (IT102022000019740); Perotto G., **Fadda M.**, Zyck A., Athanasiou A., *Metodo per produrre un rivestimento di un substrato e materiale composito comprendente tale rivestimento*, filed on 26th September 2022.

This work has been submitted for publication with the title: "Sustainable, biobased and hydrophobic coating for water resistant fish leather and textiles".

3.1. Fish leather: state of the art

Nowadays, the marine aquaculture is growing faster than other food production sectors [121]. In particular, Atlantic salmon (Salmo salar) represents 90% of the production [122]. First of all, this fast growing is causing damage to the ecosystem. For instance, Taranger et al. summarized the hazards of the salmon farming: (i) genetic interactions between the farmed species and the wild ones due to escapes of fish, (ii) lice and viral diseases of farmed salmon increased significantly the mortality of the wild salmons, (iii) discharges of organic materials and nutrients from the farming to the natural environment [123]. In addition, the faster the growing of this food sector the higher the amount of produced waste. Concerning the salmon food industry, the types of waste after the salmon fillet are: heads, backbones, bellies, trimmings, and skins [124]. In order to reduce the environmental impact of this sector, a circular economy strategy has been established where waste become valuable protein sources for cosmetic, pharmacology or agricultural applications [125].

In this contest, the Horizon 2020 project FISHSKIN [5], titled "Developing fish skin as a sustainable raw material", has the aim of valorizing the salmon skins as waste by transforming them in leather, preventing their throwing into the ocean, and therefore avoiding marine pollution and preserving marine ecosystems [126]. Beside the environmental issue, fish leather, as other exotic leathers (e.g. alligator, python, shark), has acquired a lot of interest in leather industry not only due to its appearance and natural pattern [127], but also because it is more breathable, thinner and stronger than lamb and cow leather due to the intertwining of its fibers instead of the traditional parallel distribution [128]. In spite of all these interesting properties in terms of both workability and application, today the fish leather from fish skin represents less than 1% of the global leather sales [128]. However, the leather industry is aiming to become a more sustainable sector in terms of environmental impact and chemicals [129], since 90 % of the leathers are tanned with chrome and finished with unsustainable materials and dyes

[130]. For this reason, the FISHSKIN project has the aim of finding both chrome-free tanning methods also focusing on vegetable tannins (e.g. mimosa, quebracho, chestnut tannins), and sustainable finishing and post-tanning treatments (e.g. fattening, dyeing), respecting three main keywords: sustainability, circular economy and green chemistry.
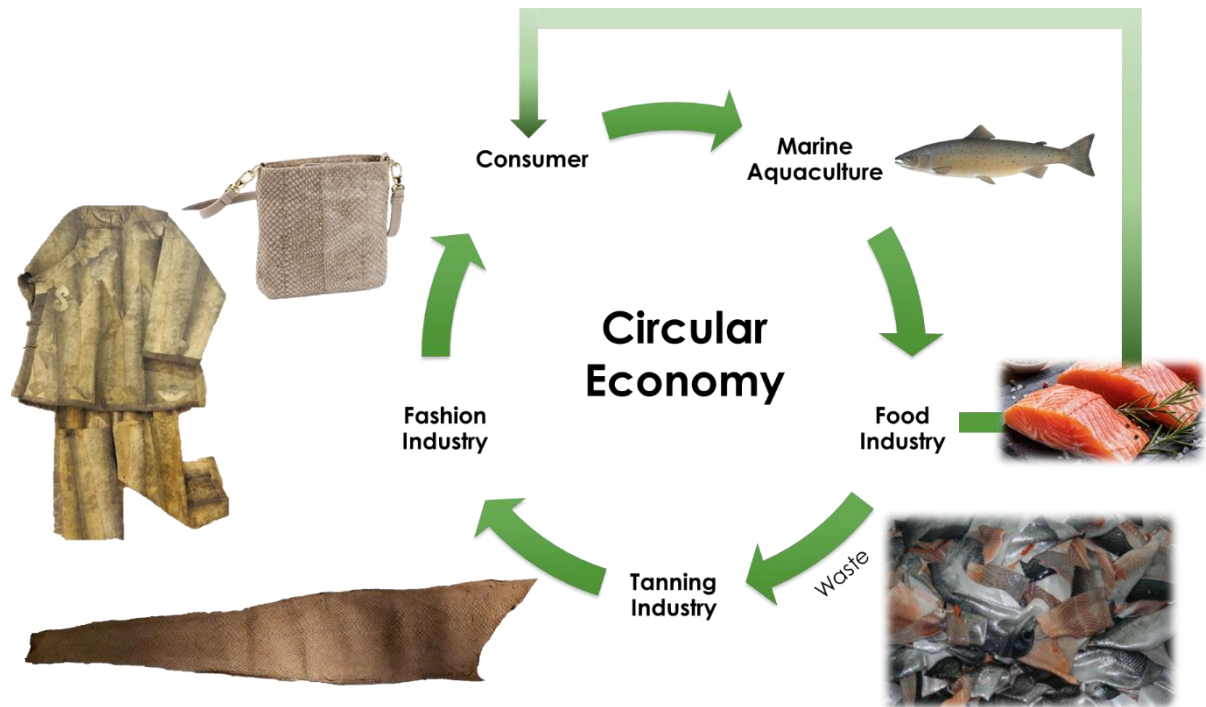

Figure 23. Circular economy model for fish leather: the increasing demand for food leads the increasing number of salmons farmed, which are filleted by the food industry for the consumer producing several waste such as skins. The skins are tanned by the leather industry with sustainable processes making fish leather for the fashion industry. The clothes, shoes, bags and accessorizes are appreciated by the consumer. The images in the figure have been taken consulting the following websites: salmon fish (https://en.wikipedia.org/wiki/Salmon), salmon fillets (https://allfreshseafood.com/products/fresh-norwegian-organic-salmon-fillet-2-8-oz-portions-1-lb), salmon fish skins (https://www.fao.org/3/a1394e/a1394e.pdf), fish leather bag (https://www.pinterest.com/pin/122793527310509999/). The picture of the salmon leather clothes (Hezhen fish skin robe. Jiejinkou Hezhen Village ethnic museum. Heilongjiang, China. Photographer Elisa Palomino (2019)) has been kindly provided by Dr. Elisa Palomino.

Referring to what has been stated above, fish leather can be considered a protein-based textile fabric since it is made of an interweaving of collagen fibers. As reported by Sherman et al. collagen is the main component of extracellular matrix and it presents a triple helical structure made of three polypeptide chains, which contain a region with a repeating amino acid motif, Gly-X-Y, where Gly is the glycine, the core of the protein, and X and Y can be any amino-acid [131]. Several types of collagen exist, but collagen type I, which is a fibrillar collagen, is the most common: it is characterized by an organization of fibrils and fibers that give structural support to many parts of the body such as bones, skin, tendons, cartilage, etc.

[131]. Collagen possesses a high number of hydrophilic groups such as amino (-NH$_2$), carboxylic (-COOH) and hydroxyl (-OH) groups which make it a hydrophilic material [132].

Therefore, it can be concluded that fish leather, which derives from fish skin, is made of collagen and it is hydrophilic. In addition, other factors such as pores and capillaries in its morphology largely influence its wettability properties, as well as surface irregularities and the air contained in the surface layer [133]. Due to the application in fashion, its hydrophilicity and hygroscopicity in terms of water and moisture represent big drawbacks to overcome for the industries. From this need, the second part of this PhD work consisted in developing a sustainable hydrophobic and water resistant coating for fish leather.

3.2. Fish leather: characterization techniques

3.2.1. Materials

Salmon skin leather was kindly provided by ViaTalenta Foundation. The salmon skin leather was obtained from a semi-vegetable tanning process, which involved both chromium and mimosa extract, of the salmon fish skins.

3.2.2. Morphological analysis

Firstly, the morphology of the surface of the fish leather was investigated by using the optical profilometer (Zeta-20, ZETA). The samples were previously mounted on a glass slide with double-side tape in order to make them as flat as possible.

The microstructure of the surface, front and back, and cross-section of the fish leather was investigated by using the Scanning Electron Microscope (SEM; JSM-6490LA, JEOL, Japan) with 10 kV acceleration voltage. The samples were previously mounted on a tilted stub, framed with silver paste, and sputter-coated (Cressington Sputter Coater – 208 HR) with a 10 nm thick layer of gold.

3.2.3. Chemical characterization

The chemical structure of fish leather was analysed by a single-reflection ATR accessory with a diamond crystal (MIRacle ATR, Pike Technologies) coupled to FTIR spectrophotometer (VERTEX 70v FTIR, Bruker). The spectral region scanned was 4000-600 cm^{-1} with a resolution of 4 cm^{-1}. The spectra were normalized to their maximum.

3.2.4. Thermal characterization

Thermogravimetric analysis (TGA) of fish leather was performed by using a TGA Q500 (TA Instruments, USA) instrument. Measurements were performed placing the samples

(7 mg) in platinum pans under inert N_2 flow (50 mL/min) in a temperature range from 30 to 800 °C with a heating rate of 10 °C/min.

3.2.5. Water contact angle

Wettability properties of fish leather were investigate by measuring with a contact angle goniometer (OCA-20 DataPhysics, Instruments GmbH, Filderstadt, Germany) at room temperature the water contact angle of 10 µL deionized water droplet laid on the surface of the sample. The contact angle was calculated from the side view with the help of the built in software. Six measurements were taken to ensure repeatability.

3.3. Fish leather: results and discussion

Before proceeding with more detailed investigations, a macroscopic analysis of fish leather was done. In Figure 24, a picture of the entire sample was reported. As can be noticed, the typical shape of the fish was observable and the regions corresponding to the head and tail were easily distinguishable, as well as the longitudinal line that crossed the skin from the tail to the head. Furthermore, the characteristic scaly nature of the skin was clearly visible, as well as the fact that the closer to the longitudinal line the bigger the scales were. Macroscopically speaking, it could be stated that fish leather did not present any repetitive pattern, any specific geometry and a high variability in the texture, resulting to be an inhomogeneous substrate.

Figure 24. Photo of salmon fish leather obtained by mimosa and chromium tanning.

3.3.1. Morphological analysis

The morphology of the fish leather was firstly investigated by using the optical profilometer with a 5X objective in order to understand how the material was organized microscopically. With this objective, images in 2D (Figure 25A) and 3D (Figure 25B) view of a part of the surface were acquired. As can be noticed in Figure 25A, a particular area was analyzed in order to appreciate the scaly nature of the leather. Therefore, on the top it is clearly evident a more homogeneous part in half-rhombic shape, where the scale was, completely surrounded by edges of variable thickness. With the same magnification, the 3D view of the same area was acquired. As can be observed in Figure 25B, the scaly motif is characterized by

48

an alternating pattern of peaks and valleys. In particular, in the same area previously described, it is noticeable a depression highlighted by green-blue colors due to the previous presence of the scale, while the surrounding edges are magenta-yellow colored, indicating an increasing of the thickness. These pictures could allow us to understand that the tanning process did not change the morphology of the skin because the scaly pattern was maintained.
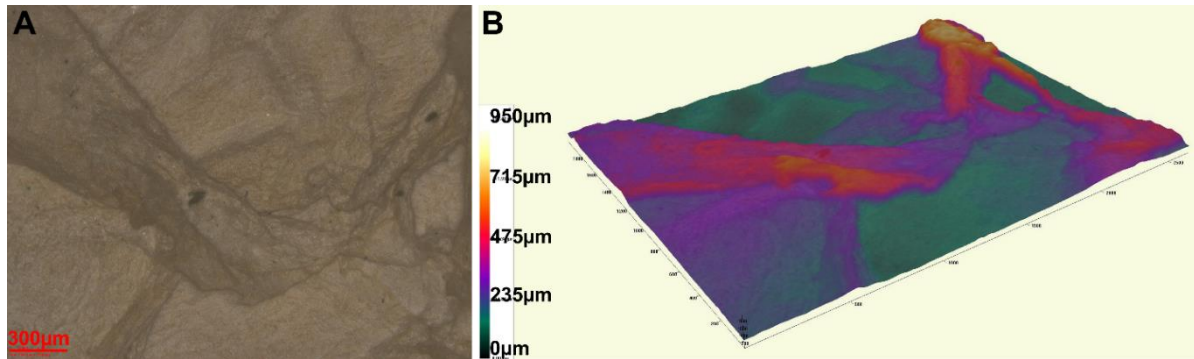

Figure 25. Fish leather surface images acquired with optical profilometer with a 5X objective in (A) 2D view with realistic colors, and in (B) 3D view colored with a palette to appreciate different surface levels: the lowest level (0 µm) is in green and the highest (950 µm) in yellow-white.

To see the sample with more details, a 20X objective was used. The analysis was conducted inside the homogeneous, half-rhombic shaped and flat area where the scale was, in order to have a better quality image and analysis. In Figure 26A the 2D view is reported, where any particular pattern can be appreciated. However, from the 3D view (Figure 26B) a certain rugosity was observable, with highest peaks at 45 µm in yellow. Mostly, a magenta-yellow alternating pattern can be observed, where the magenta highlights the valleys and the yellow the heights. The pattern is not repetitive or characterized by a specific geometry.
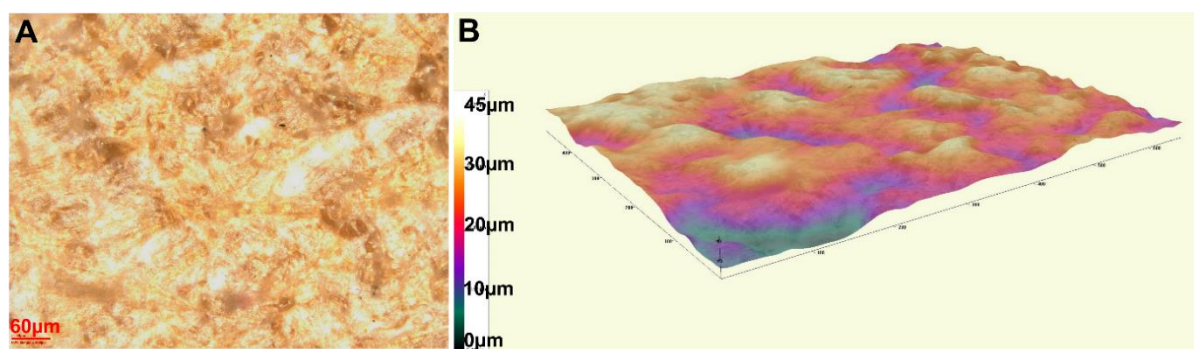

Figure 26. Detail of the surface of the area, where the scale was, acquired with optical profilometer with a 20X objective in (A) 2D view with realistic colors, and in (B) 3D view colored with a palette to appreciate different surface levels: the lowest level (0 µm) is in green, the highest (45 µm) in yellow-white.

Since a fibrous structure was expected, the morphology of the fish leather was investigated by SEM. In particular, the top view analysis was distinguished in front and back

part of the sample, where the front was relative to the scaly pattern typical of the fish skin. The images relative to the front are reported in Figure 27. It was noticed, with different magnifications, that the surface of the front part is covered in fibers that are distributed no homogeneously and in a disorganized manner, with an interweaving and random entanglement of them. Differently, it was noticed investigating the back part of the samples, as reported in Figure 28. Indeed, a more organized structure of fibers was observed. A similar structure was noticed and reported by Wairimu et al. even if for a different type of fish, the Nile perch fish [134]. Furthermore, it seemed that there was a multi-layer structure where each layer presented a precise orientation of the fibers, and it was oriented at angle of about 90° respect to the upper layer. These observations were confirmed by the SEM images of the cross section of the fish leather (Figure 29), where a multi-layer structure of fibers was well visible.
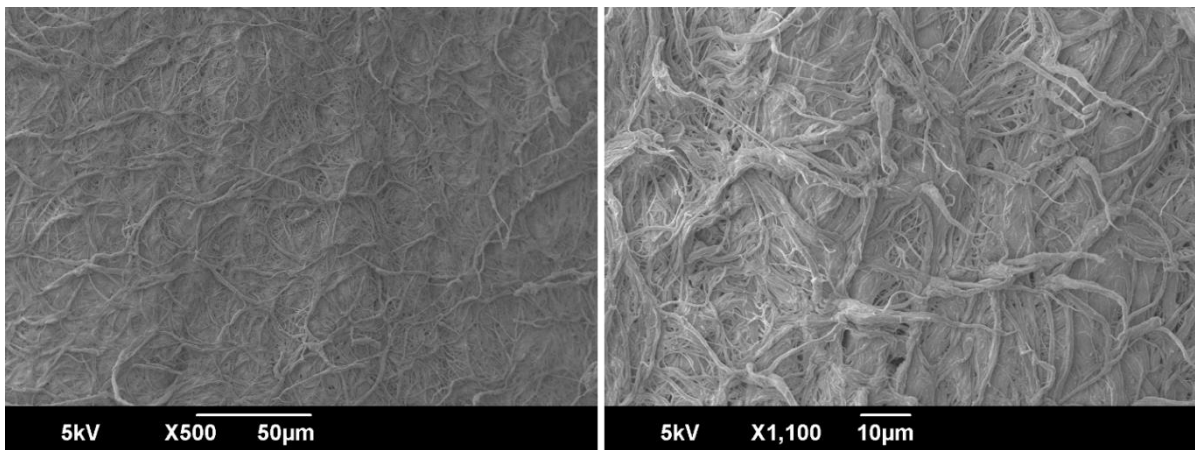
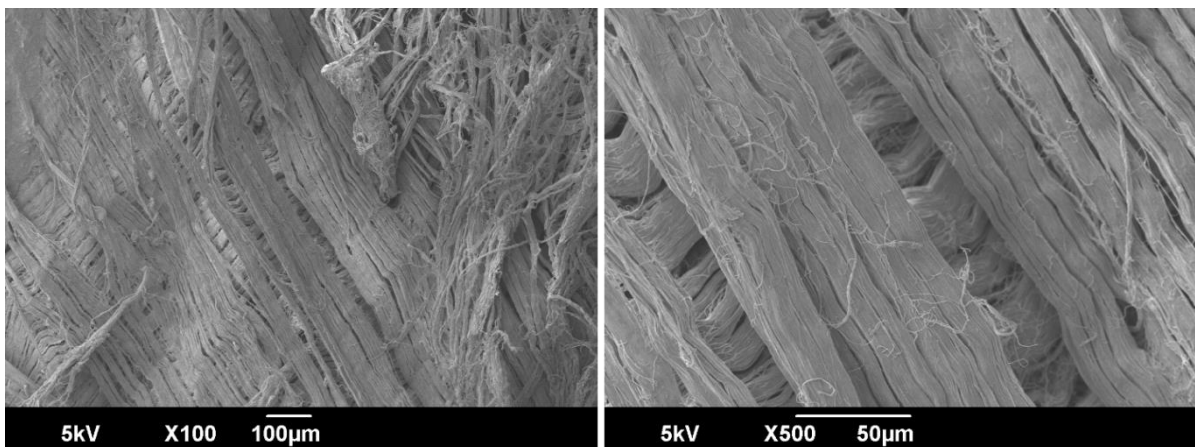**Figure 27.** SEM images of the top view of the front part of fish leather.

Figure 28. SEM images of the top view of the back part of fish leather.
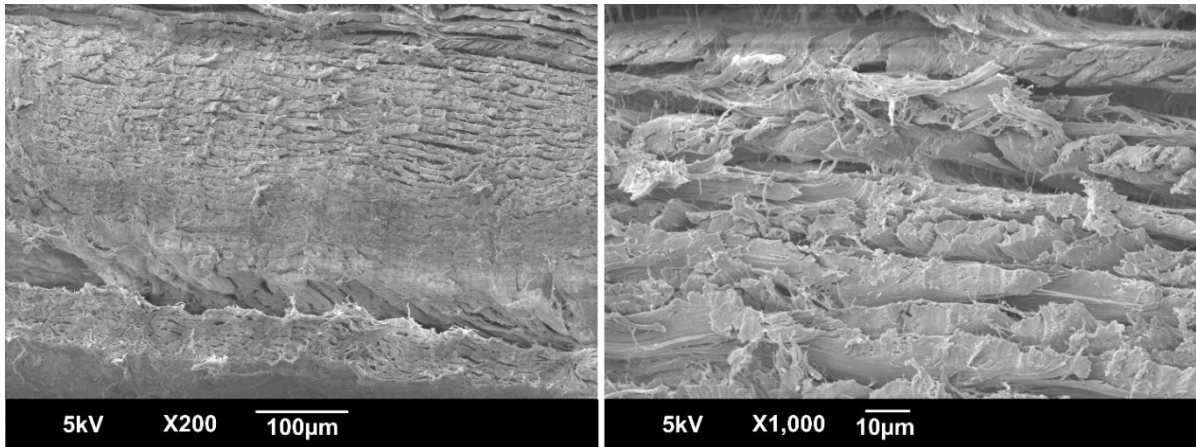
Figure 29. SEM images of the cross section of fish leather.

3.3.2. *Chemical characterization*

To study the fish leather and its functional groups, its FTIR spectrum was acquired and reported in Figure 30. As deriving from fish skin, it was expected to be made of collagen, as previously stated, but it was interesting investigate if and how the tanning process eventually changed its chemical structure. It showed the characteristic peaks and structure of the collagen Type I: the peaks at 3300 and 3080 cm-1 were assigned to the stretching of N-H and O-H, respectively, related to the Amide A; the peaks at 2925 and 2855 cm-1 were assigned to the asymmetric and symmetric stretching of CH2, respectively, related to the Amide B; the peaks at 1645 and 1545 cm-1 were assigned to the stretching of CH (Amide I), and to the vibrations on the plane of the N-H bond and to the stretching of C-N, respectively (Amide II); the peaks at 1450, 1375 and 1337 cm^{-1} were assigned to the asymmetric bending of CH_2, CH_3 and CH_2, respectively, corresponding to the stereochemistry of the pyrrolidine rings of proline and hydroxyproline; the peak at 1234 cm^{-1} was assigned to the stretching of C-N, related to the Amide III. All the assignments were done basing on these references [135-137]. Therefore, it seemed that the tanning process did not change the chemical structure of the fish leather.
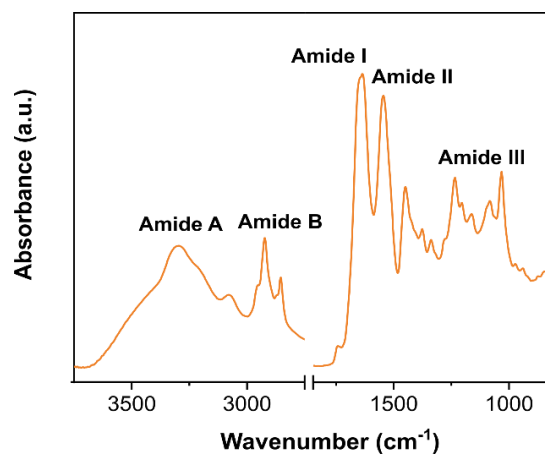

Figure 30. FTIR spectrum of fish leather with characteristic peaks.

3.3.3. Thermal characterization

The thermal stability of fish leather was evaluated by TGA in order to understand how stable was the leather to the temperature in case of treatments post-tanning. It is well known that the tanning process stabilises the skin chemically, thermally and mechanically, preventing fast degradations [138]. Fish leather thermograms and derivatives of weight loss curves are reported in Figure 31A-B, respectively. As can be noticed, untreated fish leather presented a two steps weight loss, as for the fish skin [139], as further demonstration of the fact that the material did not change after the tanning. The first peak was at 56 °C and presented a 10 % weight loss due to the loss of structural water bond, while the second one was at 315 °C and presented a 60 % weight loss due to the thermal destruction of the polypeptide chain [139]. In addition, the green residue at the end of the test (800 °C) was about 20% and was associated to the chromium used for tanning.
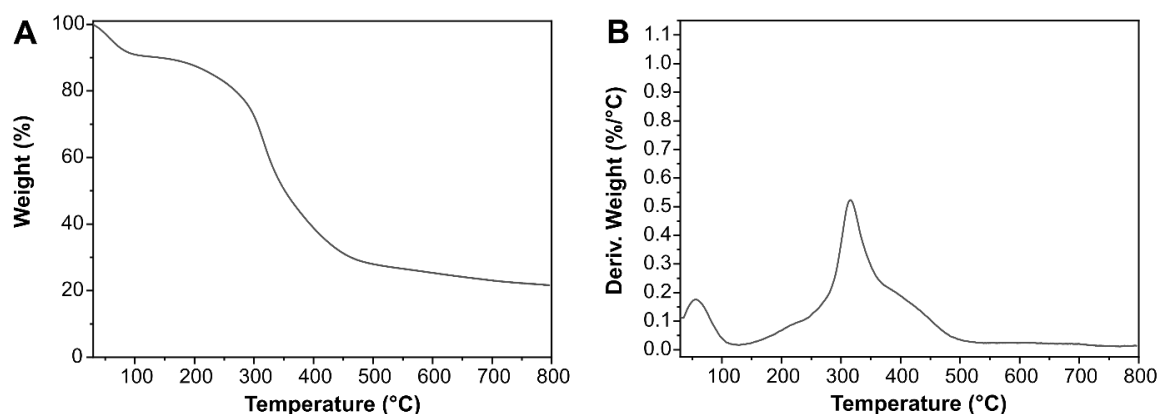

Figure 31. (A) Thermogram and (B) respective derivative of fish leather.

3.3.3.1. Water contact angle

Due to the final application of the fish leather, as raw material for fashion garments and accessorizes, such as bags, clothes, and shoes, it was fundamental to understand in which way the leather behaves once in contact with water. Therefore, the wettability properties of fish leather were evaluated by measuring and monitoring the WCA of droplets laid on the surface of the sample, and results are reported in Figure 32. At the beginning of the measurement WCA was ~ 130° due to a transient effect caused by the fibrillary microstructure of the sample. Indeed, after only 1 minute, the WCA drops well below 90 °, with the droplet being completely absorbed by the leather and WCA becoming not measurable anymore. This result might be explained with the contribution of the roughness of fish leather. Monitoring the drop, it was observable the fast absorption of the water by the surface with a WCA of ~ 80° after one minute, so the fish leather became hydrophilic. Afterwards, the water was completely absorbed

by the fish leather and the WCA was not measurable anymore. Practically speaking, the absorption of the water by the leather could cause the loss of important properties of the leather itself, such as the mechanical strength and softness, that in case of bags and accessorize are really appreciate properties by the user Therefore, this result was thought as an important disadvantage to overcome.
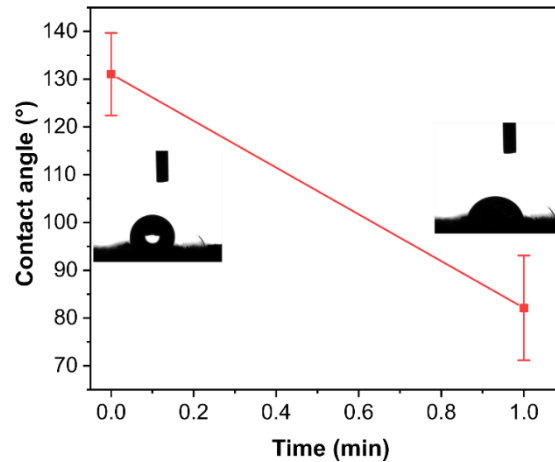

Figure 32. Water contact angle (°) of fish leather vs time (min).

3.4. Fish leather as substrate: conclusions

In conclusion, fish leather maintained the scaly-nature typical of the fish skin. It presented a fibrous structure made of collage Type I, therefore with amino, carboxyl, hydroxyl and thiol functional groups. The collagen fibers seemed randomly organized in the front part of the leather but not in the internal part, where a multi-layer structure was visible by SEM with a preferential alignment of the fibers in the single layer. Referring to the definition of biomimicry that is an imitation or adaptation of biological and natural systems [140], fish leather can be considered a biomimetic material since it maintained the morphology, the chemical structure and functionality of the fish skin after a human intervention, the tanning. In addition, the leather was demonstrated to be thermally stable under 100 °C, and the highest temperature at which the shrinkage was not observed was 80 °C, value that respects the shrinkage temperatures reported by Wairimu et al. for other types of fish, such as 63 °C for sturgeon, 78 °C for conger and 90°C for carp [141]. Finally, the fish leather was demonstrated to absorb the water very fast. Therefore, it was a need of the companies involved in the project to protect the fish leather from the water with a hydrophobic and water resistant coating due to the application in fashion to make bags, clothes or shoes. As a second part of this work, a completely sustainable coating for fish leather was developed. In the next section, the state of

the art relative to hydrophobic and water resistant coating for leather has been reported in terms of materials proposed and used up to now.

3.5. Hydrophobic and water resistant coating for leather

Focusing on finishing and, more specifically, on hydrophobic treatments and coatings for leather, most of the materials and products already used and commercialized are unsustainable, as well as the processes are expensive, as previously reviewed for cellulose-based textile fabrics. After tanning, finishing step is very important in order to enhance leather's aspect and provide to it new features and properties, such as flexibility, water resistance, abrasion resistance and thermal stability [142]. The most used techniques for leather's finishing are spray, roll and dip coating, whereas the materials are divided in binders (e.g. waxes, proteins, synthetic polymers), and additives (e.g. pigments) [142]. In the last decades the most investigated binders to improve the water-resistance of leather have been acrylates, butandienes, and polyurethanes. For instance, Nashy et al. synthetized methyl methacrylate/butyl acrylate copolymers nano-emulsion as retanning and lubrigating agent for leather improving its mechanical properties in terms of tensile strength and elongation at break, its thermal stability, and limiting its water absorption [143]. Furthermore, Mohamed et al. synthetized a styrene/butyl methacrylate copolymer to coat the leather observing an improvement of tensile strength and elongation at break, thermal stability with higher butyl methacrylate content, and water resistance with increasing styrene content [142]. Or, Wang et al. proposed a fluorinated polyurethane-acrylate investigating different hexafluorobutyl acrylate contents as finishing for leather due to its high tensile strength, hardness and excellent chemical resistance [144].

Concerning hydrophobic and water-proof coatings for leather the proposed solutions in the state of the art are similar to the one summarized for cellulose-based substrates by using nanoparticles or synthetic polymers. For instance, Ma et al. sprayed on leather two layers, one made with polyacrylate emulsion and the other one made with ethanol dispersion of hydrophobic silica nanoparticles reaching water contact angles from 120° to 170° depending on the number of sprayed nanoparticles-based layers [132]; on the other hand, Feng et al. developed a polymerized vinyltriethoxysilane coating deposited on the leather by using a low-pressure and cold plasma technology increasing the hydrophobicity of the leather itself reaching water contact angle of 140° [145]. However, even if all these treatments were consider eco-friendly ten years ago, nowadays the market and the leather industry are looking for more sustainable solutions. As recently reviewed by Lipika et al., polydimethylsiloxane could be

considered a sustainable solution to make hydrophobic coating since it is eco-friendly and suitable for many substrates due to its strong adhesion properties [146]. On the other hand, PDMS remains a synthetic polymer not bio-based nor waste-derived, as well as its strong adhesion could represent a problem in the recycling or waste management process.

For this reason, in the chapter 3 of this work a further step was done, selecting natural-based by-products as main materials to make a hydrophobic coating. Indeed, as reported by Zahid et al., there are testimonies of the first hydrophobic and water-repellent textiles in the 15th century, when linseed oil or natural waxes were used for this purpose [28]. Nowadays, due to the big environmental issue there is a change in mentality by looking at solutions that nature can give us. Therefore, various studies on oil-based hydrophobic and water-proof agents have been proposed for leather. For instance, Qiang et al. prepared a polyether organosilicone succinate ester mixed with sulfated neatsfoot oil and oxidized-sulfited fish oil to make a new leather fatliquor to improve the waterproof-ability of the leather [147].

However, more than animal-derived oils, vegetable oils today are used in several industries because they are cheap and renewable resources. Indeed, in this work soy bean oil has been considered. Soybeans are the largest oilseed crops in the world, after palm oil, due to the higher amount of proteins that possesses respect to others vegetable oils depending on the cultivation area (e.g. United States, Brazil, Argentina) [148]. Soybean oil's applications are mainly focused on food (70 %) as baking, frying and salad oil, or to produce margarine, even if a smaller quantity is used in non-food applications such as lubricants, oleochemicals, bioplastics, as substitute of paraffin wax or to produce biodiesel [148]. However, soybean oil is produced in excess in many geographical areas respect to the consumption in cooking [6]. In addition, as triglyceride, it owns both saturated and unsaturated fatty acids: the double bonds in its structure are not very active, so they could be made more active by introducing functional and highly chemically reactive groups such as epoxide, hydroxyl or acrylate groups. One of the most common transformation is the epoxidation, making the epoxidized soybean oil (Figure 33) [149].
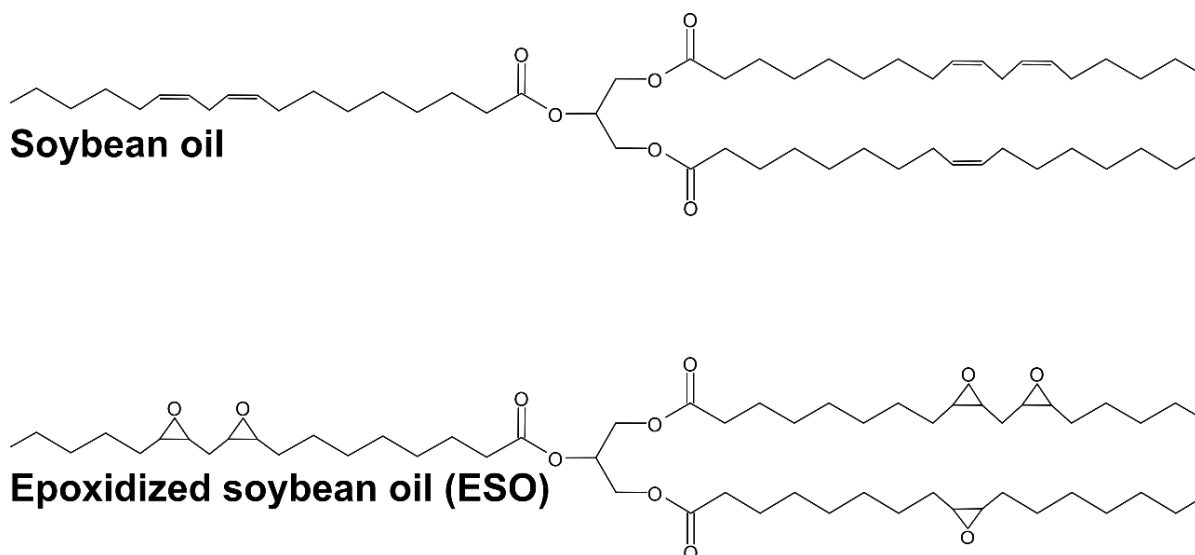
Figure 33. Molecule of soybean oil and epoxidized soybean oil

Generally, the epoxidation is performed by reacting the double bonds in the soybean oil with a peracid, which is made in a previous step by treating acetic acid or formic acid with hydrogen peroxide [150]. On the other hand, this process has got several limitations: firstly it causes the opening of the epoxide rings due to the acidic environment, therefore, limiting the number of epoxide groups, and so lowering the reactivity of the final products; last but not least, it is problematic in terms of safety due to the presence of peracid and hydrogen peroxide [150]. For these reasons, in the state of the art alternative processes to epoxidize the soybean oil are investigated [150].

3.6. Epoxidized soybean oil-based water-resistant coatings

The epoxidized soybean oil, as other epoxidized vegetable oils, has been used in various applications as plasticizer in polymers or as additive in lubricants, as well as its conversion in polyols can allow its applicability in polyurethane materials [151]. Furthermore, focusing on the aim of this work, ESO has been used to make water-resistant materials and coatings for natural films, cellulose-based fabrics, and leather. For instance, Ge et al. [152] coated starch-based films in acrylated epoxidized soybean oil-based coating to improve their moisture resistance and gas permeability. By adding a commercial photoinitiator, they crosslinked and polymerized the coating by UV-light obtaining a smooth layer on the top of the starch films, imparting hydrophobicity and limiting their water absorption. Or, Miao et al. [153] polymerized epoxidized soybean oil on paper substrates by using boron trifluride diethyl etherate as catalyst. As a result, the water vapour permeability of treated paper was lower than bio-based polymeric materials, promoting the use of vegetable-based polymers as potential

water-resistant materials. Furthermore, Cheng et al. [154] cured epoxidized soybean oil with a catalyst and, then coated with it cotton and filter paper, as substrates, in order to obtain the adhesion. Afterwards, they coated the substrates in ZnO nanoparticles solution and cured at 150 °C for 2.5 hours. To obtain superhydrophobic materials they made a final treatment in a stearic acid solution. In addition, the use of epoxidized vegetable oils, comprising the epoxidized soybean oil, has been proposed to protect the wood from humidity and UV light, which degrade faster the material (WO2009101362A1).

Focusing on leather, epoxidized oils have been used during the tanning together with a catalyst in order to obtain a crosslinked system that comprises the collagen of the leather and the oil, resulting in a flexible and water-resistant chamois leather (CN101550459B) or salmon leather (CN101240355A). Previously, Heath et al. reviewed the use of epoxides as alternatives to aldehydic tanning systems that are more toxic, describing the mechanisms and kinetic of the reaction between epoxides and proteins/collagen [155]. This review was considered as a starting point of this work, with the idea of creating a crosslinked network between the epoxidized soybean oil and the collagen of the fish leather, which has got several reactive groups in the polypeptide chain, such as amine (-NH$_2$), carboxylic acid (-COOH) and thiol groups (-SH), avoiding to use catalysts since most of the time are toxic and unsustainable and controlling only the temperature. In order to select the curing temperature, the shrinkage temperature of the fish leather substrate had to be taken into account. Fish leather, because of its fibrous collagen structure, begins to shrink at temperatures higher than 80-90 °C, depending on the type of tanning agent and its amount [156]. Because of this, the curing process for our ESO was performed at 80 °C. Last but not least, the process has been performed directly on leather, after the tanning, as finishing step. Additionally, a sustainable trimer acid with functional carboxylic groups (-COOH) has been included in the formulation and strongly crosslinked with the ESO.

3.7. Trimer acid

The used trimer acid has been selected because both it is sustainable and derives from vegetable oils, as well. Known commercially as Pripol 1040, it is a complex mixture of polycarboxylic acids produced by coupling reactions of bio-based unsaturated fatty acids (mainly oleic and linoleic) and subsequent partial hydrogenation [157] (Figure 34). Therefore, as fatty acid and due to its long chain, it was thought to be a good solution to improve the water resistance of the leather together with the ESO. The reaction that was designed for developing the coating is based on the ring opening reaction of the epoxide groups of ESO by the

carboxylic groups of the trimer acid [158]. Because the trimer acid has three functional groups per molecule and the ESO has four epoxy ring per molecule, their coupling result in a strongly crosslinked network. Moreover, the collagen in the fish leather, as previously stated, possesses carboxylic and amino groups that have been expected to potentially participate in the curing, providing improved adhesion and stability of the coating. Indeed, previously, dimer acid was considered to perform the ring opening reaction of bisphenol-A epoxy resin to synthetize an UV-curable epoxy acrylate oligomer by Liang et al. [159]; or, Li et al. prepared a vitrimer elastomer by crosslinking a commercial glycidylamine epoxy with a vegetable oil-derived dimer acid only by a two-steps curing process [160].

Therefore, in this second project two sustainable materials, epoxidized soybean oil and trimer acid, have been considered to make fish leather hydrophobic and water resistant without using catalysts. The reaction has been performed only managing temperature, and as a result a strong crosslinking between the two components of the coating has been evaluated as gel fraction. The evaluation of water contact angle and water uptake demonstrated the main functionality of the coating making the fish leather hydrophobic and water resistant, protecting it by the humidity, as well. On the other hand, the coating does not affect the properties that make the fish leather a better product respect to the traditional leather, such as breathability, flexibility and workability.
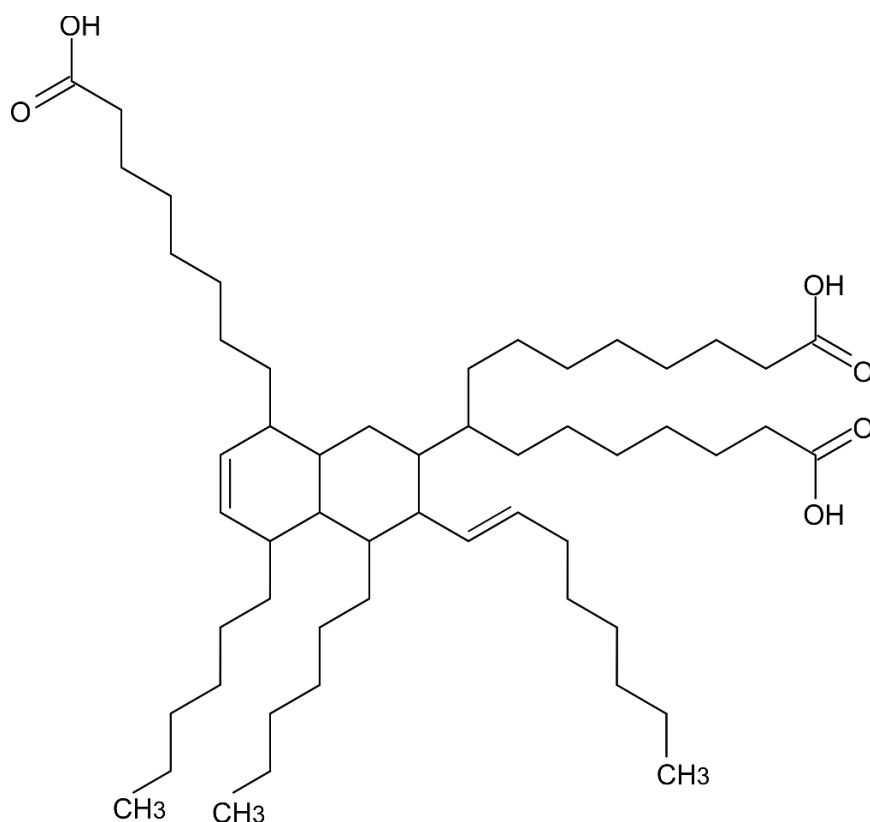

Figure 34. Molecule of trimer acid

3.8. Coating: materials and methods

3.8.1. Materials

Epoxidized soybean oil (ESO) (M_w = 950 g/mol; 4 epoxide/molecule) was purchased by Spectrum Chemical. PRIPOL^{TM} 1040-LQ-(GD) (Pripol) (M_w = 830 g/mol; 2.78 carboxylic acid groups/molecule) was kindly provided Croda. Ethyl acetate was purchased by Sigma Aldrich. Salmon skin leather was kindly provided by ViaTalenta Foundation. Deionized water was obtained from Milli-Q Advantage A10 purification system. All chemicals are analytical grade and used as received.

3.8.2. Preparation of the solutions

55.7 g of Pripol was mixed with 44.3 g of ESO until complete homogenization. The final mixture, labeled as PESO, was dissolved in ethyl acetate in different concentrations: 1, 5, 10 and 15 % (w/w). The solutions were labeled as 1% PESO, 5% PESO, 10% PESO, and 15% PESO, respectively. A schematic illustration of the procedure is shown in Figure 35.
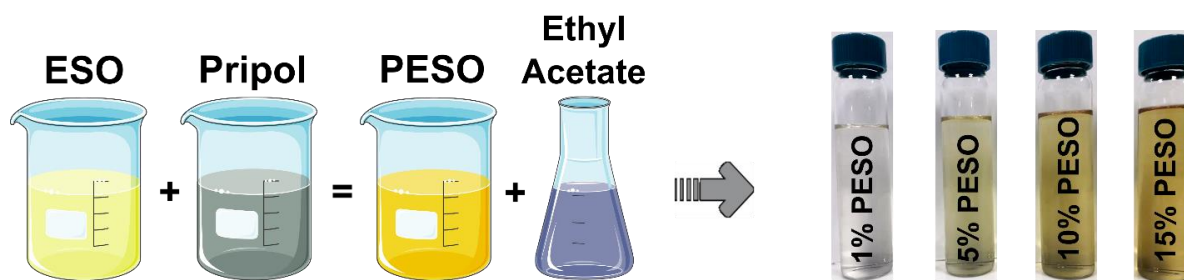

Figure 35. Solutions fabrication steps: homogeneous mixing of ESO and Pripol (PESO), and dissolution of the mixture in ethyl acetate in different concentrations: 1, 5, 10, and 15 wt%.

3.8.3. Fabrication of the coated fish leather and cotton fabrics

The fish leather or cotton fabric were cut in pieces (2 cm x 3 cm) and dip coated in the solutions. The samples were dried at room temperature in a fume hood for 3 hours until the complete evaporation of the solvent. Afterwards, they were placed in the oven at 80 °C for 2 weeks for the curing. The samples were labeled as PESO 1, PESO 5, PESO 10, and PESO 15. A schematic illustration of the fabrication process is shown in Figure 36. In addition, free standing films of the coating material were made by casting PESO in a round shape Teflon dish, and then the material was cured in the oven to give a freestanding material, labeled as Film.
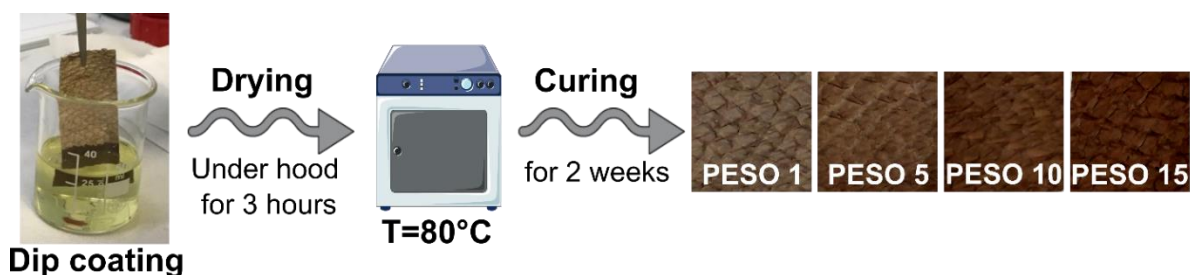
Figure 36. Fabrication steps of the coatings on fish leather: dip coating in the solutions, drying under hood for 3 hours, curing in the oven at 80 °C for two weeks. Photographs of fish leather with different amount of coating on it are reported: PESO 1, PESO 5, PESO 10, and PESO 15.

3.8.3.1.   Gel fraction

The crosslinking between ESO and Pripol was evaluated on 5 cm x 1 cm samples of PESO 1, PESO 5, PESO 10, PESO 15 coated and untreated fish leather as control. In addition, a 1 cm x 1 cm pieces of Film were used as control. In particular, the samples were weighted before and after the application of the coating to calculate the weight of the coating. The crosslinking after curing was evaluated in terms of gel fraction (GF), as the amount of sample that was crosslinked and thus, was not soluble anymore. After the curing, samples were conditioned for 48 hours at 0 % R.H. in sealed chamber by using anhydrous silica gel, and weighted (W_i). Afterwards, the samples were placed in 10 mL of ethyl acetate for 24 hours, left to dry under hood for 24 hours, conditioned in a sealed chamber for 48 hours at 0 % R.H by using anhydrous silica gel, and weighted (W_f). The GF was evaluated by the following equation:

$$GF\ (\%) = \frac{W_f}{W_i} \times 100$$

3.8.4.   Chemical characterization: ATR-FTIR and XPS

Chemical characterization of Pripol, ESO, PESO, Film, PESO 1, PESO 5, PESO 10, PESO 15, and untreated fish leather was made by using a single-reflection ATR accessory with a diamond crystal (MIRacle ATR, Pike Technologies) coupled to FTIR spectrophotometer (VERTEX 70v FTIR, Bruker). The spectral region scanned was 4000-600 cm^{-1} with a resolution of 4 cm^{-1}. The spectra were normalized to their maximum.

Elemental analysis of the surface of PESO 15 and untreated fish leather was investigated by using X-ray photoelectron spectroscopy (XPS). An electron spectrometer (Lab2, Specs, Berlin, Germany) equipped with a monochromatic X-ray source (set at 1486 eV) and with a hemispherical energy analyzer (Phoibos, HSA3500, Specs, Berlin, Germany) was used. The voltage of the Al Kα X-ray source and the current were set at 13 kV and 8 mA, respectively. The pressure in the analysis chamber was ~1×10^{-9} mbar.

3.8.5. Water contact angle

Dynamic water contact angles was measured for untreated fish leather and coated with PESO 1, PESO 5, PESO 10, PESO 15, and Film, uncoated and coated cotton using a contact angle goniometer (OCA-20 DataPhysics, Instruments GmbH, Filderstadt, Germany) at room temperature. Deionized water droplets of 10 µL were deposited on the surface and the contact angle was calculated from the side view with the help of the built in software at specific time points (0, 5, 10, 15, 20, 25, 30, 35 and 40 minutes). Six measurements for each coating were taken to ensure repeatability. A sheet of Polytetrafluoroethylene (PTFE) was used as a control to exemplify a hydrophobic and non-absorbent material.

3.8.6. Stability of the coating after washing

PESO 15 coated fish leather samples were placed in 10 mL of deionized water for 24 hours. Afterwards, they were taken out, left to dry under hood for 24 hours. The contact angle was measured by using a contact angle goniometer (OCA-20 DataPhysics, Instruments GmbH, Filderstadt, Germany) at room temperature and following the same steps described above (Section 2.7).

3.8.7. Water uptake

For the water uptake evaluation, PESO 1, PESO 5, PESO 10, PESO 15, untreated fish leather and Film specimens (0.8 cm x 0.8 cm) were conditioned at 0 % R.H. by using anhydrous silica gel and weighted by using an analytical electronic balance ($W_{0\%}$). Afterwards, they were placed in a sealed chamber at different relative humidity conditions (% R.H.), 11, 44, 84 and 100, obtained by using LiCl, K_2CO_3 and KCl saturated saline solutions and water, respectively. The samples were weighted after 1 day in the chamber ($W_{RH\%}$). The water uptake (WU) was evaluated by the following equation:

$$WU\ (\%) = \frac{W_{RH\%} - W_{0\%}}{W_{0\%}} \times 100$$

where $W_{RH\%}$ is the weight of the samples at the different % R.H. conditions and $W_{0\%}$ is the weight of the samples at 0 % R.H.. Five samples were tested to ensure the reliability of the measurement.

3.8.8. Water vapour permeability

The water vapour permeability (WVP) of untreated fish leather and coated with PESO 1, PESO 5, PESO 10, PESO 15, uncoated and coated cotton, was evaluated under 100 %

relative humidity gradient ΔRH (%) by following the ASTM E96 standard method. 400 μL of deionized water were placed in the permeation chambers of 7 mm inner diameter and 10 mm height to accomplish ΔRH. Samples were mounted on the top of the permeation chamber, sealed and placed at 0 % R.H. by using anhydrous silica gel. The chambers were weighted every hour for 7 consecutive hours by using an analythical electronic balance (0.0001 g of accuracy) to monitor the transfer of water from the chamber, through the sample, to the desiccant, evaluating the water mass loss. The water mass loss was plotted as a function of time. The slope of each line was calculated by linear regression. Afterwards, the water vapour transmission rate (WVTR) was determined by using the following equation:

$$WVTR(g(m^2 d)^{-1}) = \frac{slope}{A}$$

where A is the area of the sample.

The water vapour permeability (WVP) of the samples was calculated by the following equation:

$$WVP\ (g(mdPa)^{-1}) = \frac{WVTR \times L \times 100}{p_S \times \Delta RH}$$

where L is the thickness of the sample (m), p_s is the saturation water vapour pressure at 25 °C (Pa). Every measurement was replicated three times to ensure reliability of the results.

3.8.9. Morphological analysis

The microstructure of the surface and cross-section of the treated and untreated fish leather, treated and untreated cotton was investigated by using the Scanning Electron Microscope (SEM; JSM-6490LA, JEOL, Japan) with 10 kV acceleration voltage. The samples were previously mounted on a tilted stub, framed with silver paste, and sputter-coated (Cressington Sputter Coater – 208 HR) with a 10 nm thick layer of gold.

3.8.10. Mechanical characterization

PESO 1, PESO 5, PESO 10, PESO 15 coated and untreated fish leather were tested with uniaxial tension tests on a dual column universal testing machine (Instron 3365). The samples were cut in dog bone shape (ten samples were tested for statistical analysis) with a width of 4 mm and length of 25 mm. They were conditioned at 24 °C and 50 % R.H. in a humidity chamber (Espec SH-262 Environmental Chamber). Displacement was applied at a rate of 5 mm/min. The Young's modulus and the elongation at break were calculated from the stress–strain curves.

3.8.11. Thermal characterization

Thermogravimetric analysis (TGA) of PESO 15 coated and untreated fish leather, and Film sample was performed by using a TGA Q500 (TA Instruments, USA) instrument. Measurements were performed placing the samples (7 mg) in platinum pans under inert N_2 flow (50 mL/min) in a temperature range from 30 to 800 °C with a heating rate of 10 °C/min.

3.9. Coating: results and discussion

3.9.1. Scheme of reaction

The waterproofing of the fish leather was developed by coating it with a mixture of the two oils, ESO and Pripol, with subsequent crosslinking of the two components, to create a thin hydrophobic coating. A possible scheme of reaction is reported in Figure 37, where the molecules of ESO and Pripol are showed with all the functional groups highlighted, epoxide rings in red for ESO and carboxyl groups in blue for Pripol. In addition, the main functional groups of fish leather as collagen type I are reported: amino groups (-NH$_2$) in green, carboxyl groups (-COOH) in magenta, hydroxyl groups (-OH) in light blue, and tiol groups (-SH) in orange. After the curing in the oven at 80°C for two weeks of the materials, the ring-opening reaction of the ESO with mainly the functional carboxyl groups of the Pripol has been expected, creating a crosslinked network between the two materials. The crosslinking efficiency was evaluated in terms of gel fraction (GF), which usually is used to evaluate the degree of crosslinking in a hydrogel polymer network, therefore to quantify the percentage of the insoluble part. In this system, it has been expected that the oil-based mixture would not dissolve in ethyl acetate solvent if the crosslinking worked well. Furthermore, since the fish leather has got the functional groups listed beforehand that could react with ESO after the opening of the epoxide ring, we can speculate that these groups will be taking part in the crosslinking reaction with ESO, effectively binding the coating with the substrate, as represented in Figure 37. Of course, since the particular substrate, this concept was not possible to demonstrate properly.
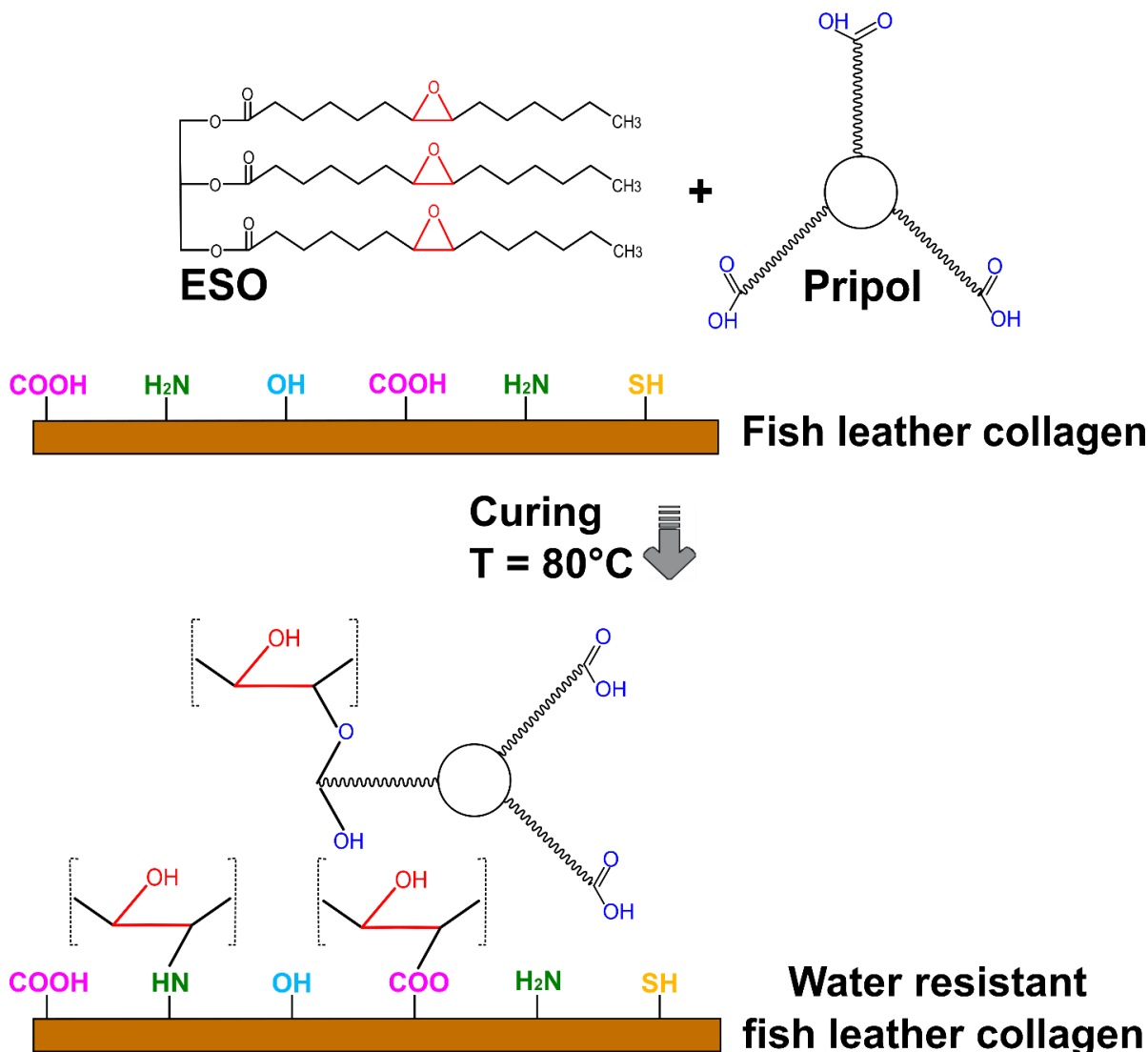
Figure 37. Scheme of reaction between ESO and Pripol, with open-ring reaction and crosslinking after curing. Possible reactions with the functional groups of leather are supposed.

3.9.2. *Gel fraction*

The weights and gel fraction (GF) of PESO 1, PESO 5, PESO 10, PESO 15 and Film are reported in Table 5. The coating resulted to be 2, 8, 11, 22 % of the mass of the final material for PESO 1, PESO 5, PESO 10, and PESO 15, respectively. The efficacy of the curing step, evaluated in terms of GF, showed that for all samples it was very high, being always > 97%, demonstrating that the temperature and time used were enough to have the crosslinking. The GF of the Film sample was high (> 92 %) demonstrating the successful crosslinking of the Pripol with the ESO.

Sample	Weight $\pm$ s.d. (mg)	GF $\pm$ s.d. (%)
PESO 1	4.7 ± 0.7	98.1 ± 1.0
PESO 5	19.2 ± 3.0	98.9 ± 0.1
PESO 10	30.1 ± 1.7	97.8 ± 0.2
PESO 15	53.2 ± 2.4	97.3 ± 0.5
Film	220.2 ± 9.1	92.3 ± 1.1

Table 5. Weight (mg) and GF (%) of PESO 1, PESO 5, PESO 10 and PESO 15 coatings on FL.

3.9.3. Chemical characterization: ATR-FTIR and XPS

To study the crosslinking reaction between Pripol and ESO, from the chemical point of view, FTIR was used on the blend of the two components (PESO) and on Film sample, reporting the spectra of the raw materials. Spectra are showed in Figure 38A. As can be noticed, the peak assigned to the stretching of C=O was observable at 1707 cm^{-1} and at 1741 cm^{-1} for Pripol and ESO, respectively. In particular, this difference in the wavenumber found its explanation in the fact that for Pripol is a carboxylic acid whereas for ESO is an ester group. From the spectrum of PESO, both peaks were visible at the same wavenumbers, revealing a good homogeneity in the mixture. However, the peaks presented different intensities before and after the curing. In particular, comparing PESO and Film spectra, before the curing the carboxyl peak revealed a higher intensity than the ester peak, whereas after the curing the ester group presented higher intensity than the carboxyl peak. This observation found its explanation in the fact that before the curing there were more free carboxyl groups of Pripol, which after the curing reacted with ESO creating ester groups and, therefore, the intensity of the ester peak increased, while the intensity of carboxyl peak decreased. All these evidences confirmed the reaction between Pripol and ESO and the formation of a crosslinked network after the curing step. Finally, as a further confirmation of this fact, in the ESO spectrum the peak at 823 cm^{-1} related to the epoxy groups, highlighted by the red arrows, was visible also in PESO but not in Film. This result was another demonstration of the crosslinking reaction of the epoxy groups with the carboxyl groups of the Pripol. All the assignments were done basing on these references [161-163].

To study the substrate and its functional groups involved in the reaction with the coating material, the FTIR spectra of untreated and coated fish leather were acquired and reported in Figure 38B. In particular, it shows, from the bottom to the top, the FTIR spectra of the untreated fish leather, PESO 1, PESO 5, PESO 10 and PESO 15 samples. All these samples showed the characteristic peaks and structure of the collagen Type I [145-147]. These spectra revealed a

strong contribute of the substrate, since the chemical structure of the collagen was still clearly visible after the application of the coating. However, as highlighted by the reddish bands, an increase of the intensity of the peaks at 2925 and 2855 cm⁻¹ was observed between the untreated and the coated fish leather, especially in the fish leather with most of the coating on it (PESO 15). Indeed, these peaks were present also in Film, as explained above. As expected, the higher the amount of the coating on fish leather the higher the intensities of the peaks. The same behaviour can be observed for the peak at 1741 cm⁻¹, assigned to the stretching of C=O, visible both in the untreated and coated fish leather, with an increasing of its intensity with the increasing of the amount of the coating on fish leather. Both these results confirmed the presence of the coating on the fish leather.
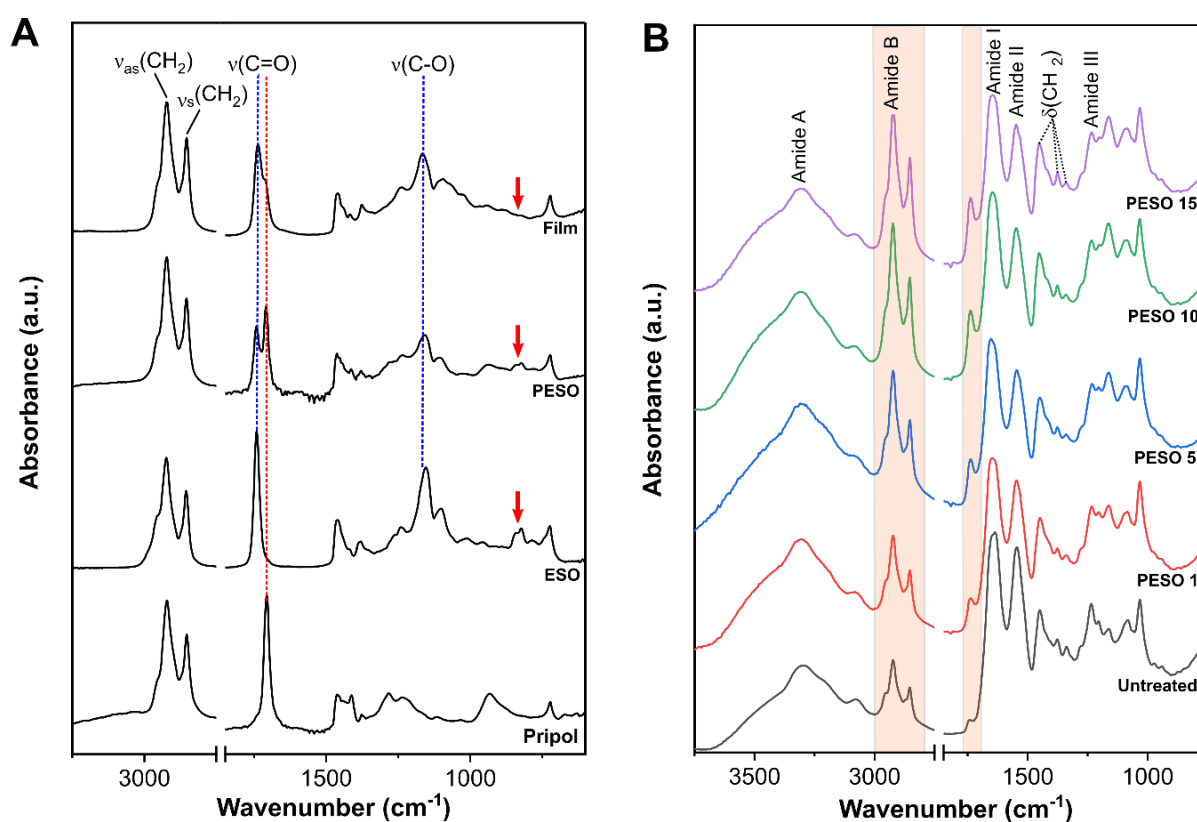

Figure 38. (A) ATR-FTIR spectra (from the bottom) of Pripol, ESO, PESO, and Film with the characteristic peaks of ESO (blue dotted line) and Pripol (red dotted line). Red arrows highlight the peaks related to the epoxy groups of ESO. (B) ATR-FTIR spectra (from the bottom) of untreated fish leather, PESO 1, PESO 5, PESO 10 and PESO 15 coating with all the characteristic peaks of collagen Type I. The reddish bands highlight the peaks at 2925, 2855 and 1741 cm⁻¹.

To further characterize the change in surface chemistry due to the coating, XPS was used, comparing the untreated and PESO 15 coated fish leather. The XPS spectrum related to the C 1s for the untreated and coated fish leather are reported in Figure 39A-B. From the analysis of the peak related to C 1s of the untreated fish leather three peaks were found and based on their binding energy were assigned to C=O (green), C-O (blue) and C-C (red). These

groups represented the functional groups that were expected to be found in the collagen Type I comprising the fish leather. The coated sample showed an additional group, O-C=O (in magenta in the graph) and a slight increase in the intensity of C-C and C-H peak. Both changes were signature of the presence of the coating, that is rich in O-C=O, C-C and C-H due to Pripol and ESO.
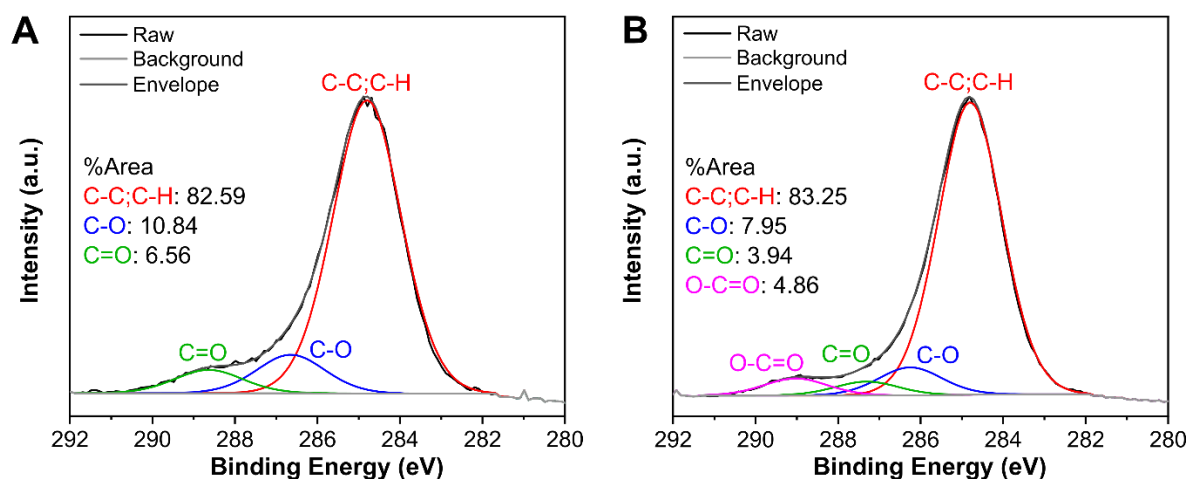

Figure 39. XPS spectra of C 1s for (A) untreated and (B) PESO 15 coated fish leather.

3.9.4. Water contact angle

The water contact angle (WCA) of untreated fish leather, PESO 1, PESO 5, PESO 10, PESO 15, Film and PTFE after 60 seconds is reported in Figure 40A. As can be noticed, untreated fish leather presented a hydrophilic behaviour with a WCA of ~ 80° whereas the coated fish leather, independently of the amount of the coating on it, presented a WCA of ~ 130°. Therefore, the coating made the fish leather hydrophobic, comparable with the PTFE that showed a WCA of ~ 110°. Furthermore, the WCA of Film was ~ 100°: the WCA of PESO 15 was higher due to the fibrillary microstructure of the surface of the FL, confirming that the coating was not a thick layer that changed the morphology of the substrate but rather conformal to it.

To demonstrate the water resistance effect of the coating on fish leather, the WCA of PESO 15 coating was monitored up to 40 min, using untreated fish leather, Film and PTFE as controls. Results are reported in Figure 40B. As can be noticed, untreated fish leather showed very briefly a high WCA, due to the fibrous nature of the leather. After only one minute, though, WCA already decreased down to 80°, after which there was complete absorption of the water and WCA dropped below the detection limit. On the other hand, PESO 15 showed a hydrophobic behaviour that lasted up to 40 minutes with a final WCA of ~ 100°. The Film sample was used as comparison with the coated leather. The WCA of the Film was ~ 100° after

60 seconds and decreased to ~ 80° after 40 minutes, showing a decrease similar to the PESO 15's. To understand the change of WCA with time, we compared PESO 15 with PTFE sheet. As expected, the PTFE showed a hydrophobic behaviour that was maintained throughout the experiment: a slight decrease of the WCA and of the droplet's volume was observed while the base diameter remained constant as reported in Figure 40C. These results were associated to the evaporation of the water as previously observed [164]. PESO 15 showed a change in WCA and droplet volume with the same trend in time, maintaining the same base diameter throughout the measurement as reported in Figure 40C. The same behaviour was observed for Film confirming that the coating materials can confer hydrophobic and water resistant properties, as PTFE (Figure 40C). Because of this we can explain that the changes in the WCA for PESO 15 were due to the evaporation of the water and not related to the absorption of water by the fish leather. Basing on this conclusion, the volume absorbed by PESO 15 was calculated by adding the volume of the evaporated water (deduced from the PTFE data) to the volume of the drops on PESO 15 previously showed in Figure 40C. As can be noticed, PESO 15 did not absorb water for up to 40 minutes, as also confirmed by the pictured of the drop at 0, 20 and 40 minutes, in Figure 40D. From these results, it can be concluded that PESO 15 coating was not only hydrophobic but also water resistant.

Same study was done for PESO 1, PESO 5, and PESO 10 coatings on fish leather. In particular, the WCA of these samples was monitored until complete absorption of the water and/or when WCA dropped below the detection limit (Figure 41A). Basing on the drop base diameter and volume (Figure 41B), it was concluded that PESO 1 did not give any water resistant effect to the leather, starting to absorb water in the first 5 minutes, while PESO 5 and PESO 10 maintained their hydrophobicity without absorbing any water until 15 and 25 minutes, respectively.

In conclusion, PESO 15 coating had got the best performance in terms of water resistance.
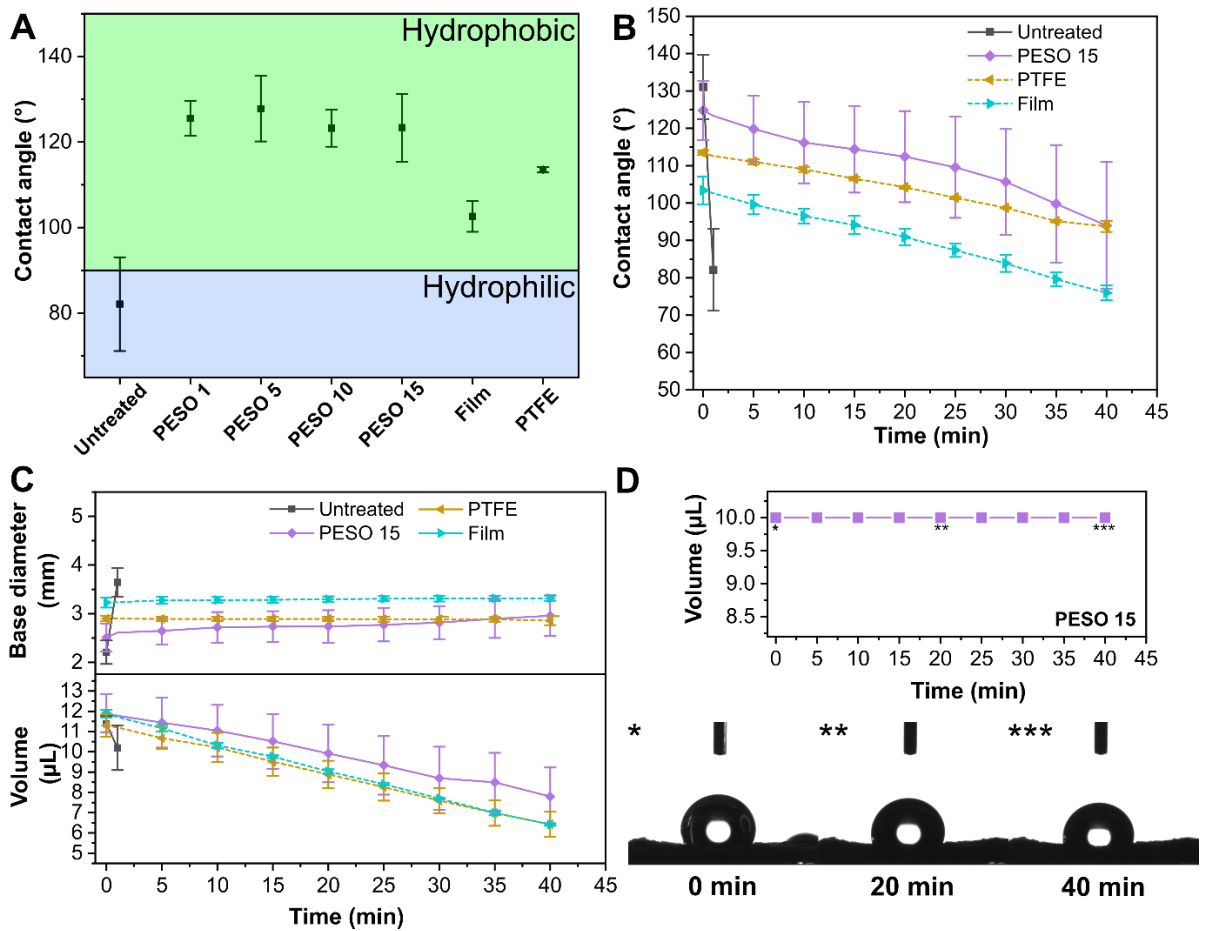
Figure 40. (A) WCA (°) of untreated fish leather, PESO 1, PESO 5, PESO 10, PESO 15, Film and PTFE after 60 s. (B) WCA (°) vs time (min) of untreated fish leather, PESO 15, Film and PTFE. (C) Drop base diameter (mm) and volume (μL) of untreated fish leather, PESO 15, Film and PTFE. (D) Drop volume (μL) vs time of PESO 15 with pictures of the drops on PESO 15 at 0, 20 and 40 minutes.
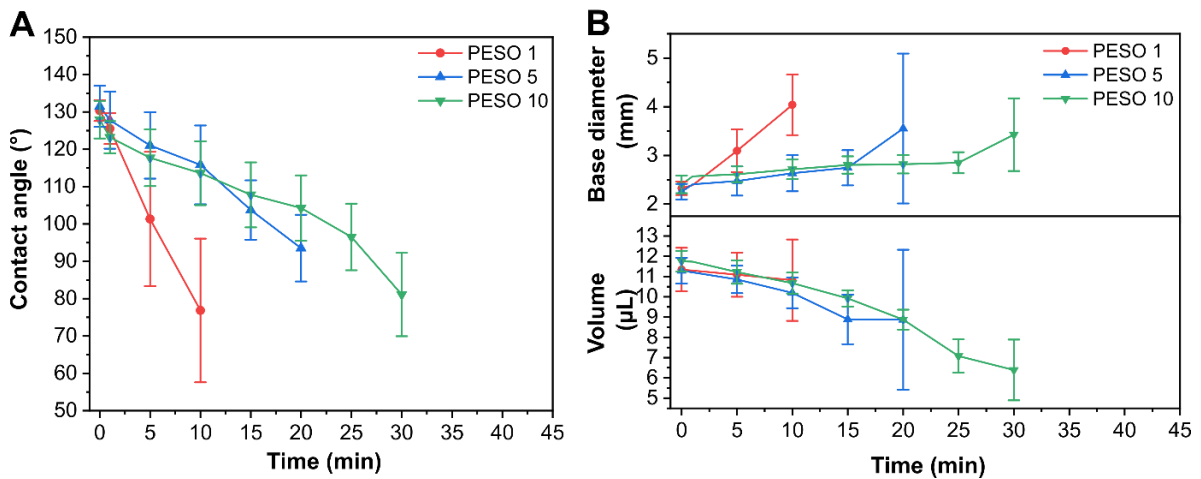
Figure 41. (A) WCA (°) vs time and (B) Drop base diameter (mm) and volume (μL) of PESO 1, PESO 5 and PESO 10.

3.9.5. Water uptake

Together with improved hydrophobicity and water resistance property, it was tested if the coating could offer protection from moisture absorption to the fish leather, thinking mainly of the storage of the material. Samples were conditioned at different relative humidities (% R.H.) and the water uptake was evaluated. Figure 42 reports the water uptake of untreated fish leather, PESO 1, PESO 5, PESO 10, PESO 15 coatings on fish leather, and a free standing film of the coating material (Film). As ca be observed, Film did not show an increase in mass, due to its hydrophobic and oil-based nature. Coated and untreated fish leather increased in mass when exposed to high relative humidity, due to moisture absorption, but the coated samples showed a reduced water absorption. For instance, the ANOVA test ($p < 0.05$) revealed that at 44 and 84 % R.H., two realistic humidity conditions, PESO 5, PESO 10 and PESO 15 protected the substrate from the moisture, reducing the absorption of water from 17% to 12% at 84 % R.H.
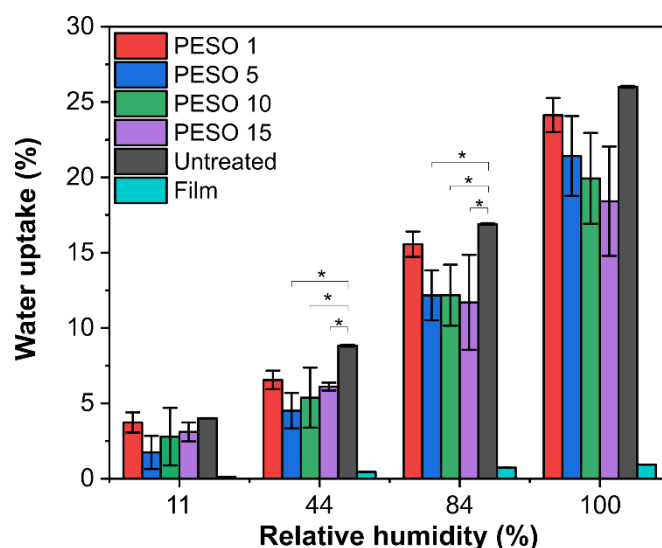

Figure 42. Water uptake (%) of untreated fish leather, PESO 1, PESO 5, PESO 10, PESO 15, and Film at different %R.H. * ANOVA test for $p < 0.05$.

3.9.6. Water vapor permeability

As mentioned, one of the appealing features of fish leather is its higher breathability, when compared to traditional leather, such as cow or goat leather. The breathability was evaluated in terms of WVP. To ensure that the coating did not affect this property, WVP of untreated fish leather was measured and compared with WVP of PESO 1, PESO 5, PESO 10, and PESO 15 coatings on fish leather. Results are reported in Figure 43. As can be noticed, the coating, from the one with the less amount of coating on it (PESO 1) to the one with the highest (PESO 15) did not affect the WVP, and, consequently, the breathability of the fish leather. In

particular, this result can be connected to the fact that the coating did not change the porosity and the microstructure of the substrate, as discussed later on.

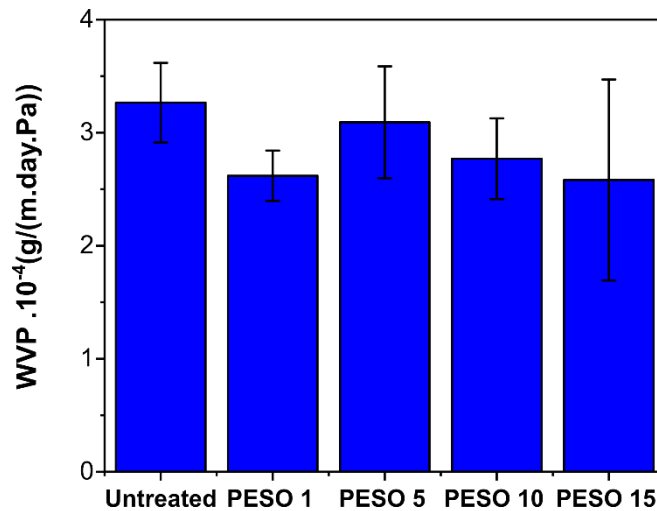**Figure 43.** WVP (g / m · day · Pa) of untreated fish leather, PESO 1, PESO 5, PESO 10, and PESO 15.

3.9.7. *Stability of the coating after washing*

Thinking of the application, it is desirable that the treatment that we developed for fish leather does not lose its functionality after soaking the material in water, to simulate a rainy day or washing. To investigate its stability, PESO 15, the best coating in terms of hydrophobicity and water resistance, was completely immersed in water for 24 hours, as shown in Figure 44A. Afterwards, the samples were kept out and left to dry for 24 hours, after which the WCA was measured. The results are reported in Figure 44B (WCA at 0 minutes) and Figure 44C (WCA at 40 minutes). As can be noticed, the contact angle at 0 minutes was ~ 130°, while at 40 minutes was ~ 90°. By comparing the behaviour of the PESO 15 with PTFE, it was noticed that, similarly as before, the change of WCA and of the drop volume with time was due to the evaporation of water and not absorption to the substrate. Furthermore, as highlighted by the red circles around the drops in the pictures, no capillarity effects were observed, demonstrating no absorption of the water by the coated samples. These results confirmed the stability of the coating functionality for fish leather after immersion for 24 hours in water. Practically, if the coated fish leather was wet after a heavy rain, the coating would continue to protect the leather after having dried it.
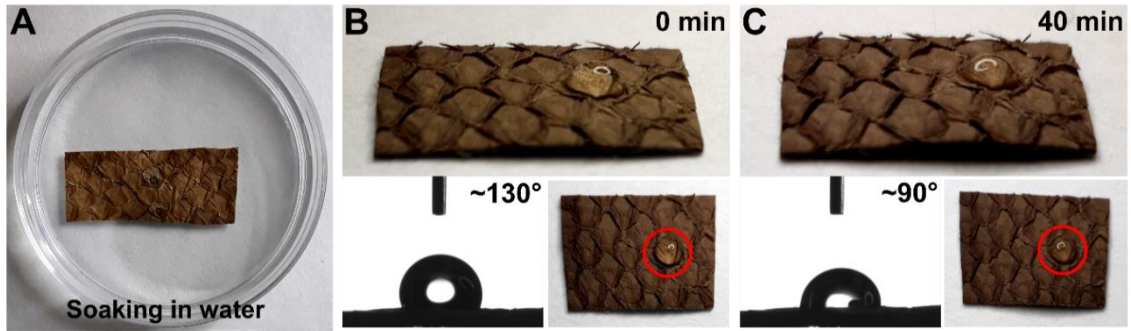
Figure 44. Evaluation of the stability of the coating functionality after washing with all the main steps: (A) soaking of PESO 15 in water for 24 hours to simulate the rain, WCA (°) with pictures of the drop at (B) 0 and (C) 40 minutes. Red circles highlighted no capillarity effects due to the absorption of the water by the substrate.

3.9.8. Morphological analysis

For the morphological analysis a comparison between the untreated fish leather and PESO 15 coating was conducted. PESO 15 was taken in consideration because it was the coating that demonstrated the best performances in terms of hydrophobicity and water resistance. Figure 45 reports the SEM images of the top-view of the untreated fish leather and PESO 15. As can be noticed, no evident changes in the surface microstructure were observed, confirming that the coating was not a thick layer applied on the top of the substrate, but was well adapted onto the fibers.
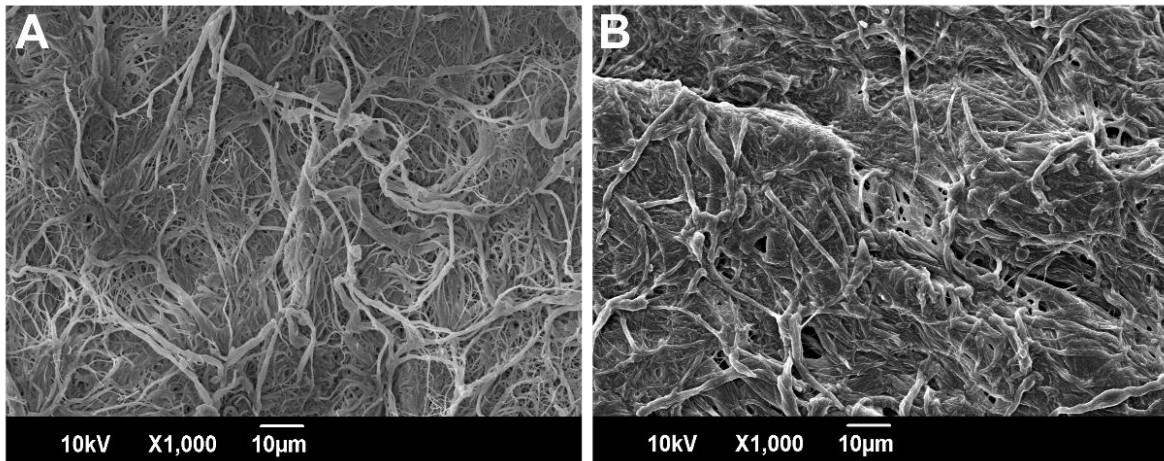
Figure 45. SEM images of the surface of (A) untreated fish leather and (B) PESO 15 coated fish leather.

To understand in which way the coating was distributed inside the fish leather, SEM images of the cross section of untreated fish leather and PESO 15 were acquired and compared, as reported in Figure 46A-B with x1000 magnification, and Figure 46D-E with x5000 magnification. As reported in Chapter 3, these images revealed that the untreated fish leather was comprised by a multi-layer structure in which each layer was a bundle of tanned collagen

fibers. In particular, the higher magnifications image showed that the single fibers were organized in smaller fibrils. This is the typical structure of collagen [165], the main component of the leather. From the comparison with PESO 15 images, no visible changes in the microstructure were observed, testifying the very thin layer of PESO deposited onto the fibrous leather.

In addition, to visualize the coating and its interaction with the substrate, a more concentrated coating was made using a 50 % wt PESO solution in ethyl acetate. The SEM images of the coating are reported in Figure 46C and Figure 46F. Compared to the untreated sample, a multi-layer structure, where the fibers were incorporated in the oily matrix, was visible. Moreover, higher magnifications of the collagen layers, revealed how the coating was deposited between each fiber but not in between the smaller fibrils.
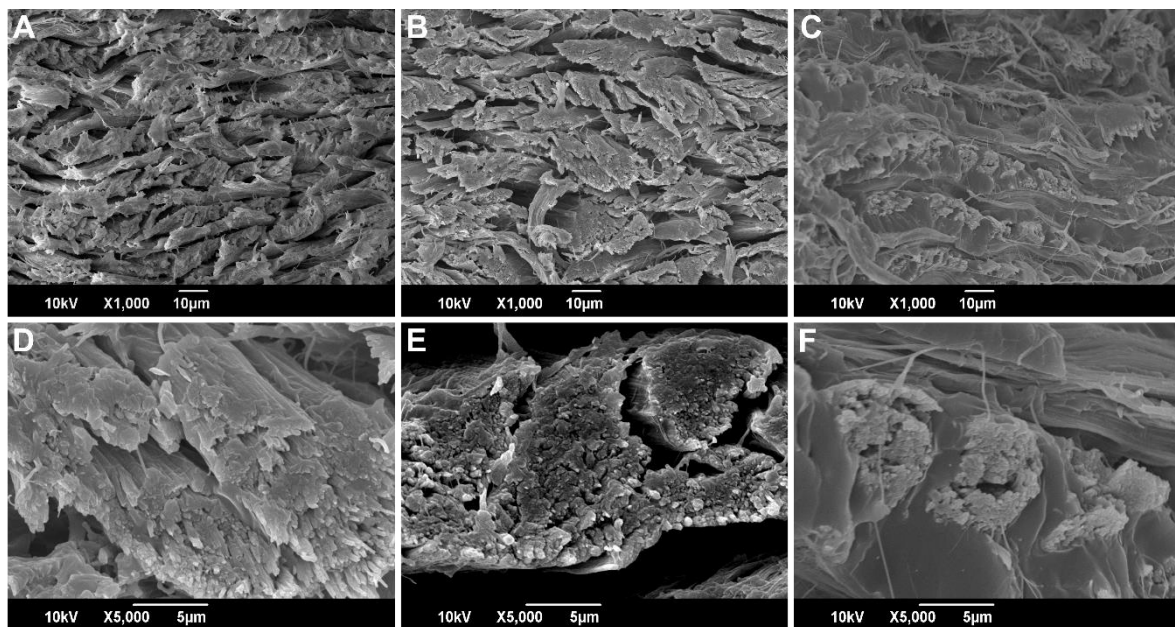
Figure 46. SEM images of the cross section with x1000 magnification of (A) untreated fish leather, (B) PESO 15 coating and (C) PESO 50 coating. SEM images of the cross section with x5000 magnification of (D) untreated fish leather, (E) PESO 15 coating and (F) PESO 50 coating.

3.9.9. *Mechanical characterization*

A part from breathability, from the point of view of the designers other interesting properties of fish leather respect to the traditional leather are the flexibility and softness, in terms of workability and final applications. For this reason, mechanical properties of untreated fish leather were evaluated and compared with PESO 1, PESO 5, PESO 10, and PESO 15 coatings on fish leather, as reported in Figure 47. From the stress-strain curves (Figure 47A), the untreated fish leather presented the typical trend of the collagen fibers [166] with three regions (dotted lines in the graph): toe, heel and linear. As reported by Gutmann et al., the toe

region is due to the removal of macroscopic crimps in the collagen fibrils, the heel region is caused by the reduction of the disorder in the lateral molecular packing, and the linear region is due to a stretching of collagen triple helices or of the crosslinks between helices [166]. As can be noticed, PESO 1 presented nearly the same behaviour as the untreated fish leather, therefore, the coating did not influence the mechanical properties of the substrate. On the other hand, PESO 5, PESO 10, and PESO 15 showed a new linear region (Linear 1) that was associated to the mechanical contribution of the coating, replacing the toe and heel regions. In Table 6, the modulus of the Linear 1 and Linear 2 (referred to the linear region previously cited, and associated to the fish leather) regions are reported for the different samples. As can be noticed, the moduli of the Linear 1 were the same without any significant difference (ANOVA test, $p < 0.05$), confirming that the Linear 1 region was determined by the coating on the substrate. Similarly, the ANOVA test did not show any significant difference between the moduli of Linear 2. The mechanical properties of the coating had a visible impact on the fish leather, hiding the contribution of the substrate in terms of toe and heels region. However, the presence of Linear 2 region confirmed that the fish leather maintained its flexibility even if in presence of the coating. Practically, this result was especially satisfying because the coated fish leather maintained its workability and softness. This result was also confirmed by the evaluation of the ductility in terms of the elongation at break (Figure 47B). The ANOVA test ($p < 0.05$) did not reveal any significant difference between the samples confirming that the coating, in the quantity deposited, did not change the ductility of the FL but it was determined solely by the substrate.

Sample	Linear 1 – Modulus ± s.d. (MPa) *	Linear 2 – Modulus ± s.d. (MPa) *
Untreated	-	38.99 ± 16.93
PESO 1	-	45.97 ± 18.83
PESO 5	55.12 ± 19.45	61.36 ± 15.13
PESO 10	51.38 ± 30.06	45.89 ± 21.90
PESO 15	55.94 ± 20.08	41.99 ± 13.31

Table 6. Modulus (MPa) of the two linear regions (Linear 1 and Linear 2) individuated by the stress-strain curves of untreated fish leather, PESO 1, PESO 5, PESO 10 and PESO 15. *ANOVA test ($p < 0.05$).
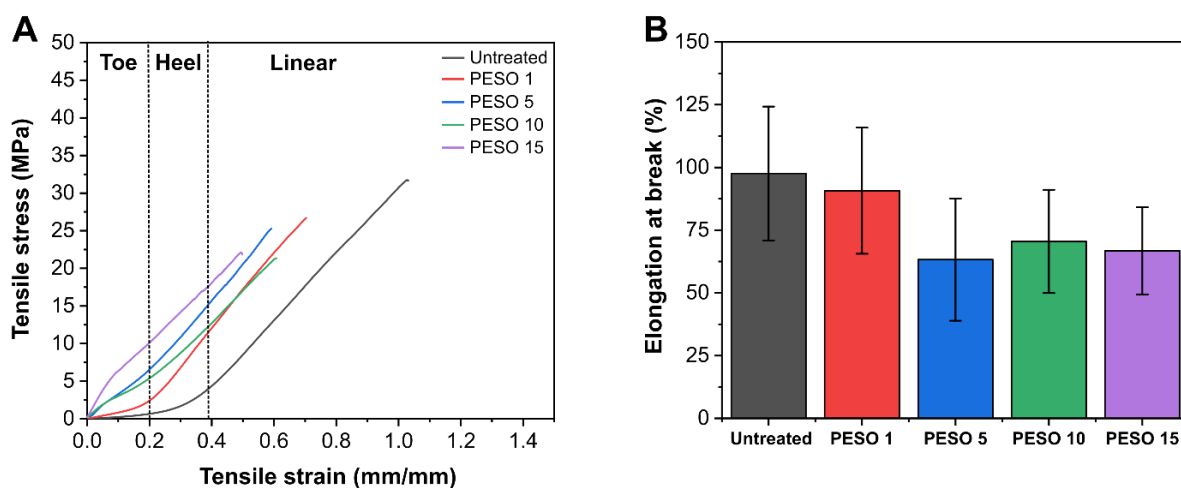
Figure 47. (A) Representative stress-strain curves and (B) elongation at break (%) of untreated fish leather, PESO 1, PESO 5, PESO 10, and PESO 15. ANOVA test was performed for $p < 0.05$.

3.9.10. Thermal characterization

The thermal stability of PESO 15 was evaluated and compared with two controls, untreated fish leather and Film, by TGA. The thermograms and the derivatives of weight loss curves are reported in Figure 48A-B, respectively. As can be noticed, untreated fish leather presented a two steps weight loss. The first peak was at 56 °C and presented a 10 % weight loss due to the loss of structural water bond, while the second one was at 315 °C and presented a 60 % weight loss due to the thermal destruction of the polypeptide chain [139]. On the other hand, PESO 15 coated fish leather presented four thermal peaks. The first two peaks were at the same temperatures as untreated fish leather, whereas the only difference was in the 3 % weight loss after the first peak comparing to the 10 % observed for the untreated fish leather. This fact might be explained with the fact that PESO coating reduced moisture absorption protecting the fish leather from thermal degradation at this early stage and, therefore, improving its thermal stability. The other two peaks were at 379 °C and 445 °C and were associated to the degradation of the coating as confirmed by Film's derivative thermogram, as previously observed for ESO [153].

Figure 48. (A) Mass loss and (B) derivatives of the thermograms of untreated fish leather, PESO 15 and Film.
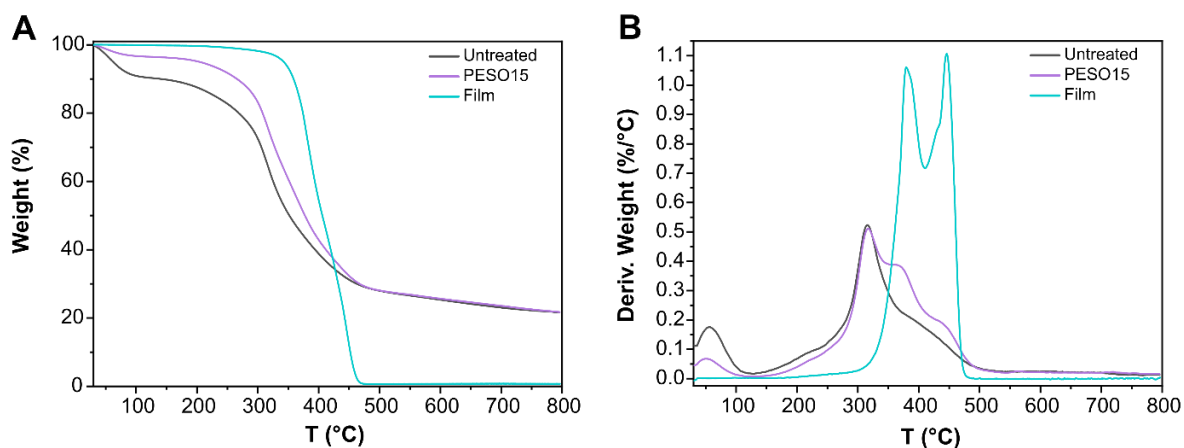
3.9.11. Application of the coating on cotton

As previously introduced, cotton fabrics are organized in weaved fibers made of cellulose, and, consequently, absorb rapidly the water, due to the hydroxyl functional groups. The state of the art about hydrophobic coating for cotton fabrics has been already discussed in Section 1.4. As previously described, most of the proposed and developed solutions to protect the cotton from water were allowed for a certain period (e.g. PDMS treatments) and then the usage of these monomers and molecules was considered fully or partially unsustainable for the environment or/and for the human health because of new regulamentation, as explained in Section 1.4. Most of the coating and treatments were fluorine, nanoparticles, or PDMS-based. For this reason, the epoxidized soybean oil-based coating, initially developed for fish leather, can be considered a possible solution to overcome the limitations of textiles, such as cotton fabrics, explained in details in Section 1.4. Since the successful results in terms of protection from water obtained by applying the coating on fish leather, its functionality was tested also on cotton. Therefore, PESO 15 coating was applied on cotton textile by following the same fabrication and curing steps developed for fish leather. This formulation was chosen because it resulted the best one for the fish leather since it protected it from water for longer. To verify the functionality of the coating on cotton, only some characterization techniques have been considered. In particular, they were: morphological analysis to investigate if and how the coating changed the cotton substrate, water contact angle measurement to see if the coating protected the cotton from water with similar results obtained for fish leather, and water vapour permeability to understand if the application of the coating affected the breathability of the cotton.

The microstructure of the surface and cross section of untreated and treated cotton samples was investigated by SEM, as reported in Figure 49. As can be noticed, the coating changed the colour of the cotton from white to yellowish without affecting its microstructure both the surface and cross-section into the inter-waved fibers. On the other hand, as shown in Figure 49D and highlighted by the red arrow, the coating was well visible around the cotton fiber by using x6000 magnification. These results gave information about the possible distribution of the coating around the single fiber or fibril of the fish leather substrate, since its complex structure did not allow to have precise information about it.
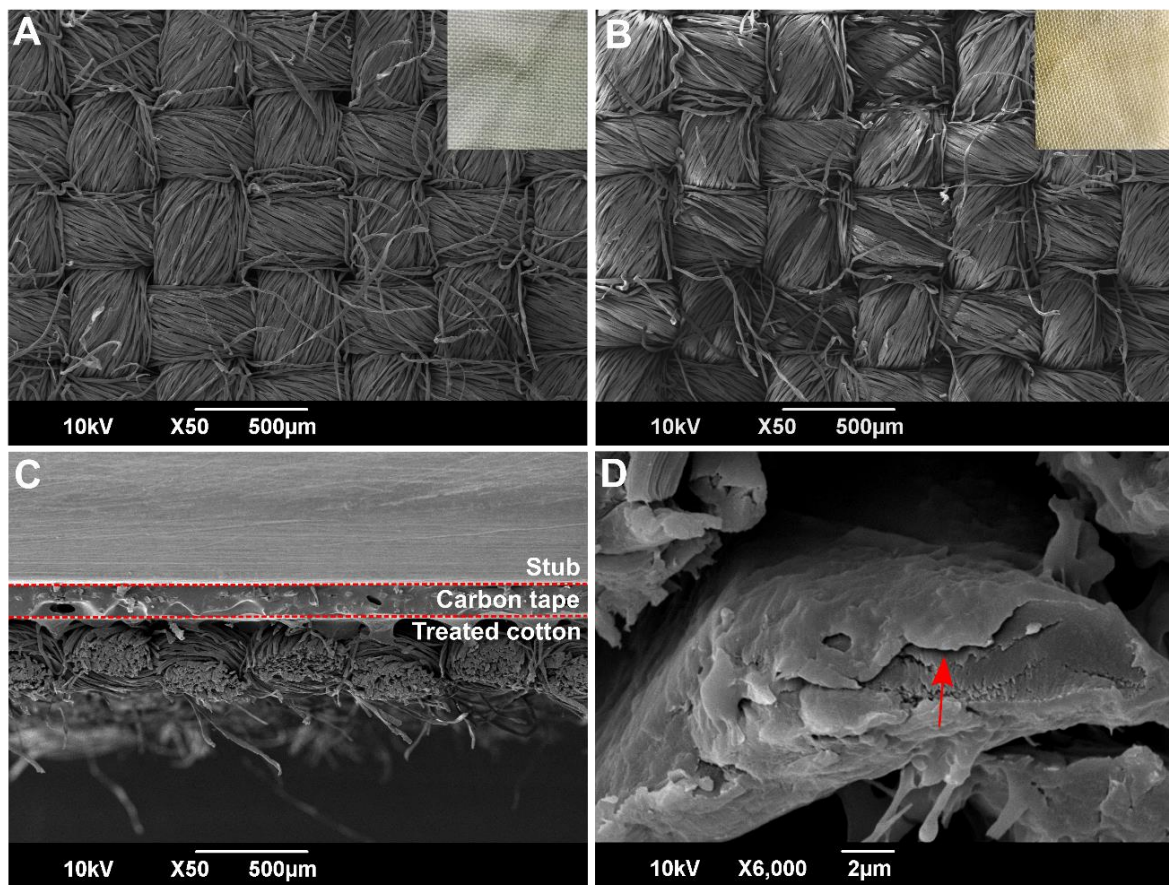
Figure 49. SEM images of the top view of the surface of (A) untreated and (B) treated cotton with attached pictures of respective sample. SEM images of the cross section of treated cotton at (C) x50 and (D) x6000 magnification. The red arrow highlights the coating as thin layer around the fiber.

Furthermore, to test the main functionality of the coating, the WCA of the treated cotton was measured. As expected, the untreated cotton revealed a hydrophilic behaviour with fast water absorption, whereas, as can be noticed in Figure 50, PESO 15 coating made the cotton hydrophobic with WCA of about 145 °. In addition, the hydrophobic behaviour was maintained by the coating up to 25 minutes, with a slight decrease of WCA to 136 °, while drop base diameter did not change up to 20 minutes. Therefore, the little decreasing of the drop's volume

was associated to water evaporation phenomenon until 20 minutes. Afterwards, the WCA decreased drastically becoming hydrophilic, as well as the drop's volume, while the drop's base diameter increased, demonstrating the water absorption by the sample. Therefore, the coating made the cotton water resistant up to 20 minutes, comparing to the 40 minutes of the treated fish leather. Possible explanations of this difference between the two substrates could be found, first of all, in the surface chemistry of cotton. As previously demonstrated by Mazzon et al. [167], the functional groups on the surface of cotton are due to the cellulose fibers that show mainly –OH groups, without carboxyl, amino, and thiol groups of collagen. Therefore, cotton has got less functional group, which the epoxide ring can react with, preferring, during the curing, a bond with the carboxyl groups of Pripol. The second reason stays in the roughness of the substrate: comparing the SEM images of the surface of the fish leather and of the cotton it can be noticed that the roughness of the fish leather is higher than the roughness of the cotton due to, for example, a different organization of the fibers. Therefore, it could be that the roughness helps in the water resistance preservation for more time. Last but not least, the thickness of the substrate can influence this feature: since the coating stays around the single fibers, in fish leather the number of fibers and complexity of inter-weaving give to the coating more available surface on which it can be adhere respect to cotton.
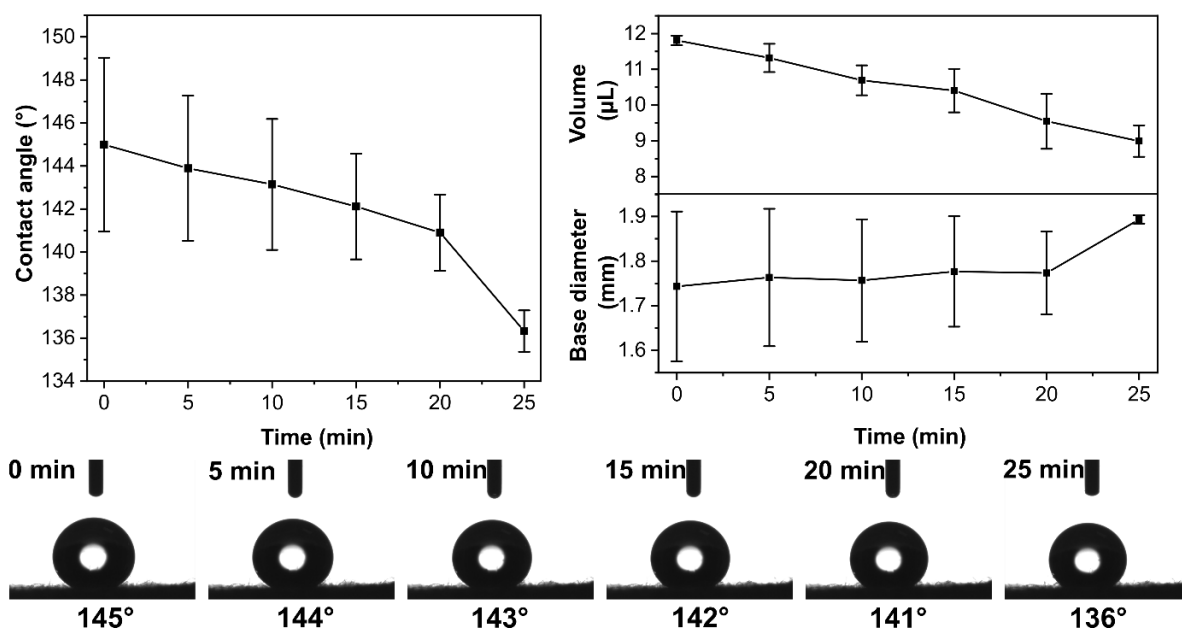
Figure 50. WCA (°), droplet's volume (µL) and base diameter (mm) vs time of PESO 15 coated cotton, with attached photos of the drop (10 µL) with the value of the respective contact angle every 5 minutes for 25 minutes.

Finally, also cotton is a very breathable substrate, therefore breathability of the coated cotton was evaluated in terms of WVP by using the previously described standard method, in order to understand if the coating affected the breathability of the cotton. Results are reported

in Table 7, demonstrating that the coating did not affect the breathability of the cotton, and presenting similar behaviour to polyurethane coating on cotton fabrics without changing the permeability of the substrate [167].

Sample	WVP $(g \cdot m^{-1} \cdot day^{-1} \cdot Pa^{-1})*$
Untreated	$(1.95 \pm 0.09) \cdot 10^{-4}$
Treated	$(2.08 \pm 0.07) \cdot 10^{-4}$

Table 7. WVP of untreated and treated cotton. * ANOVA test ($p<0.05$)

3.10. Coating: conclusions

In conclusion, a fully sustainable and by-product derived system and coating was developed, from the substrate to the coating materials, both food industry waste materials. In particular, epoxidized soybean oil and a sustainable trimer acid were applied as coating by dip coating and were successfully crosslinked after a certain period of curing in the oven without using toxic catalysts. The main functionalities of the coating in terms of protection of fish leather substrate from water and moisture were assessed. In particular, the WCA analysis demonstrated that the coating made the leather from hydrophilic to hydrophobic and water resistant up to 40 minutes, protecting it from the moisture at realistic humidity conditions. The WCA was around 130 °, result absolutely comparable with the WCAs reported in Section 3.5 for hydrophobic nanoparticles-based or PDMS-based coating for leather, even if no results about the water resistance were reported. Furthermore, as previously stated, fish leather has important features respect to the traditional leather, such as breathability, flexibility and softness. It was demonstrated that the coating did not affect its breathability, as well as its mechanical properties in terms of ductility and workability. This information was confirmed by SEM images where the coating was so thin that it was not distinguishable into the multi-layer fibrous structure of the fish leather. The hydrophobicity of the coating was demonstrated to be stable and preserved even after immersion in water of the coated leather. In addition, it was suitable also for a different textile substrate, such as cotton fabrics, obtaining a superhydrophobic behavior, similarly to the nanoparticles/PDMS-based treatments for cotton presented in Section 1.4, even if studies on their water resistance were not reported.

Conclusions

In conclusion, as previously stated, functional or multi-functional coatings can be useful in a wide range of applications, such as by decorating, protecting the substrate, and giving to it new functionalities. In addition, nowadays, one of the main trends in developing coatings is the environmental sustainability, for instance avoiding to use petroleum-derived materials, reducing the waste, and, more recently, selecting by-products as possible new range of materials. To give an example, chitosan, which is a bio-polymer and derives from an abundant food waste, shrimps and crabs' shells, is widely proposed in packaging applications to developed antimicrobial food coatings in order to extend the shelf life of the products and reducing the food spoilage. In this thesis work two examples of functional coatings were showed, both proposing a new solution for food packaging and implementing new circular economy systems.

In chapter 2, a sustainable polymer, PVAc-VL, and the strong antioxidant molecule, curcumin, were used together for the first time in order to develop a coating suitable not only for glass but also for natural substrate. Demonstrated properties of the coating, such as non toxicity of the implied materials, transparency to see the food through the package, UV filtering ability to preserve the food from light deterioration, and reduced bacterial adhesion to avoid the spreading of bacteria and extend the shelf life of the packaged food, were considered valuable for food packaging applications.

In chapter 3, two by-products of the food industry, salmon fish skin and soybean oil, were valorize for fashion industry applications. In particular, the epoxidized soybean oil was cross-linked with a sustainable trimer acid to protect the fish leather from water and moisture, without affecting its breathability and flexibility. This solution is considered a valuable alternative to fluorine-based or nanoparticles-based hydrophobic coatings, widely studied and reviewed, which are unsustainable.

The presented and developed systems are only an example of the wide range of applications and potentialities that functional or multi-functional coatings have, for instance reducing the produced waste or valorizing by-products of the industry, making our life and our impacts on the planet more sustainable.

Future perspective

As previously stated, coatings are very useful for our society, for instance for our health, safety, and comfort. For this reason they have a great impact on the environment for example by reducing the amount of produced energy to heat up or cool down buildings, or reducing the amount of waste that we produce in terms of food, electronics or textiles.

As future perspectives of this PhD work, multi-functional coatings and systems can be implemented. Regarding the first project, the developed composite coating presented a big issue, the resistance to high temperature. Due to the application in packaging, the migration standard test with Tenax was conducted at different temperature. It was noticed that the coating started the melting process at 60 °C, becoming sticky. Therefore, one future perspective for this work could be, first of all, to understand the behavior of the coating at different temperatures related to realistic packaging conditions, such as freezer (- 20 °C), fridge (+ 4 °C) or oven/microwave (40-200 °C). Various mechanical features or release behaviors of the filler might be observed per each considered temperature. For instance, the melting of the polymer at 60 °C could be solved by blending the PVAc-VL or creating a multi-layer structure with a more stable polymer. A further development could be the coating application directly on food, such as fresh vegetables and fruits as protection from external agents and pathogens: for instance, coated strawberries, or similar fruits/vegetables that are easily perishable, will be protected from smog and pollutants when exposed in a grocery shop on the road, or they will maintain their freshness longer. Of course, this will need, first of all, additional tests, such as migration tests following international and national standards and limits.

On the other hand, regarding the second project, again the possibilities are many. For instance, the additional antimicrobial or anti-molding property could be interesting since the coating will be in contact with human body, especially in case of clothes and shoes. In this case, different molecules and solutions can be taken in consideration, starting from the addition of an essential oil to the oil-based coating, widely demonstrated to be antioxidant and antimicrobial in the state of the art, or other antioxidant and antibacterial natural compounds. Or, improving the water resistant property of the coating on cotton might represent another possibility by simply making the crosslinking between cotton and coating stronger by, for instance, coating the cotton with collagen, increasing in this way the number of functional groups available in the substrate.

References

1.   Cunningham, M.F., et al., *Future green chemistry and sustainability needs in polymeric coatings.* Green Chemistry, 2019. **21**(18): p. 4919-4926.

2.   Valdes, A., et al., *State of the art of antimicrobial edible coatings for food packaging applications.* Coatings, 2017. **7**(4): p. 56.

3.   Chen, H., et al., *Application of protein-based films and coatings for food packaging: A review.* Polymers, 2019. **11**(12): p. 2039.

4.   Pourhashem, G., *Coating a Sustainable Future.* 2020, MDPI. p. 713.

5.   *FISHSKIN.*

6.   Joshi, S., et al., *Intensification of biodiesel production from soybean oil and waste cooking oil in the presence of heterogeneous catalyst using high speed homogenizer.* Ultrasonics Sonochemistry, 2017. **39**: p. 645-653.

7.   Qu, J., et al., *Transparent thermal insulation coatings for energy efficient glass windows and curtain walls.* Energy and Buildings, 2014. **77**: p. 1-10.

8.   Becker, P.F.B., C. Effting, and A. Schackow, *Lightweight thermal insulating coating mortars with aerogel, EPS, and vermiculite for energy conservation in buildings.* Cement and Concrete Composites, 2022. **125**: p. 104283.

9.   Dastjerdi, R., M. Montazer, and S. Shahsavan, *A novel technique for producing durable multifunctional textiles using nanocomposite coating.* Colloids and Surfaces B: Biointerfaces, 2010. **81**(1): p. 32-41.

10.   Mazzon, G., et al., *Antioxidant and hydrophobic Cotton fabric resisting accelerated ageing.* Colloids and Surfaces A: Physicochemical and Engineering Aspects, 2021. **613**: p. 126061.

11.   Zucchelli, M., et al., *Stone sustainable protection and preservation using a zein-based hydrophobic coating.* Progress in Organic Coatings, 2021. **159**: p. 106434.

12.   Lenzuni, M., et al., *Development of biodegradable zein-based bilayer coatings for drug-eluting stents.* RSC advances, 2021. **11**(39): p. 24345-24358.

13.   Francis, L.F. and C. Roberts, *Chapter 6-Dispersion and Solution Processes. Materials Processing.* 2016, Boston: Academic Press.

14.   Gigante, V., et al., *Liquid and Solid Functional Bio-Based Coatings.* Polymers, 2021. **13**(21): p. 3640.

15.   Vanderroost, M., et al., *Intelligent food packaging: The next generation.* Trends in food science & technology, 2014. **39**(1): p. 47-62.

16.   Arora, A. and G. Padua, *Nanocomposites in food packaging.* Journal of Food science, 2010. **75**(1): p. R43-R49.

17.   Parliament, E., *Directive (EU) 2019/904 of the European Parliament and of the Council of 5 June 2019 on the Reduction of the Impact of Certain Plastic Products on the Environment.* 2019.

18.   Nechita, P. and M. Roman, *Review on polysaccharides used in coatings for food packaging papers.* Coatings, 2020. **10**(6): p. 566.

19.   Cazón, P., et al., *Polysaccharide-based films and coatings for food packaging: A review.* Food Hydrocolloids, 2017. **68**: p. 136-148.

20.   Tanpichai, S., et al., *Chitosan coating for the preparation of multilayer coated paper for food-contact packaging: Wettability, mechanical properties, and overall migration.* International Journal of Biological Macromolecules, 2022. **213**: p. 534-545.

21.   Battisti, R., et al., *Gelatin-coated paper with antimicrobial and antioxidant effect for beef packaging.* Food Packaging and Shelf Life, 2017. **11**: p. 115-124.

22.   Schmid, M., et al., *Properties of whey-protein-coated films and laminates as novel recyclable food packaging materials with excellent barrier properties.* International Journal of Polymer Science, 2012. **2012**.

23.   Bang, G. and S.W. Kim, *Biodegradable poly (lactic acid)-based hybrid coating materials for food packaging films with gas barrier properties.* Journal of Industrial and Engineering Chemistry, 2012. **18**(3): p. 1063-1068.

24.   Ozcalik, O. and F. Tihminlioglu, *Barrier properties of corn zein nanocomposite coated polypropylene films for food packaging applications.* Journal of Food Engineering, 2013. **114**(4): p. 505-513.

25.   Al-Naamani, L., S. Dobretsov, and J. Dutta, *Chitosan-zinc oxide nanoparticle composite coating for active food packaging applications.* Innovative Food Science & Emerging Technologies, 2016. **38**: p. 231-237.

26.   Munteanu, B.S., et al., *Antioxidant/antibacterial electrospun nanocoatings applied onto PLA films.* Materials, 2018. **11**(10): p. 1973.

27.   Bastarrachea, L.J., et al., *Active packaging coatings.* Coatings, 2015. **5**(4): p. 771-791.

28.   Zahid, M., et al., *Environmentally benign non-wettable textile treatments: A review of recent state-of-the-art.* Advances in Colloid and Interface Science, 2019. **270**: p. 216-250.

29. Jiang, J., et al., *Novel fluorinated polymers containing short perfluorobutyl side chains and their super wetting performance on diverse substrates.* ACS applied materials & interfaces, 2016. **8**(16): p. 10513-10523.

30. Cai, L., et al., *Synthesis of novel polymethacrylates with siloxyl bridging perfluoroalkyl side-chains for hydrophobic application on cotton fabrics.* Applied Surface Science, 2016. **371**: p. 453-467.

31. Freberg, B.I., et al., *Occupational exposure to airborne perfluorinated compounds during professional ski waxing.* Environmental science & technology, 2010. **44**(19): p. 7723-7728.

32. Zahid, M., et al., *Robust water repellent treatment for woven cotton fabrics with eco-friendly polymers.* Chemical Engineering Journal, 2017. **319**: p. 321-332.

33. Wang, Q., et al., *Fluorine-free superhydrophobic coatings from polydimethylsiloxane for sustainable chemical engineering: Preparation methods and applications.* Chemical Engineering Journal, 2021. **426**: p. 130829.

34. Yin, Y., et al., *Superhydrophobic–superhydrophilic switchable wettability via TiO2 photoinduction electrochemical deposition on cellulose substrate.* Chemical Engineering Journal, 2016. **289**: p. 99-105.

35. Zhu, T., et al., *Rational design of multi-layered superhydrophobic coating on cotton fabrics for UV shielding, self-cleaning and oil-water separation.* Materials & Design, 2017. **134**: p. 342-351.

36. Kadam, V., et al., *Waste management in coated and laminated textiles.* Waste Management in the Fashion and Textile Industries, 2021: p. 215-231.

37. Cheng, Q.-Y., et al., *Cellulose nanocrystal coated cotton fabric with superhydrophobicity for efficient oil/water separation.* Carbohydrate polymers, 2018. **199**: p. 390-396.

38. Dong, X., et al., *A self-roughened and biodegradable superhydrophobic coating with UV shielding, solar-induced self-healing and versatile oil–water separation ability.* Journal of materials chemistry A, 2019. **7**(5): p. 2122-2128.

39. Cheng, Q.-Y., et al., *Fully sustainable, nanoparticle-free, fluorine-free, and robust superhydrophobic cotton fabric fabricated via an eco-friendly method for efficient oil/water separation.* ACS Sustainable Chemistry & Engineering, 2019. **7**(18): p. 15696-15705.

40.   Cheng, Q.-Y., et al., *Robust and nanoparticle-free superhydrophobic cotton fabric fabricated from all biological resources for oil/water separation.* International journal of biological macromolecules, 2019. **140**: p. 1175-1182.

41.   Deshwal, G.K., N.R. Panjagari, and T. Alam, *An overview of paper and paper based food packaging materials: health safety and environmental concerns.* Journal of food science and technology, 2019. **56**(10): p. 4391-4403.

42.   Li, Z., et al., *A closed-loop and sustainable approach for the fabrication of plastic-free oil-and water-resistant paper products.* Green Chemistry, 2019. **21**(20): p. 5691-5700.

43.   Parvathy, P. and S.K. Sahoo, *Hydrophobic, moisture resistant and biorenewable paper coating derived from castor oil based epoxy methyl ricinoleate with repulpable potential.* Progress in Organic Coatings, 2021. **158**: p. 106347.

44.   Thakur, S., M. Misra, and A.K. Mohanty, *Sustainable hydrophobic and moisture-resistant coating derived from downstream corn oil.* ACS Sustainable Chemistry & Engineering, 2019. **7**(9): p. 8766-8774.

45.   Li, Z., M. Rabnawaz, and B. Khan, *Response surface methodology design for biobased and sustainable coatings for water-and oil-resistant paper.* ACS Applied Polymer Materials, 2020. **2**(3): p. 1378-1387.

46.   Lavrov, N., *Vinyl acetate copolymer-based adhesive materials.* Polymer Science Series C, 2007. **49**(3): p. 255-257.

47.   Zhang, N., et al., *Application of Polyvinyl Acetate/Lignin Copolymer as Bio-Based Coating Material and Its Effects on Paper Properties.* Coatings, 2021. **11**(2): p. 192.

48.   Liauw, C.M., et al., *The effect of surface hydrophobicity on the attachment of fungal conidia to substrates of polyvinyl acetate and polyvinyl alcohol.* Journal of Polymers and the Environment, 2020. **28**(5): p. 1450-1464.

49.   Zhang, N., et al., *The copolymer of polyvinyl acetate containing lignin-vinyl acetate monomer: Synthesis and characterization.* European Polymer Journal, 2020. **123**: p. 109411.

50.   Kaboorani, A., et al., *Nanocrystalline cellulose (NCC): A renewable nano-material for polyvinyl acetate (PVA) adhesive.* European Polymer Journal, 2012. **48**(11): p. 1829-1837.

51.   Friis, N. and A. Hamielec, *Kinetics of vinyl chloride and vinyl acetate emulsion polymerization.* Journal of Applied Polymer Science, 1975. **19**(1): p. 97-113.

52. Grassie, N., I. McLean, and I. McNeill, *Thermal degradation of vinyl chloride-vinyl acetate copolymers—I. Bulk degradation studies by thermal volatilization analysis.* European Polymer Journal, 1970. **6**(5): p. 679-686.

53. Brar, A. and S. Charan, *Sequence determination of vinyl acetate–methyl acrylate copolymers by NMR spectroscopy.* Journal of applied polymer science, 1994. **53**(13): p. 1813-1822.

54. Duquesne, S., et al., *Vinyl acetate/butyl acrylate copolymers—part 1: mechanism of degradation.* Polymer degradation and stability, 2004. **83**(1): p. 19-28.

55. Stark, W. and M. Jaunich, *Investigation of Ethylene/Vinyl Acetate Copolymer (EVA) by thermal analysis DSC and DMA.* Polymer Testing, 2011. **30**(2): p. 236-242.

56. Schneider, C., et al., *Applications of ethylene vinyl acetate copolymers (EVA) in drug delivery systems.* Journal of Controlled Release, 2017. **262**: p. 284-295.

57. Chaabouni, O. and S. Boufi, *Cellulose nanofibrils/polyvinyl acetate nanocomposite adhesives with improved mechanical properties.* Carbohydrate polymers, 2017. **156**: p. 64-70.

58. Samaha, S., H. Nasr, and A. Hebeish, *Synthesis and characterization of starch-poly (vinyl acetate) graft copolymers and their saponified form.* Journal of Polymer Research, 2005. **12**(5): p. 343-353.

59. Chen, L., et al., *Synthesis and characterization of starch-g-poly (vinyl acetate-co-butyl acrylate) bio-based adhesive for wood application.* International journal of biological macromolecules, 2018. **114**: p. 1186-1193.

60. Don, T.-M., C.-F. King, and W.-Y. Chiu, *Preparation of chitosan-graft-poly (vinyl acetate) copolymers and their adsorption of copper ion.* Polymer journal, 2002. **34**(6): p. 418-425.

61. Silva, M., et al., *Characterization of poly (vinyl acetate)/sugar cane bagasse lignin blends and their photochemical degradation.* Journal of thermal analysis and calorimetry, 2011. **106**(2): p. 407-413.

62. Mormann, W. and M. Al-Higari, *Acylation of starch with vinyl acetate in water.* Starch-Stärke, 2004. **56**(3-4): p. 118-121.

63. Junistia, L., et al., *Synthesis of higher fatty acid starch esters using vinyl laurate and stearate as reactants.* Starch-Stärke, 2008. **60**(12): p. 667-675.

64. Lina, B.A., H. Messinger, and A. Bär, *13-week oral toxicity study of vinyl laurate in rats.* Regulatory Toxicology and Pharmacology, 2015. **71**(1): p. 101-107.

65.   Messinger, H. and A. Bär, *Subchronic toxicity, toxicity to reproduction and prenatal developmental toxicity of vinyl laurate.* Regulatory Toxicology and Pharmacology, 2014. **70**(1): p. 80-86.

66.   Kraisomdet, P., et al., *Amphiphilic dextran-vinyl laurate-based nanoparticles: formation, characterization, encapsulation, and cytotoxicity on human intestinal cell line.* Progress in biomaterials, 2020: p. 1-9.

67.   Sun, S., et al., *A thermoresponsive chitosan− NIPAAm/vinyl laurate copolymer vector for gene transfection.* Bioconjugate chemistry, 2005. **16**(4): p. 972-980.

68.   Abidi, N. and E. Hequet, *Cotton fabric graft copolymerization using microwave plasma. II. Physical properties.* Journal of applied polymer science, 2005. **98**(2): p. 896-902.

69.   Benee, L., M. Snowden, and B. Chowdhry, *Novel gelling behavior of poly (N-isopropylacrylamide-co-vinyl laurate) microgel dispersions.* Langmuir, 2002. **18**(16): p. 6025-6030.

70.   Aldakkan, B.S., et al., *Stimuli-Responsive, Hydrolyzable Poly (Vinyl Laurate-co-vinyl Acetate) Nanoparticle Platform for In Situ Release of Surfactants.* ACS Applied Materials & Interfaces, 2021.

71.   *Amended Final Safety Assessment of Polyvinyl Acetate.* Journal of the American College of Toxicology, 1996. **15**(2): p. 166-176.

72.   *Commission Regulation (EU) No 10/2011.* 14 January 2011.

73.   Kim, D.-C., S.-K. Ku, and J.-S. Bae, *Anticoagulant activities of curcumin and its derivative.* BMB reports, 2012. **45**(4): p. 221-226.

74.   Kulkarni, S., A. Dhir, and K.K. Akula, *Potentials of curcumin as an antidepressant.* TheScientificWorldJOURNAL, 2009. **9**: p. 1233-1241.

75.   Virk, R.S., et al., *Curcumin-Containing Orthopedic Implant Coatings Deposited on Poly-Ether-Ether-Ketone/Bioactive Glass/Hexagonal Boron Nitride Layers by Electrophoretic Deposition.* Coatings, 2019. **9**(9): p. 572.

76.   Murgia, D., et al., *Development of a Multifunctional Bioerodible Nanocomposite Containing Metronidazole and Curcumin to Apply on L-PRF Clot to Promote Tissue Regeneration in Dentistry.* Biomedicines, 2020. **8**(10): p. 425.

77.   Aggarwal, B.B., A. Kumar, and A.C. Bharti, *Anticancer potential of curcumin: preclinical and clinical studies.* Anticancer research, 2003. **23**(1/A): p. 363-398.

78. Wilken, R., et al., *Curcumin: A review of anti-cancer properties and therapeutic activity in head and neck squamous cell carcinoma.* Molecular cancer, 2011. **10**(1): p. 1-19.

79. Khorasani, M.Y., et al., *The role of curcumin and its derivatives in sensory applications.* Materials Science and Engineering: C, 2019. **103**: p. 109792.

80. Ak, T. and İ. Gülçin, *Antioxidant and radical scavenging properties of curcumin.* Chemico-biological interactions, 2008. **174**(1): p. 27-37.

81. Teow, S.-Y., et al., *Antibacterial action of curcumin against Staphylococcus aureus: a brief review.* Journal of tropical medicine, 2016. **2016**.

82. Tyagi, P., et al., *Bactericidal activity of curcumin I is associated with damaging of bacterial membrane.* PloS one, 2015. **10**(3): p. e0121313.

83. Zia, J., et al., *Low-density polyethylene/curcumin melt extruded composites with enhanced water vapor barrier and antioxidant properties for active food packaging.* Polymer, 2019. **175**: p. 137-145.

84. Roy, S. and J.-W. Rhim, *Preparation of carbohydrate-based functional composite films incorporated with curcumin.* Food Hydrocolloids, 2020. **98**: p. 105302.

85. Roy, S. and J.-W. Rhim, *Preparation of antimicrobial and antioxidant gelatin/curcumin composite films for active food packaging application.* Colloids and Surfaces B: Biointerfaces, 2020. **188**: p. 110761.

86. Roy, S. and J.-W. Rhim, *Preparation of bioactive functional poly (lactic acid)/curcumin composite film for food packaging application.* International Journal of Biological Macromolecules, 2020. **162**: p. 1780-1789.

87. Nieto-Suaza, L., et al., *Characterization of Aloe vera-banana starch composite films reinforced with curcumin-loaded starch nanoparticles.* Food Structure, 2019. **22**: p. 100131.

88. Chen, H.-z., et al., *Novel pH-sensitive films containing curcumin and anthocyanins to monitor fish freshness.* Food Hydrocolloids, 2020. **100**: p. 105438.

89. Quilez-Molina, A.I., et al., *Responsive Bio-Composites from Magnesium Carbonate Filled Polycaprolactone and Curcumin-Functionalized Cellulose Fibers.* Advanced Sustainable Systems, 2021. **5**(10): p. 2100128.

90. Ghosh, T., K. Nakano, and V. Katiyar, *Curcumin doped functionalized cellulose nanofibers based edible chitosan coating on kiwifruits.* International Journal of Biological Macromolecules, 2021. **184**: p. 936-945.

91. Alehosseini, A., et al., *Electrospun curcumin-loaded protein nanofiber mats as active/bioactive coatings for food packaging applications.* Food Hydrocolloids, 2019. **87**: p. 758-771.

92. Chen, L., et al., *Photoinduced antimicrobial activity of curcumin-containing coatings: Molecular interaction, stability and potential application in food decontamination.* ACS omega, 2020. **5**(48): p. 31044-31054.

93. Heredia-Guerrero, J.A., et al., *All-natural sustainable packaging materials inspired by plant cuticles.* Advanced Sustainable Systems, 2017. **1**(1-2): p. 1600024.

94. Oleyaei, S.A., et al., *Synergistic reinforcing effect of TiO2 and montmorillonite on potato starch nanocomposite films: thermal, mechanical and barrier properties.* Carbohydrate Polymers, 2016. **152**: p. 253-262.

95. Hirschler, R., *Whiteness, yellowness, and browning in food colorimetry: a critical review.* Color in food, 2012: p. 118-129.

96. Lee, M.H., S.Y. Kim, and H.J. Park, *Effect of halloysite nanoclay on the physical, mechanical, and antioxidant properties of chitosan films incorporated with clove essential oil.* Food Hydrocolloids, 2018. **84**: p. 58-67.

97. Ezati, P. and J.-W. Rhim, *pH-responsive chitosan-based film incorporated with alizarin for intelligent packaging applications.* Food Hydrocolloids, 2020. **102**: p. 105629.

98. Hwang, G.B., et al., *The anti-biofouling properties of superhydrophobic surfaces are short-lived.* ACS nano, 2018. **12**(6): p. 6050-6058.

99. Naderizadeh, S., et al., *Bioresin-based superhydrophobic coatings with reduced bacterial adhesion.* Journal of colloid and interface science, 2020. **574**: p. 20-32.

100. Ke, N., et al., *The xCELLigence system for real-time and label-free monitoring of cell viability*, in *Mammalian cell viability*. 2011, Springer. p. 33-43.

101. López-Tobar, E., et al., *Encapsulation and isomerization of curcumin with cyclodextrins characterized by electronic and vibrational spectroscopy.* Vibrational Spectroscopy, 2012. **62**: p. 292-298.

102. Liu, X., et al., *Protective effect of curcumin against ultraviolet A irradiation-induced photoaging in human dermal fibroblasts.* Molecular medicine reports, 2018. **17**(5): p. 7227-7237.

103. Li, H., et al., *Protective effect of curcumin against acute ultraviolet B irradiation-induced photo-damage.* Photochemistry and Photobiology, 2016. **92**(6): p. 808-815.

104. Quilez-Molina, A.I., et al., *UV-blocking, transparent, and antioxidant polycyanoacrylate films.* Polymers, 2020. **12**(9): p. 2011.

105. Wei, S., V. Pintus, and M. Schreiner, *Photochemical degradation study of polyvinyl acetate paints used in artworks by Py–GC/MS.* Journal of analytical and applied pyrolysis, 2012. **97**: p. 158-163.

106. Hu, K., et al., *Core–shell biopolymer nanoparticle delivery systems: Synthesis and characterization of curcumin fortified zein–pectin nanoparticles.* Food chemistry, 2015. **182**: p. 275-281.

107. Kolev, T.M., et al., *DFT and experimental studies of the structure and vibrational spectra of curcumin.* International Journal of Quantum Chemistry, 2005. **102**(6): p. 1069-1079.

108. Daemi, H. and M. Barikani, *Synthesis and characterization of calcium alginate nanoparticles, sodium homopolymannuronate salt and its calcium nanoparticles.* Scientia Iranica, 2012. **19**(6): p. 2023-2028.

109. Jejurikar, A., et al., *Degradable alginate hydrogels crosslinked by the macromolecular crosslinker alginate dialdehyde.* Journal of Materials Chemistry, 2012. **22**(19): p. 9751-9758.

110. Cai, L., et al., *Characterization of gelatin/chitosan ploymer films integrated with docosahexaenoic acids fabricated by different methods.* Scientific reports, 2019. **9**(1): p. 1-11.

111. Salerno, M., *Improved estimation of contact compliance via atomic force microscopy using a calibrated cantilever as a reference sample.* Measurement, 2012. **45**(8): p. 2103-2113.

112. Said, N.S. and N.M. Sarbon, *Physical and mechanical characteristics of gelatin-based films as a potential food packaging material: a review.* Membranes, 2022. **12**(5): p. 442.

113. Rhim, J.-W., *Physical and mechanical properties of water resistant sodium alginate films.* LWT-Food science and technology, 2004. **37**(3): p. 323-330.

114. Tedeschi, G., et al., *Sustainable fabrication of plant cuticle-like packaging films from tomato pomace agro-waste, beeswax, and alginate.* ACS Sustainable Chemistry & Engineering, 2018. **6**(11): p. 14955-14966.

115. Pulla-Huillca, P.V., et al., *Wettability of gelatin-based films: The effects of hydrophilic or hydrophobic plasticizers and nanoparticle loads.* Journal of Food Engineering, 2021. **297**: p. 110480.

116. Mun, S.-H., et al., *Synergistic antibacterial effect of curcumin against methicillin-resistant Staphylococcus aureus.* Phytomedicine, 2013. **20**(8-9): p. 714-718.

117.   Yun, D.G. and D.G. Lee, *Antibacterial activity of curcumin via apoptosis-like response in Escherichia coli.* Applied microbiology and biotechnology, 2016. **100**(12): p. 5505-5514.

118.   Wang, H., et al., *Release kinetics and antibacterial activity of curcumin loaded zein fibers.* Food Hydrocolloids, 2017. **63**: p. 437-446.

119.   Jayapal, K.P., et al., *Recombinant protein therapeutics from CHO cells-20 years and counting.* Chemical engineering progress, 2007. **103**(10): p. 40.

120.   Wagner, E.D. and M.J. Plewa, *CHO cell cytotoxicity and genotoxicity analyses of disinfection by-products: an updated review.* Journal of Environmental Sciences, 2017. **58**: p. 64-76.

121.   Frühe, L., et al., *Supervised machine learning is superior to indicator value inference in monitoring the environmental impacts of salmon aquaculture using eDNA metabarcodes.* Molecular Ecology, 2021. **30**(13): p. 2988-3006.

122.   Burridge, L., et al., *Chemical use in salmon aquaculture: a review of current practices and possible environmental effects.* Aquaculture, 2010. **306**(1-4): p. 7-23.

123.   Taranger, G.L., et al., *Risk assessment of the environmental impact of Norwegian Atlantic salmon farming.* ICES Journal of Marine Science, 2015. **72**(3): p. 997-1021.

124.   Ramírez, A., *Salmon by-product proteins*. 2007: FAO.

125.   Fraga-Corral, M., et al., *Aquaculture as a circular bio-economy model with Galicia as a study case: How to transform waste into revalorized by-products.* Trends in Food Science & Technology, 2022. **119**: p. 23-35.

126.   Palomino, E. and G. Defeo, *Material Design Innovation: Fish Leather, a new environmentally friendly material.* 2018.

127.   Alla, J., et al., *Fish skin and exotic leathers.* Journal of the American Leather Chemists Association, 2017. **112**(02): p. 36-43.

128.   Hsia, C. *The Importance of Leather: How Fish Skin Leather Can Help Reduce Waste in a Seafood System.* 2021 10/24/2022]; Available from: https://www.fishfulfuture.com/blog/fish-skin-leather.

129.   Boström, M. and M. Micheletti, *Introducing the sustainability challenge of textiles and clothing.* Journal of Consumer Policy, 2016. **39**(4): p. 367-375.

130.   Tyagi, P.K. and G. Mukherjee, *A Step Towards Cleaner Production: Chrome Free Tanning: A Review.* Journal of Huazhong University of Science and Technology ISSN. **1671**: p. 4512.

131.   Sherman, V.R., W. Yang, and M.A. Meyers, *The materials science of collagen.* Journal of the mechanical behavior of biomedical materials, 2015. **52**: p. 22-50.

132.   Ma, J., et al., *A facile spraying method for fabricating superhydrophobic leather coating.* Colloids and Surfaces A: Physicochemical and Engineering Aspects, 2015. **472**: p. 21-25.

133.   Serenko, O., et al., *Effect of the morphology of leather surface on the hydrophobic-hydrophilic properties.* Advances in Materials Physics and Chemistry, 2014. **2014**.

134.   Wairimu, P.M., E.W. Nthiga, and M.A. Ollengo, *The structural and chemical properties of the nile perch fish leather.* 2020.

135.   Júnior, Z.S.S., et al., *Effect of papain-based gel on type I collagen-spectroscopy applied for microstructural analysis.* Scientific reports, 2015. **5**(1): p. 1-7.

136.   Xiao, H., G. Cai, and M. Liu, *Hydroxyl radical induced structural changes of collagen.* Spectroscopy, 2007. **21**(2): p. 91-103.

137.   Sanden, K.W., et al., *The use of Fourier-transform infrared spectroscopy to characterize connective tissue components in skeletal muscle of Atlantic cod (Gadus morhua L.).* Journal of biophotonics, 2019. **12**(9): p. e201800436.

138.   Onem, E., et al., *Comparison of different tanning agents on the stabilization of collagen via differential scanning calorimetry.* Journal of Thermal Analysis and Calorimetry, 2017. **129**: p. 615-622.

139.   Ramanathan, G., et al., *Extraction and characterization of collagen from the skin of Arothron stellatus fish—A novel source of collagen for tissue engineering.* Journal of Biomaterials and Tissue Engineering, 2014. **4**(3): p. 203-209.

140.   Suresh Kumar, N., et al., *A review on biological and biomimetic materials and their applications.* Applied Physics A, 2020. **126**(6): p. 445.

141.   WAIRIMU, P., M.A. Ollengo, and E.W. Nthiga, *Physical properties of chrome-tanned nile perch (lates niloticus) fish leather.* 2019.

142.   Mohamed, O., et al., *Styrene and butyl methacrylate copolymers and their application in leather finishing.* Journal of Applied Polymer Science, 2009. **111**(3): p. 1488-1495.

143.   Nashy, E.S.H., M.M. Essa, and A.I. Hussain, *Synthesis and application of methyl methacrylate/butyl acrylate copolymer nanoemulsions as efficient retanning and lubricating agents for chrome-tanned leather.* Journal of applied polymer science, 2012. **124**(4): p. 3293-3301.

144. Wang, Y., et al., *Preparation, mechanical properties and surface morphologies of waterborne fluorinated polyurethane-acrylate.* Progress in Organic Coatings, 2013. **76**(5): p. 876-883.

145. Feng, Y.-e., et al., *Improvements in Leather Surface Hydrophobicity through Low-pressure Cold Plasma Polymerization.* Journal of the American Leather Chemists Association, 2014. **109**(03): p. 89-95.

146. Singh, A.K., *Polydimethylsiloxane based sustainable hydrophobic/oleophilic coatings for oil/water separation: A mini review.* Cleaner Materials, 2022: p. 100136.

147. Qiang, T.T., et al. *Preparation, characterization of silicone succinate ester and its application in leather industry.* in *Advanced Materials Research.* 2011. Trans Tech Publ.

148. Gerde, J.A., et al., *Soybean oil.* Bailey's industrial oil and fat products, 2005: p. 1-68.

149. Saremi, K., et al., *Epoxidation of soybean oil.* Annals of biological research, 2012. **3**(9): p. 4254-4258.

150. He, W., et al., *Epoxidation of soybean oil by continuous micro-flow system with continuous separation.* Organic Process Research & Development, 2013. **17**(9): p. 1137-1141.

151. Liu, Z. and S.Z. Erhan, *Ring-opening polymerization of epoxidized soybean oil.* Journal of the American Oil Chemists' Society, 2010. **87**(4): p. 437-444.

152. Ge, X., et al., *Developing acrylated epoxidized soybean oil coating for improving moisture sensitivity and permeability of starch-based film.* International journal of biological macromolecules, 2019. **125**: p. 370-375.

153. Miao, S., et al., *Preparation and characterization of epoxidized soybean oil-based paper composite as potential water-resistant materials.* Journal of Applied Polymer Science, 2015. **132**(10).

154. Cheng, Q.-Y., et al., *Sustainable and biodegradable superhydrophobic coating from epoxidized soybean oil and ZnO nanoparticles on cellulosic substrates for efficient oil/water separation.* ACS Sustainable Chemistry & Engineering, 2017. **5**(12): p. 11440-11450.

155. Heath, R., et al., *Epoxide tannage: a way forward.* 2005.

156. Valeika, V., J. Širvaitytė, and K. Beleška, *Estimation of chrome-free tanning method suitability in conformity with physical and chemical properties of leather.* Materials science, 2010. **16**(4): p. 330-336.

157. Demongeot, A., et al., *Coordination and catalysis of Zn 2+ in epoxy-based vitrimers.* Polymer Chemistry, 2016. **7**(27): p. 4486-4493.

158. Blank, W.J., Z. He, and M. Picci, *Catalysis of the epoxy-carboxyl reaction.* Journal of Coatings Technology, 2002. **74**(926): p. 33-41.

159. Liang, S., et al., *Preparation and characterization of dimer fatty acid epoxy-acrylate resin hybrid emulsion for photocurable coatings.* Colloid and Polymer Science, 2019. **297**(9): p. 1199-1211.

160. Li, Y., et al., *Catalyst-free vitrimer elastomers based on a dimer acid: robust mechanical performance, adaptability and hydrothermal recyclability.* Green Chemistry, 2020. **22**(3): p. 870-881.

161. Barcena, H., A. Tuachi, and Y. Zhang, *Teaching green chemistry with epoxidized soybean oil.* Journal of Chemical Education, 2017. **94**(9): p. 1314-1318.

162. Adhvaryu, A. and S. Erhan, *Epoxidized soybean oil as a potential source of high-temperature lubricants.* Industrial Crops and Products, 2002. **15**(3): p. 247-254.

163. Park, S.-J., F.-L. Jin, and J.-R. Lee, *Thermal and mechanical properties of tetrafunctional epoxy resin toughened with epoxidized soybean oil.* Materials Science and Engineering: A, 2004. **374**(1-2): p. 109-114.

164. Xiang, Y., et al., *Temperature Dependence of Water Contact Angle on Teflon AF1600.* Langmuir, 2022. **38**(4): p. 1631-1637.

165. Nogami, R., et al., *Three-dimensional architecture of the acetabular labrum in the human hip joint.* Medical Molecular Morphology, 2020. **53**(1): p. 21-27.

166. Gutsmann, T., et al., *Force spectroscopy of collagen fibers to investigate their mechanical properties and structural organization.* Biophysical journal, 2004. **86**(5): p. 3186-3193.

167. Mazzon, G., et al., *Hydrophobic treatment of woven cotton fabrics with polyurethane modified aminosilicone emulsions.* Applied Surface Science, 2019. **490**: p. 331-342.